Thesis presented to the Technological Institute of Aeronautics, in partial fulfillment of the requirements for the degree of Doctor of Science in the Program of Physics, Field of Plasmas Physics.

Armstrong Godoy Junior

BLACK TiO$_2$ THIN FILMS PRODUCTION BY HOLLOW CATHODE HYDROGEN PLASMA FOR PHOTOCATALYTIC APPLICATIONS

Thesis approved in its final version by signatories below:

Prof. Dr. Argemiro Soares da Silva Sobrinho
Advisor

Prof. Dr. André Luis de Jesus Pereira
Co-advisor

Prof. Dra. Emília Villani
Pro-Rector of Graduate Courses

Campo Montenegro
São José dos Campos, SP – Brazil
2021

BIBLIOGRAPHIC REFERENCE

CESSION OF RIGHTS

BLACK TiO$_2$ THIN FILMS PRODUCTION BY HOLLOW CATHODE HYDROGEN PLASMA FOR PHOTOCATALYTIC APPLICATIONS

Armstrong Godoy Junior

Thesis Committee Composition:

Prof. Dr.	Gilberto Petraconi Filho	President	-	ITA
Prof. Dr.	Argemiro Soares da Silva Sobrinho	Advisor	-	ITA
Prof. Dr.	André Luis de Jesus Pereira	Co-advisor	-	ITA
Prof. Dr.	Homero Santiago Maciel	Intern Member	-	ITA
Prof. Dr.	Korneli Grigoriev Grigorov	External Member	-	BAS
Prof. Dr.	José Humberto Dias da Silva	External Member	-	UNESP

ITA

To my parents, Alexsandra and Armstrong, and my
brother, Alefe.

Acknowledgments

Firstly and foremost I wish to express my deepest gratitude to God, who gave me force and conditions to arrive until here.

I am deeply grateful to Marcelle for encouraging me and be patient throughout this project. She kept me going on, never wavered in her support and this thesis would not have been possible without her incentive.

Also, I am extremely grateful to my family: my mother, Alexsandra; father, Armstrong; and brother, Alefe. Without their tremendous understanding and encouragement in the past few years, it would be impossible for me to complete my study.

I would like to pay my special regards to my esteemed supervisor and co-supervisor, Prof. Dr. Argemiro and Prof. Dr. André, respectively, for their assistance at every stage of the research project. In addition, I would like to thank you for the encouragement at all times, which was essential for my journey considering the difficult moment that the world has been going through due to the pandemic caused by COVID-19. It is worth mentioning that these two human beings not only guided me but also became friends, which I will certainly take with me along my journey.

My gratitude extends to the professors Dr. Douglas Leite, Dr. Rodrigo Pessoa, and Dr. Marcilene Gomes for their mentorship during my stay at ITA.

I am indebted to Garufe e Jorge for always being helpful to me in the design of parts and repair of components of the systems used in this thesis.

I wish to express my sincere appreciation to all my lab mates, specially Aleandro, Barbara, Bernardo, Caliari, Cristian, Eduardo, Fagundes, Folli, Isabela, Miranda, Paulo, Rodrigo Moraes, and Roberson, for a cherished time spent together in the lab, and in social settings. My appreciation also goes out to my colleagues from ITA: Vinícius, Batta, Lilian, Bruno, Julia, Gracci, Vanessa, Andrew, Cauê, Maycon, and Fernando.

Thank should also go to Helen and Neto for the nice moments and helps in the Ozônio lab.

Lastly, I would like to acknowledge CAPES, FAPESP, and CNPq agencies for their financial support.

Science is the belief in the ignorance of experts.

Richard P. Feynman

Abstract

This thesis aims to demonstrate a new method to produce thin black TiO_2 films from pure TiO_2 films in the anatase phase. The method consists of immersing the TiO_2 films for fifteen minutes in a hydrogen plasma generated by a PECVD-RF system with a hollow cathode geometry, resulting in an efficient darkening of the TiO_2. The growth of pure TiO_2 films in the anatase phase on glass and c-Si substrates was carried out using a magnetron sputtering system and subsequent heat treatment at 450 °C for 2h in order to achieve a preponderance of the anatase phase. Before and after the H_2 plasma treatment, the samples were characterized for their morphological, microstructural, chemical, optical, electrical, and wettability characteristics. For this purpose, analyzes of mechanical profilometry, scanning electron microscopy by field emission and atomic force, UV-Vis-NIR spectrophotometry, X-ray diffraction, Raman spectroscopy, X-ray excited photoelectron spectroscopy, measurements of sheet resistance by four-point probe, and goniometry. In addition, the photocatalytic potential of the films produced through the degradation of the methylene blue dye was evaluated, in addition to an investigation of the characteristics of the hydrogen plasma generated during the hydrogenation process. The results obtained show that the use of a hollow cathode for the hydrogenation process was decisive for the efficient hydrogenation of the black TiO_2 films. After treatment in hydrogen plasma, the films show a significant increase in the absorption of light across the solar spectrum, a significant decrease in sheet resistance, and a significant increase in the surface area. These results are mainly related to an increase in O vacancies and an increase in the presence of OH hydroxyl groups on the surface of the films. These characteristics led to a significant improvement in its photocatalytic activity under UV-Vis irradiation.

Resumo

Esta tese visa demonstrar um novo método para se produzir filmes finos de black TiO_2 a partir de filmes puros de TiO_2 na fase anatase. O método consiste na imersão dos filmes de TiO_2 por apenas poucos minutos em um plasma de hidrogênio gerado por um sistema PECVD-RF com uma geometria de catodo oco, resultando em um eficiente escurecimento do TiO_2. O crescimento dos filmes puros de TiO_2 na fase anatase sobre substratos de vidro e c-Si se deu por meio do método de pulverização catódica (*magnetron sputtering*) e posterior tratamento térmico a 450 °C durante 2 h a fim de se conseguir uma preponderância da fase anatase. Antes e após o tratamento em plasma de H_2, as amostras foram caracterizadas quanto às suas características morfológicas, microestruturais, química, ótica, elétricas e de molhabilidade. Para isso, foram realizadas análises de perfilometria mecânica, microscopia eletrônica de varredura por emissão de campo e de força atômica, espectrofotometria UV-Vis-NIR, difração de raios-X, espectroscopia Raman, espectroscopia de fotoelétrons excitados por raios-X, medidas de resistência de folha por sonda de quatro pontas e goniometria. Além disso, foi avaliado o potencial fotocatalítico dos filmes produzidos por meio da degradação do corante azul de metileno, além de uma investigação das características do plasma de hidrogênio gerado durante o processo de hidrogenação. Os resultados obtidos mostram que a utilização de um catodo oco para o processo de hidrogenação foi determinante para uma eficiente hidrogenação dos filmes de black TiO_2. Após o tratamento em plasma de hidrogênio os filmes apresentam um aumento significativo na absorção de luz em todo o espectro solar, uma diminuição significativa da resistência de folha, e um aumento significativo da área superficial. Estes resultados estão relacionados principalmente a um aumento das vacâncias de O e com o aumento da presença de grupos hidroxila OH na superfície dos filmes. Essas características levaram a uma melhoria significativa na sua atividade fotocatalítica sob irradiação UV-Vis.

List of figures

List of Tables

List of Abbreviations and Acronyms

AFM   Atomic Force Microscopy

Ar   Argon

BAS   Academia de Ciências da Bulgária

CAPES   Coordination for the Improvement of Higher Education Personnel (*Coordenação de Aperfeiçoamento de Pessoal de Nível Superior)*

CB   Conduction Band

CNPq   National Council for Scientific and Technological Development (Conselho Nacional de Desenvolvimento Científico e Tecnológico)

DC   Direct Current

DSSC   Dye-Sensitized Solar Cells

FEG-SEM   Field Emission Gun Scanning Electron Spectroscopy

FWHM   Full Width at Half Maximum

H_2 Hydrogen

HC   Hollow Cathode

HCHP   Hollow Cathode Hydrogen Plasma

HRTEM   High-Resolution Transmission Electron Microscopy

HT   Heat Treatment

IEAv   Institute of Advanced Studies (*Instituto de Estudos Avançados*)

INPE   National Institute for Space Research (*Instituto Nacional de Pesquisas Espaciais*)

ITA   Technological Institute of Aeronautics (*Instituto Tecnológico de Aeronáutica*)

LABAS   Associated Laboratory of Sensors and Materials

LPP-ITA   Plasma and Process Laboratory at ITA (*Laboratório de Plasmas e Processos do ITA*)

MB   Methylene Blue

MO   Methyl Orange

N_2 Nitrogen

O_2 Oxygen

RF   Radiofrequency

RhB   Rhodamine B

Si   Silicon

Ti   Titanium

TiO_2 Titanium Dioxide

UNESP   Universidade Estadual de São Paulo

UV   Ultraviolet

VB   Valance Band

Vis   Visible

V_o Oxygen Vacancy

XPS   X-Ray Photoelectron Spectroscopy

XRD   X-ray Diffraction

Contents

1 Introduction

1.1 Background

Nowadays, semiconductor materials have received widespread interest in studies, since these materials are the basis of a variety of electronic/optoelectronic devices that can be applied in sectors aimed at solving environmental and energy issues [1–3]. Considering technologies such as solar cells, hydrogen production, or water purification, a key characteristic desired for the application of semiconductors is the absorption of all radiation, or at least the most part, of sunlight that reaches the Earth [4]. This is a challenge to be faced, since many of the semiconductor-based materials used for this purpose generally have wide bandgaps, which does not allow the absorption of the entire electromagnetic spectrum of the sun, covering the ultraviolet (UV), visible (Vis), and near-infrared (NIR) range [5]. For this reason, many researchers have been engaged in the treatment/modification of these materials to improve their optoelectronic properties, seeking maximum absorption of radiation in the visible region [6–8].

In 2011, Chen et al. published the results from a novel structural modification carried out in pristine TiO_2 (also called titania) nanoparticles [6]. It was reported that this new modified TiO_2, called "black TiO_2", was able to absorb electromagnetic radiation from the ultraviolet (UV) to the near-infrared (NIR) range. This increase in absorption was a consequence of the bandgap narrowing from 3.3 eV (pristine anatase TiO_2) to 1.54 eV (black TiO_2) obtained after heat treatment (200 °C) in a hydrogen atmosphere for 5 days under high pressure (20 bar) [6]. This hydrogenation treatment induced the creation of defects and structural disorder in the TiO_2 nanoparticles promoted by the incorporation of hydrogen atoms and removal of oxygen atoms, which was responsible for the bandgap narrowing and consequent light absorption increase [6].

Considering the extreme experimental conditions used by Chen et al. as high hydrogen pressure (which is a flammable gas) and the long process time, several studies started to be developed with the proposal to optimize the hydrogenation methodology [9,10]. So far, the most used methods are based on laser process [11], plasma-assisted treatment [12], chemical reduction [13], and low-/high-pressure heat treatments [14–16]. Among these methods, plasma-based processes have been used through different configurations: thermal plasma furnace [13,17], non-thermal dielectric barrier discharge (DBD) [18], plasma spray [19,20], chemical vapor deposition (CVD) [21,22], and others [12,23]. In this context, the CVD method is one of the most promising ones for synthesizing black TiO_2, mainly for its relatively mild conditions

(low pressure and short time process) and intense chemical reactions that this technique provides without harming the material's internal microstructure.

1.2   Problem Statement

Taking into account what was exposed previously, many research groups started to try to use CVD-based systems looking for an effective way to produce black titania. In 2013, Yan et al. treated anatase TiO_2 nanoparticles with H_2 plasma using inductively coupled plasma (ICP) equipment under 26.5 - 28.3 mTorr, at a temperature of 390 °C for 180 min. The ICP power was fixed at 3000 W and the synthesized material was applied to lithium-ion batteries [24]. One year later, in 2014, Teng et al. synthesized black TiO_2 powders using a hot filament CVD configuration under H_2 atmosphere. The treatment was carried out for 3h at 350 °C and 500 °C. The samples were applied in photocatalysis experiments on the degradation of rhodamine B (RhB) under simulated sunlight irradiation [25]. In the following year, black TiO_2 nanofibers were obtained by a CVD radio frequency hydrogen plasma system using an RF power of 15 W and temperatures ranging from 300 °C to 500 °C for 3h [26]. Ren et al. synthesized black TiO_2 nanoparticles by ICP instrument for 20 min under a hydrogen atmosphere (25.8 - 27.1 mTorr) at 150 °C. The ICP power was adjusted to 3000 W and the material produced was applied in photothermal cancer therapy [27]. In 2018, Islam et al. produced black TiO_2 thin films by a microwave (2.45 GHz)-assisted plasma CVD (MPCVD) system, and their photocatalytic activity was tested by photoelectrochemical water oxidation experiments under UV and visible light [22]. The hydrogenation process was performed under work pressure and discharge power at 40 Torr and 400 W, respectively, for 30 min. One year later, Pylnev and Wong also synthesized hydrogenated titania thin films using an MPCVD (2.45 GHz) system [21]. The treatment lasted 30 min under a working pressure of 10 Torr at 350 W. The authors evaluated the photocatalytic activity of the synthesized black TiO_2 thin films by methylene blue (MB) dye degradation when irradiated by a UV-Vis light source.

It is very clear to realize that, among the studies mentioned above, only one performed the hydrogenation process for less than 30 min. Besides, most of the works had to use extreme values of power to get great results. These two process variables (time and power) are directly related to energy consumption, and, consequently, to the cost, which affects considerably the costs of production mainly when we are talking about production on a large scale.

Moreover, most researchers concentrate efforts on the synthesis of black titania in powder form steady of thin-film form. As is known, TiO_2 in a nanopowder form is conducive

to surface reactions due to its large active surface area. However, the difficulty in precipitating and recovering the nanopowder from the treated liquid limits its application [28]. Therefore, the use of thin films in contaminated liquid photocatalytic processes is interesting and convenient.

1.3   Objective

Based on what is aforementioned, the main goal of this thesis is to present a new approach to produce black titania thin films that consist of a fast and efficient method based on a radiofrequency plasma-enhanced chemical vapor deposition system (RF-PECVD) under a hydrogen (H_2) atmosphere using a hollow cathode geometry. It is worth highlighting here that the hydrogenation method presented in this work, so far, is unprecedented.

In addition, the work also aims to characterize the morphological, microstructural, chemical, optical, electrical, and wettability properties of the produced black TiO_2 thin films. The photocatalytic activity of this material was also investigated by methylene blue (MB) dye degradation.

In addition, a brief study regarding the hollow cathode hydrogen plasma (HCHP) generated during the hydrogenation process is explored.

1.4   Organization of the Thesis

A general introduction, the problem statement, and the objectives of the thesis are presented in chapter 1.

Chapter 2 presents a brief review regarding black TiO_2 based on the main papers presented in the literature. This chapter gives special attention to the main methods used so far to obtain black TiO_2-based materials, the characteristics expected from its synthesis, and the main applications.

Then, in chapter 3, some theoretical foundations that provide a background for the discussions in this thesis are presented. There, are presented some concepts concerning hollow cathode plasmas and others concerning photocatalysis.

Chapter 4 describes the methods and experimental procedures carried out for synthesize, hydrogenate, and characterize the produced anatase TiO_2 thin films. Also, the details concerning the H_2 plasma characterization are presented.

The results obtained from the deposition and hydrogenation of the anatase TiO_2 thin films, as well as from the characterization of the hollow cathode hydrogen plasma are presented

in chapter 5. The morphological, microstructural, chemical and optical properties of the films are presented and discussed. Also, the photocatalytic activity of these films is explored.

Chapter 6, the general conclusions related to each of the topics developed are presented, as well as suggestions for future work.

Chapter 7 exposes the references used in this work and, in Chapter 8, the papers published during this D.Sc. duration, which was also a prerequisite to defending this thesis. Also, the works presented in scientific conferences are presented.

2   Literature Review

2.1   Introduction

Since the first report in 2011 concerning the synthesis of black titania, this material started to be explored by many research groups around the world. However, compared with other research themes, black TiO_2-based materials are still slightly explored. This fact can be well visualized in **Figure 2.1**, which shows the panorama of the number of scientific publications on this topic from 2011 to May 2021. These data were collected through the bibliographic research platform Web of Science using the expression "Black TiO_2" as keyword.

It is possible to observe that the number of publications since 2011 was quite small, having a more significant evolution in 2018. However, this quantity is still not an expressive number when compared to the number of publications of pristine TiO_2, for example, which reaches the order of thousands of publications per year. This is a strong indication that there is still a lot to be explored concerning this material mainly considering that it was reported for the first time recently.
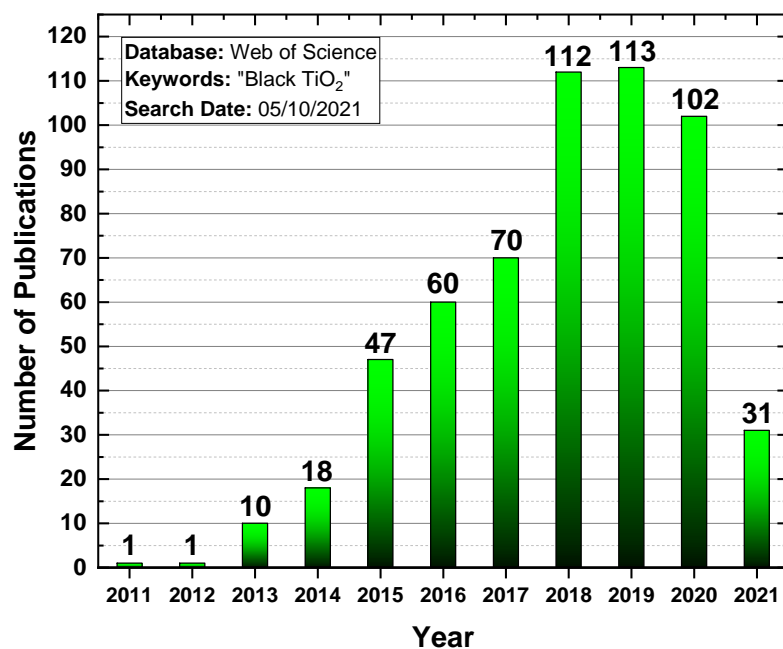
Figure 2.1. Quantity of scientific publications on black TiO$_2$ since 2011.

In addition, among these publications, it is interesting to highlight that a great part of the research groups that published on this subject is from China and just two groups in Brazil, being one of them our group, has published a scientific article related to this topic until the date of the survey, as shown in **Figure 2.2**.
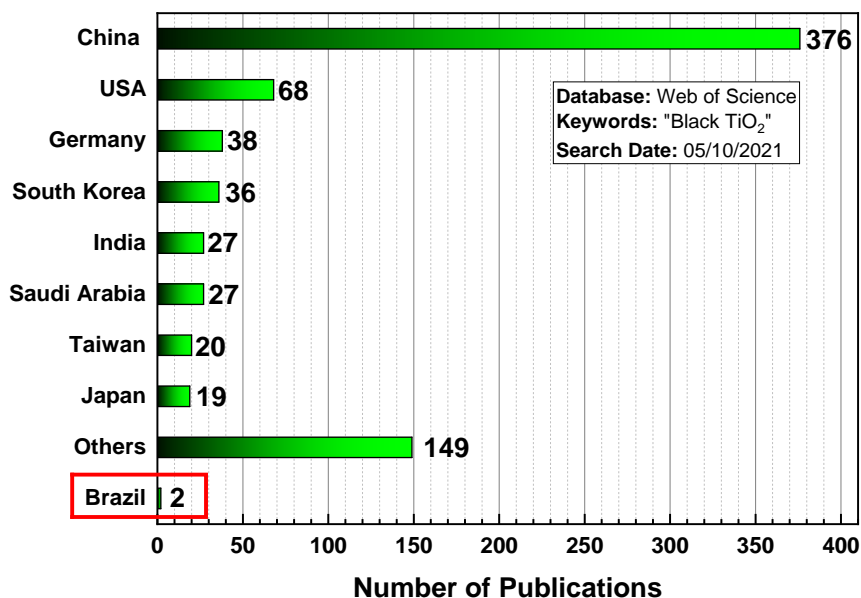
Figure 2.2. Quantity of scientific articles about black TiO$_2$ published by country from 2011 to 2021.

Therefore, it is evident that should be of great interest the study of materials used for renewable energy technologies, especially back TiO_2 in this case, considering that Brazil is one of the few countries in the world that owns the privilege of receiving one of the greatest incidences of solar light during the whole year.

As was mentioned above, it is undeniable that black TiO_2-based materials are still a novelty for the scientific community both at a global level and mainly at a national level. For this reason, in addition to the importance of this material for solving current and future environmental problems, there is still much to be studied about this topic, considering that it is still a relatively recent material and many questions must be explored and answered.

In this sense, this chapter presents a brief review of the literature concerning black TiO_2-based materials. Some important topics are highlighted, as the main methods used for the synthesis, the main characteristics desired after the synthesis, as well as the main areas where this material can be applied. Lastly, considering that this thesis focused on the application of the produced black TiO_2 thin films in photocatalysis for pollutant degradation, the main papers published so far concerning this topic are exposed in section 2.6.

2.2 Black TiO_2

Pristine/white TiO_2 is widely used in photodegradation of organic pollutants, solar cells, photocatalytic water splitting for hydrogen generation, gas sensors, biosensors, textile industries, as well as cosmetics, drugs, and even food industries. The large use of TiO_2 can be associated mainly with its whitish color and the fact that this material is chemically stable, non-toxic, cheap, and photosensitivity [29,30]. However, due to the large bandgap (3.0-3.2 eV), this material has a performance limitation when applied in processes/sectors where the use of solar energy/light irradiation is necessary for activating chemical reactions or charge mobility. That is a consequence of the large bandgap that limits the light absorption only in the UV range, which corresponds to less than 5% of sunlight [31,32].

Amid this impasse, several research groups are concentrating efforts to try to increase the light absorption rate of TiO_2-based materials. In this sense, these researchers use several strategies, as the doping of TiO_2 with metals and also non-metals [33–35], a recurrent strategy. The doping process can improve the light absorption range of the TiO_2, but sometimes only in parts of the spectrum of the sun's emission. In addition, the doping sometimes can accelerate the recombination rate of electron-hole pairs, which is not interesting for photocatalytic and photovoltaic applications [36–38].

In this context, in 2011, Chen et. al. published the results from a novel structural modification carried out in pristine TiO_2 nanoparticles [6]. They reported that this new modified TiO_2, called "black TiO_2", was able to absorb light energy from the UV to the near-infrared (NIR) range, as shown in **Figure 2.3**.
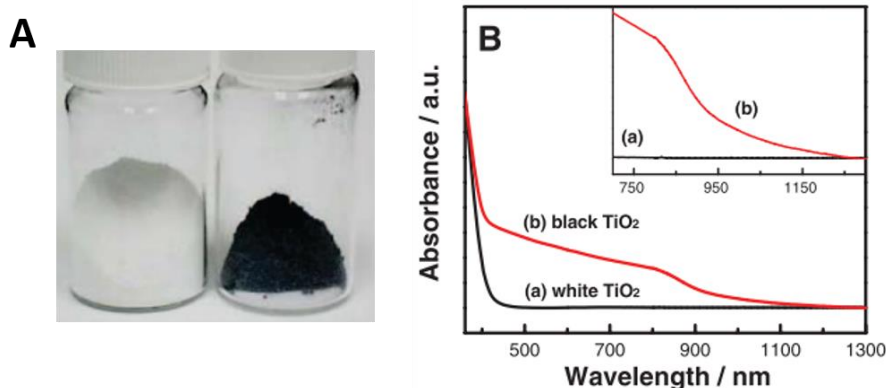
Figure 2.3. a) White and black TiO_2 nanoparticles produced by Chen et al. and b) absorption spectra of both samples. Reproduced from [6].

This increase in the absorption was related to the bandgap narrowing from 3.3 eV (pristine anatase TiO_2) to 1.54 eV (black TiO_2) obtained after heat treatment (200 °C) under high pressure (20 bar) at hydrogen atmosphere for 5 days promoted by a Hy-Energy Pressure-Composition Isotherms (PCTPro) [6]. This hydrogenation treatment induced the creation of structural disorder in the TiO_2 nanoparticles promoted by the incorporation of hydrogen atoms and removal of oxygen atoms (oxygen vacancies - V_o), which was responsible for the bandgap narrowing. This combination of changes promoted optical, electrical, and photocatalytic performance increase. **Figure 2.4** shows the microstructure of the black TiO_2 monocrystal proposed by the authors. The black dots represent the dopant (hydrogen) and the outer layer represents the disorder.
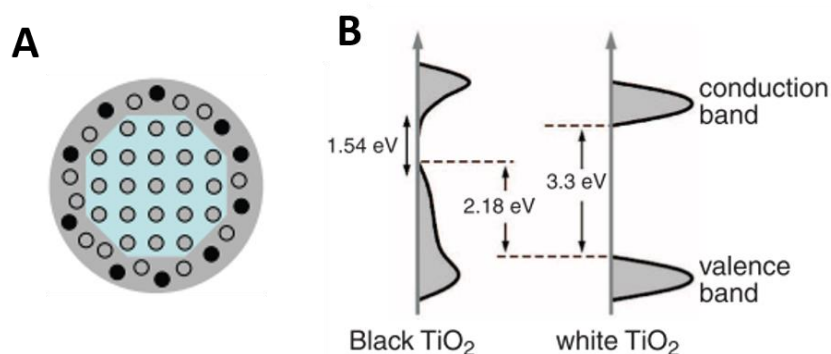
Figure 2.4. a) Proposed microstructure from a black TiO_2 nanocrystal. Black dots represent the dopant (hydrogen) and the outer layer represents the disorder. b) Schematic diagram of the density of states from the black and white TiO_2. Reproduced from [6].

In summary, the reason for the optical, electrical, and photocatalytic performance improvements is that the lattice disorder induced by the hydrogen treatment promotes the creation of midgap and also tail states inside the bandgap. Those changes decrease the bandgap and, consequently, increase the light absorption range. Xiu et al. created a table that summarizes the main differences between pristine and black TiO_2 [39]:

Table 2.1. Main characteristics difference between pristine and black TiO_2. Adapted from [39].

Pristine TiO_2	Black TiO_2
Wide bandgap	Narrow bandgap
High recombination rate of photogenerated electron-hole pairs	Low recombination rate of photogenerated electron-hole pairs
Narrow light absorption range (UV)	Large light absorption range (UV–Vis-NIR)
Fewer V_o	More V_o
Low photocatalytic activity	High photocatalytic activity

Although the results published by Chen et al. have shown themselves very promising, the extreme experimental conditions used during the hydrogenation process, as high hydrogen pressure (which is a flammable gas) and the long process time, motivated several research groups to develop alternative methods with the proposal to optimize the black TiO_2 production methodology. In view of this, **section 2.2.2** presents the main of these methodologies used in different studies that can be found in the literature. Furthermore, in addition to optimizing process parameters, these research groups have also been concentrating efforts on production routes that can further improve the desired properties after the synthesis of black TiO_2. Hence,

beneath is exposed the main characteristics expected from the black TiO_2-based materials after being produced.

2.2.1 Black TiO_2 Properties

After the synthesis of black TiO_2-based materials, the researchers aim to achieve some essential properties that make viable the application of these materials in photocatalytic and photovoltaic applications. Among these properties, the following can be highlighted: structural disorder of the surface, relatively high concentration of V_o, as well as an increase in the concentration of Ti^{3+} ions in its crystalline structure, presence of Ti-OH and Ti-H groups on its surface, in addition to narrowing the gap energy [40,41].
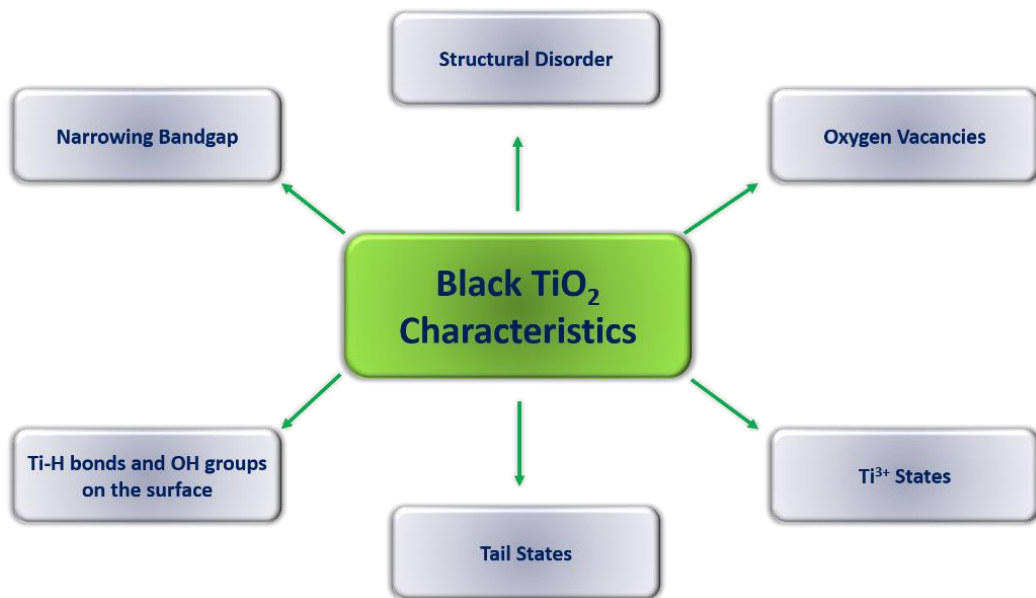
Figure 2.5. Main characteristics expected from the synthesis of black TiO_2-based materials.

The expected structural disorder is caused mainly due to the creation of V_o in the TiO_2 lattice. The presence of V_o and Ti^{3+} defect states are responsible for the creation of tail states and midgap states inside the band gap, respectively, and, consequently, the bandgap narrowing, as is represented in **Figure 2.6** [42–44]. The black color is, therefore, a consequence of this bandgap narrowing, and also is a piece of clear evidence that the material is absorbing light in the visible range.
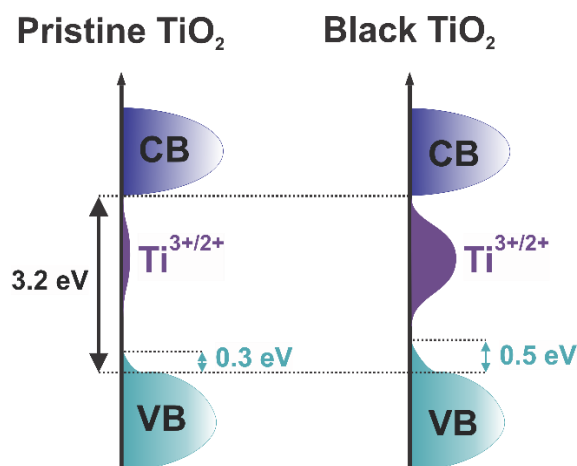
Figure 2.6. Schematic diagram representing the details of the in-gap states of pristine and black TiO$_2$.

Besides, an amount of Ti-H bonds and OH groups are created on the surface of black TiO$_2$ after the hydrogenation process. These OH groups are the main oxidative group in photocatalysis reactions in the dissolution of organic molecules [45].

In addition to all the characteristics mentioned above, some papers also report the increase in the surface area after hydrogenation, which is also crucial for better performance in photocatalytic and even photovoltaic processes [46–50].

It is worth mentioning that is not every synthesis process that makes the material possible to have all these characteristics. This is even one of the challenges that researchers try to tackle, as will be shown below.

2.2.2   Synthesis Methods

The first studies reported the production of black TiO$_2$ by processes that demanded long periods and the use of extreme pressure and temperature conditions. However, over the years, these conditions have become milder mainly because of the efforts that researchers have devoted to developing more efficient methods.

Among the several proposed methods, some of those have been more explored. The main ones are heat treatment at high-/low-pressure of pure hydrogen or different gases combinations (H$_2$/N$_2$, H$_2$/Ar, N$_2$/Ar, Ar) [38,46,51–73], chemical reduction [13,74–78], high-energy particles bombardment (laser, electron) [11,79,80], plasma treatment [17,25,81–87], electrochemical reduction-anodization [88–92], and others [93–95].
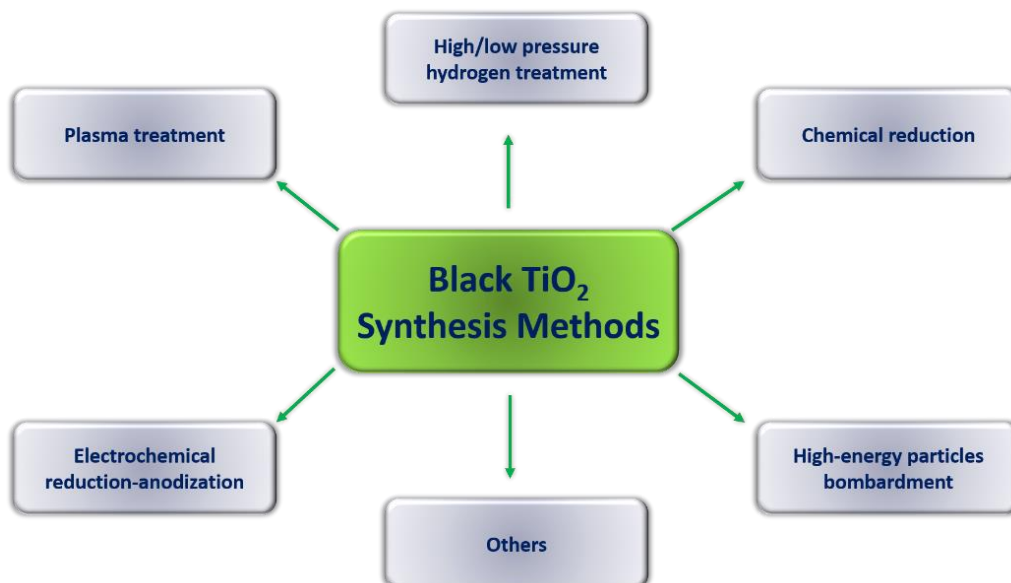
Figure 2.7. Main black TiO_2 synthesis methods reported in the literature so far.

In general, the focus of the researchers was the reduction of the work pressure, due to the dangerous nature of H_2 under high pressure, or the use of other gases combined with hydrogen, as well as the reduction of process time. Furthermore, the possibility of using milder process conditions means that the material matrix is not negatively modified.

It was aligned with these ideas that plasma processes began to be proposed as potential routes for the synthesis of black TiO_2. Plasma processes began to be used for blackening/hydrogenate TiO_2-based materials only in 2013 with Wang et al [96]. On this occasion, the authors reported the preparation of black $TiO_{2-x}H_x$ nanoparticles using a thermal plasma furnace. Was generated a hydrogen plasma with an input power of 200 W, and the nanoparticles were kept inside the furnace for 2 hours at a temperature of 500 °C.

That report concerning TiO_2 hydrogenation by plasma process motivated many other researchers to begin studying this theme with the purpose to obtain this material with the expected characteristics in a short time by an efficient treatment. The graph in **Figure 2.8** shows how the amount of publications related to the production of black TiO_2 using plasma processes has evolved.
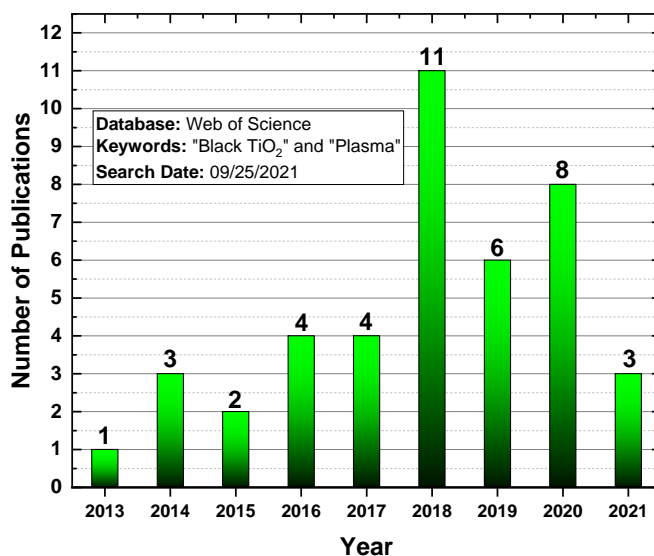
Figure 2.8. Quantity of scientific publications on black TiO$_2$ produced by plasma processes since 2013.

The next section exposes the main contributions in the literature concerning the use of plasma-based methods to produce black TiO$_2$. The objectives and general idea of the works are mentioned throughout the next sections, but the most important details of each of these papers are organized in **Tables 2.2** - **2.6**.

2.2.2.1 Plasma Enhanced Vapor Deposition – PECVD

The first works reporting the use of PECVD systems for the production of black TiO$_2$ were published in 2013. The first one was developed by Yan et al. and the main objective was hydrogenating commercial TiO$_2$ anatase nanoparticles and apply them in lithium-ion batteries [24]. Soon after, Wu and collaborators produced hydrogenated TiO$_2$ nanotube films for application in supercapacitors [97].

Table 2.2. Main operation parameters and main characteristics of the black TiO_2 produced by solution PECVD-based processes.

Year/ref.	2013/[24]	2013/[98]	2014/[99]	2015/[26]	2018/[22]
Gas/Pressure (mTorr)	H_2 (50 sccm) / 26.5-28.3	H_2 (100 sccm) / 375	H_2 (50 sccm) / 25.8-27.1	H_2 (500 sccm)	H_2 (100 sccm) / 40000
Power (W)	3000 (ICP)	40 (RF)	3000 (ICP)	15 (RF)	400 (microwave)
Process Time (min)	180	90	0.5-20	180	30
Process Temperature (°C)	390	320	150	300-500	-
Morphology	Nanoparticles	Nanotube films	Nanoparticles	Nanofibers	Mesoporous thin films
Defects	Ti^{3+}	Ti^{3+}, OH	Ti^{3+}	Ti^{3+}, V_o	Ti^{3+}, V_o, Ti-H, Ti-OH
Bandgap (eV)	-	-	-	-	-
Phase	Anatase	Anatase	Anatase/rutile	Anatase	Amorphous/anatase
Application	Lithium-ion batteries	Supercapacitors	Photocatalysis (MB degradation and CO_2 reduction)	Photoelectrochemical processes	Photoelectrochemical water oxidation

After the publication of his first work in 2013, Yan et al. published another work in 2014 [98] where they use the same PECVD system as the previous work. However, was used lower process temperature and commercial TiO_2 P25 nanoparticles, instead of pure anatase. Furthermore, instead of applying them in lithium-ion batteries, he applied them in MB degradation photocatalysis and CO_2 reduction.

A year later, Lepcha et al. produced electrospun black TiO_2 nanofibers and stained them to be applied in photoelectrochemical processes [26]. Finally, in 2018 Islam and his collaborators produced mesoporous black TiO_2 thin films by hydrogenating them using a PECVD system activated by a microwave power source [22]. The authors tested the samples in photoelectrochemical water oxidation.

2.2.2.2 Thermal Plasma Furnace

The first work reporting the use of a thermal plasma furnace system for synthesizing black TiO_2 was published in 2013 [96]. Wang et al. produced black TiO_2 nanoparticles with a core-shell microstructure and applied them in photocatalytic processes for both MO degradation and hydrogen generation. In 2016, Tian and his colleagues published a study on the production of hydrogenated TiO_2 also synthesized by a thermal plasma furnace system [99]. In this study, they applied the material in photoelectrochemical water-splitting. In that same year, Xu et al. produced black TiO_2 nanoparticles with a core-sell type structure to be applied in lithium-ion batteries [100].

Table 2.3. Main operation parameters and main characteristics of the black TiO_2 produced by thermal plasma furnace-based processes.

Year/ref.	2013/[96]	2016/[99]	2016/[100]
Gas/Pressure (mTorr)	H_2	H_2	H_2
Power (W)	200	200	200
Process Time (min)	240-480	60	120
Process Temperature (°C)	500	350-500	400
Morphology	Core-shell nanoparticles	Nanowires	Core-shell Nanoparticles
Defects	Ti^{3+}, Ti-H	Ti^{3+}, V_o	Ti^{3+}
Bandgap (eV)	0.8	2.76-2.96	-
Phase	Amorphous/anatase/rutile	TiO_2-B	Anatase
Application	Photocatalysis (H_2 generation and MO degradation)	Photoelectrochemical water-splitting	Lithium-ion batteries

2.2.2.3 Reactive Sputtering

Singhand and collaborators published in 2016 a study showing how they produced black TiO_2 thin films using a reactive sputtering system [101]. The authors did not apply the produced films. However, from the characteristics obtained, they could infer that the material is suitable for photoelectrochemical and photocatalytic applications.

Liang and his colleagues produced amorphous black TiO_2 thin films, which they found to be the reason for getting a wider bandgap than normal (3.78 eV) [102]. After that work, Pylnev et al. prepared, in 2018, black TiO_2 thin films also using a reactive sputtering system [103]. The authors investigated the H_2 flow rate influence on the properties of the thin films and found that the produced black TiO_2 presented lower photocatalytic activity compared with the pristine one.

Table 2.4. Main operation parameters and main characteristics of the black TiO_2 produced by reactive sputtering processes.

Year/ref.	2016/[101]	2017/[102]	2018/[103]
Gas/Pressure (mTorr)	Ar/H_2 / 25	Ar/H_2 / 4	Ar/H_2 / 8
Power (W)	75 (RF)	380 (pulsed DC)	200 (DC)
Thin-film Thickness (nm)	-	280	~500
Process Temperature (°C)	300	-	300
Morphology	Thin film	Thin film	Thin film
Defects	Ti^{2+}/Ti^{3+}	-	V_o
Bandgap (eV)	2.56	3.78	2.6 - 3.55
Phase	Anatase	Amorphous	Anatase/rutile
Application	-	-	Photocatalysis (MB degradation)

2.2.2.4 Solution Plasma Process

In addition to the more conventional processes mentioned above, some researchers have used plasma in an aqueous medium to produce black TiO_2. In 2017, Jedsukontorn et al. used such a system to produce black TiO_2 nanoparticles [104]. Despite not having applied these nanoparticles in any application, the authors well explored the parameters of the system used and showed how they influenced the properties of the synthesized material.

A year later, An et al. proposed a modified sol-gel method using underwater discharge plasma [105]. They synthesized nanospheres and tested them in photocatalysis by degradation of rhodamine B and phenol. In the same year, Han and his colleagues synthesized black titania by plasma electrolytic oxidation [106]. The main point of the work was to evaluate the influence of the oxidation time on the synthesized material properties. Some details related to the works mentioned above are represented in **Table 2.5**.

Table 2.5. Main operation parameters and main characteristics of the black TiO_2 produced by solution plasma-based processes.

Year/ref.	2017/[104]	2018/[105]	2018/[106]
Solution	HNO_3	$TiOCl_2$/HCl/H_2O	$Na_2SiO_3 \cdot 9H_2O$/NaOH
Pressure (Torr)	Atmospheric	Atmospheric	-
Power (W)	-	800	5000 (pulsed power source)
Process Time (min)	240	5,10	0.46-15.0
Process Temperature (°C)	60	65	-
Morphology	Nanoparticles	Spheres	Coating
Defects	Ti^{3+}, Ti-OH	Ti^{3+}, V_o	Ti^{2+}/Ti^{3+}
Bandgap (eV)	2.44	2.99, 2.88	-
Phase	Anatase/rutile	Anatase/rutile	Amorphous/rutile
Application	-	RhB, and phenol degradation by photocatalysis	-

2.2.2.5 Others

In addition to the works presented above, two others used slightly different methods but are also based on plasma processes. The first one was published in 2013 by Li et al. and was based on a hot filament hydrogen plasma system [107]. In this study, the authors synthesized black TiO_2 nanoparticles for the RhB degradation by photocatalysis. The second study deals with the use of an air plasma treatment system, where the authors evaluated the influence of treatment time on the properties of black TiO_2 thin films [108].

Table 2.6. Main operation parameters and main characteristics of the black TiO₂ produced by other processes.

Year/ref.	2013/[107]	2016/[108]
Synthesis Method	Hot Filament CVD	Air plasma treatment
Pressure (mTorr)	-	0.7
Power (W)	-	22.7
Process Time (min)	180	0-1
Process Temperature (°C)	350, 500	-
Morphology	Nanoparticles	Thin film
Defects	V_o, Ti-H	Ti^{3+}, V_o
Bandgap (eV)	2.8-3.5	3.00-3.62
Phase	Anatase/rutile	Amorphous
Application	RhB degradation by photocatalysis	-

2.2.3   Main Applications

Due to the interesting properties and versatility, black TiO₂-based materials have been applied in several areas, such as photocatalysis for pollutant removal from water [25,43,62,70,76,109–113] and for hydrogen production [53,77,78,94,111–119], dye-sensitized solar cells [123,124], supercapacitors [89,125,126], batteries [63,82,127–134], and photoelectrochemical water-splitting [74,76,99,135–138].
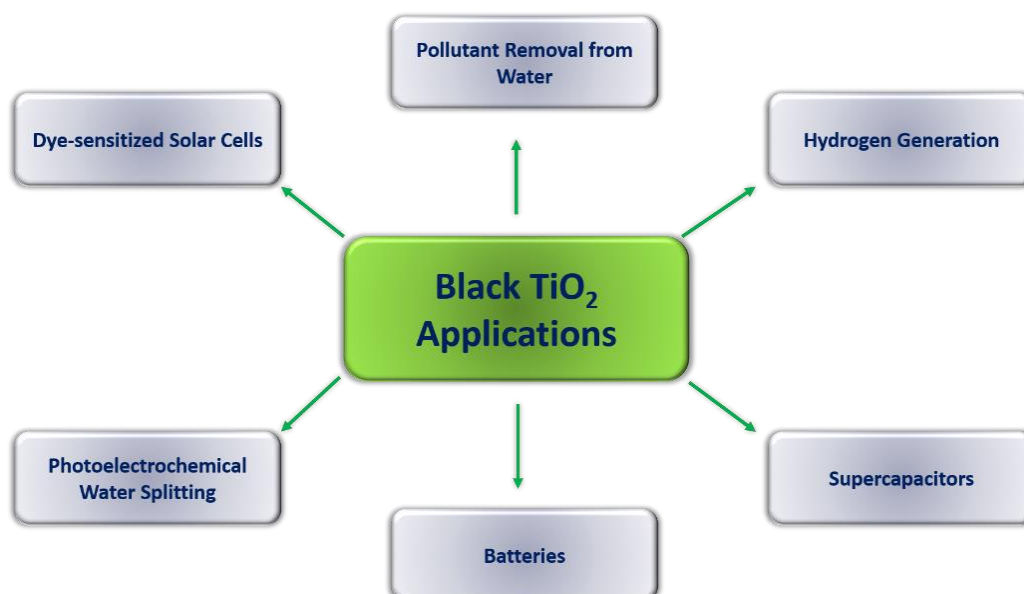
Figure 2.9. Main application fields in which black TiO₂-based materials have been applied.

In addition to the more common applications listed above, black TiO₂ has also been applied in other interesting areas, as CO_2 reduction [139,140], solar desalination [10,141], and photothermal therapy [27,79,142].

3 Theoretical Foundations

3.1 Introduction

This thesis is grounded on a variety of concepts related to the study of plasmas, materials sciences, and photocatalytic processes. Therefore, is necessary to address some topics related to these major themes that will provide a basis for a better understanding of the obtained results in this thesis. Hence, this chapter summarizes the main concepts related to hollow cathode plasmas, photocatalytic processes, and the use of pristine and black TiO_2-based materials on photocatalysis.

3.2 Hollow Cathode Plasmas

The use of plasma systems in the hollow cathode (HC) configuration is well established and has been extensively studied [145–158]. The first HC was used in 1916 by Friedrich Paschen operating with a DC discharge in an atmosphere of helium gas [149]. Although several authors have already observed an abrupt increase in the discharge current when using hollow cathode geometry compared to planar cathodes [147], the first experimental evidence of this HC effect was reported in 1954 by Little and von Engel [157]. In this episode, an abrupt increase in the discharge current (almost 10^3 times more) was measured when two parallel plates of the cathode in question were gradually brought together from a distance of a few millimeters. It was concluded on this occasion that, for the same DC potential established between the anode and the cathode, was possible to obtain a discharge current 10^3 times higher and corresponding plasma density only by establishing a suitable geometry for the cathode.

After that, several authors reported the possibility of using alternating current (AC) instead of DC to generate the HC discharge in order to obtain an even denser plasma [147]. In this context, the hollow cathode discharges generated by radiofrequency (RF) sources were first studied by Horwitz [145] and, later, by many other researchers, who described other types of configuration for the use of hollow cathodes with RF sources [144,147,155–157].

In general, the physical and chemical processes that occur inside an HC are more intense when compared to a conventional parallel plate configuration [147]. This is a consequence of a combination of effects that occur in plasma. These main effects are briefly described below and are illustrated in **Figure 3.1**.
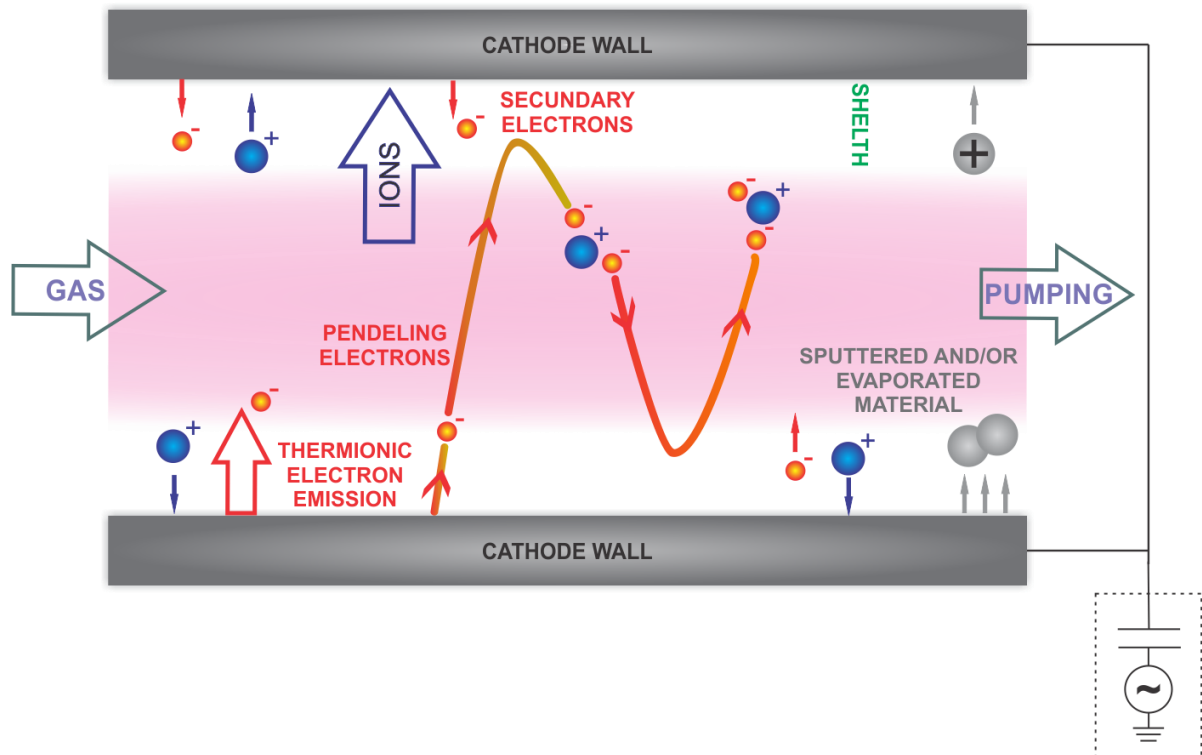
Figure 3.1. Schematic representation of the main phenomena that occur in a hollow cathode plasma. Adapted from [158].

High-energy electrons emitted from the walls of the cathode oscillate between the repellent potentials of the walls. These electrons are accelerated by the sheath's electric field and, during their oscillatory movement, they can suffer several collisions with the gas along their paths, increasing the degree of ionization and consequently the density of the plasma [147,157]. This oscillatory motion of electrons was named by L. Bárdoš as pendular motion [147]. The origin of these electrons is due to two mechanisms:

(i) Thermionic effect due to overheating of the cathode walls as a consequence of ion bombardment on it;

(ii) as a consequence of the bombardment of positive ions on the cathode walls, which leads to the ejection of secondary electrons [147].

Furthermore, species from the cathode walls may eventually be further/sputtered due to both ion bombardment and walls' heating. This species can be ionized and also contribute to the phenomena described above [147].

3.3   Photocatalysis

The photocatalysis process is inspired by the natural process of photosynthesis [159]. Basically, this process is characterized by the ability to conduct chemical reactions using light energy [160,161]. The process that has been known today as photocatalysis was first reported in 1972 by Honda and Fujishima when the photo-induced decomposition of water was discovered [162].

The photocatalysis process can be summarized in three steps:

Figure 3.2. Necessary steps to occur photocatalysis process.

(i) electron-hole pairs are generated in the bulk phase after being irradiated by light with energy higher than the material bandgap;

(ii) these electrons and holes migrate to the surface of the photocatalytic material;

(iii) the photogenerated electrons will act in the reduction reactions and the holes in the oxidation reactions [163].

In general, this photocatalytic process is mainly used for three purposes: water splitting, degradation of pollutants, and CO_2 conversion [160]. However, because of their intrinsic properties, in most cases, materials suitable for photocatalytic processes are also suitable for photovoltaic devices.

Considering that this thesis will focus on the evaluation of the photocatalytic performance of black TiO_2 thin films on the degradation of pollutants, it is worth highlighting the main mechanisms and reactions that occur in this type of process. A schematic representation of these mechanisms is presented in **Figure 3.3**, and the equations **3.1 – 3.6** explain the main chemical reactions.
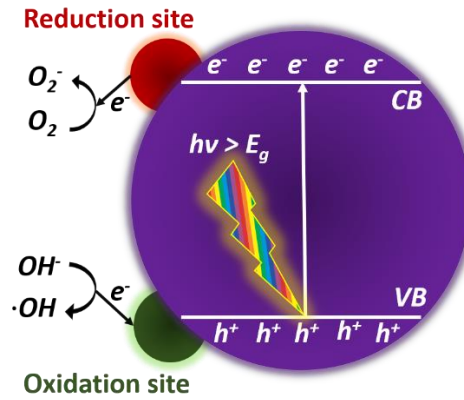
Figure 3.3. Representation of the mechanisms that govern processes of pollutant degradation.

$$Photocatalyst \ + \ hv \rightarrow h_{VB}{}^+ + e_{CB}{}^- \tag{3.1}$$

$$h_{VB}{}^+ + e_{CB}{}^- \rightarrow energy \ (heat) \tag{3.2}$$

$$H_2O \ + \ h_{VB}{}^+ \rightarrow * \ OH \ (hydroxyl \ radical) \ + \ H^+ \tag{3.3}$$

$$O_2 \ + \ e_{CB}{}^- \rightarrow O_2{}^- * (superoxide \ radical) \tag{3.4}$$

$$* \ OH \ + \ pollutant \rightarrow H_2O + CO_2 \tag{3.5}$$

$$O_2{}^- * \ + pollutant \rightarrow H_2O + CO_2 \tag{3.6}$$
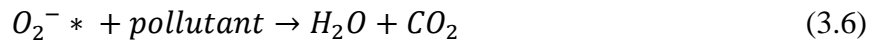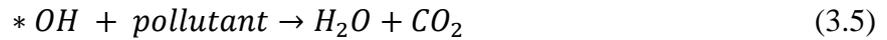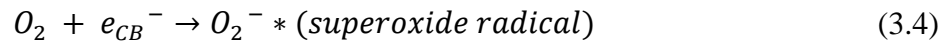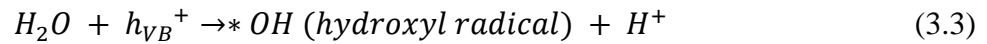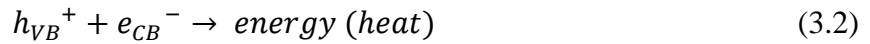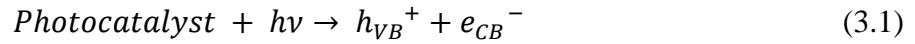
where hv is the light energy, $h_{VB}{}^+$ and $e_{CB}{}^-$ represents the holes and electrons photogenerated, respectively [40]. After being irradiated by light energy, electrons from the valence band (VB) of the photocatalytic material are excited and migrate to the conduction band (CB) leaving behind holes in the VB (**eq. 3.1**). Photogenerated holes can react with H_2O molecules and form hydroxyl radicals (*OH), while photogenerated electrons can react with O_2 and form superoxide radicals ($O_2{}^{-*}$), which is represented in equations **3.3** and **3.4**, respectively. In turn, as described in equations **3.5** and **3.6**, *OH and $O_2{}^{-*}$ radicals can react with pollutants present in the system, most often organic pollutants, forming H_2O and CO_2 as a product.

Is important to highlight that, amidst the reactions of equations **3.2** and **3.3**, the photogenerated electron-hole pairs can recombine and release energy as heat (see equation **3.2**) [40]. This recombination can occur both in the bulk and on the surface of the photocatalyst [164]. This, consequently, decreases the photocatalytic efficiency of the process/material and, hence, is an important issue to taking into account during the synthesis and characterization of the photocatalysts [40].

3.4 Pristine and Black TiO$_2$ Thin Films for Photocatalysis

Assuming that the TiO$_2$ produced in this thesis will be applied in photocatalysis processes, two important questions must be answered before its synthesis: (i) will we work with this material in which morphology (nanoparticles, thin films, nanotubes, etc)?; and (ii) which TiO$_2$ phase will allow us better performance in photocatalysis processes?

Most photocatalytic studies use TiO$_2$ in the form of nanoparticles. Indeed, nanoparticles have some important advantages compared to thin films/bulks, mainly concerning their high surface area. However, the reuse of these nanoparticles in a photocatalytic system is difficult and may also end up modifying the natural properties of the environment in which they are being applied, since their removal is difficult. In addition, TiO$_2$ thin films can be easily used in several other relevant applications, as in photovoltaic devices. Therefore, for some situations, the use of TiO$_2$ as thin-film /bulk is necessary and more suitable.

Furthermore, considering that TiO$_2$ can be found in three main phases (anatase, rutile, and brookite), the choice of which phase will be used is extremely important to achieve the best possible yield in the process in which this material will be applied. **Table 3.1** shows the main parameters of each TiO$_2$ phase [165,166].

Table 3.1. Main parameters from TiO$_2$ phases [165,166].

Phase	Anatase	Rutile	Brookite
Crystal structure	Tetragonal	Tetragonal	Orthorhombic
Atoms per unit	4	2	8
Lattice parameters (nm)	$a = b \cong 0.39$; c $\cong$ 0.95	$a = b \cong 0.46$; c $\cong$ 0.30	$a =$ c $\cong 0.54$; b $\cong$ 0.91
Space group	*I4$_1$/amd*	*P4$_2$/mnm*	*Pbca*
Density (g/cm^3)	3.83	4.24	4.17
Electron mobility (cm^2/V.s)	~10	~1	-
Bandgap (eV)	3.26	3.05	2.96

In the case of photocatalytic and photovoltaic applications, the phase that manifests the highest performance, in general, is the anatase phase [167,168]. This is because the anatase phase presents relatively higher electron mobility. This characteristic is related to a more open structure, as shown in **Figure 3.4** [38].
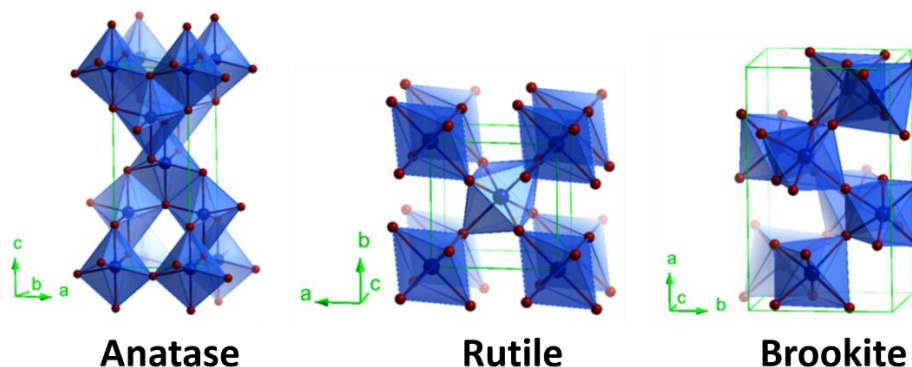
Figure 3.4. Main crystal structures of TiO_2. Adapted from [38].

Taking this into account, the vast majority of researchers who have been producing black TiO_2-based materials aim to synthesize that in the anatase phase. Is important to say that the minority of studies in the literature present a phase change during the process of converting pristine into black TiO_2 [169]. The main idea is to achieve a process efficient enough to obtain the properties described in **Chapter 2**, but at the same time mild enough time not to change the phase of the material.

4 **Materials and Experimental Procedures**

The experimental procedures of this thesis are divided into two main parts: one related to the deposition of the anatase pristine TiO_2 thin films and another related to the hydrogenation of these films to form the black TiO_2 thin films. For both cases, is described in this chapter the analytical instruments and conditions used to produce and analyze these films before and after the hydrogenation process. Finally, is presented the experimental setup used for the photocatalytic activity evaluation.

4.1   Deposition of Anatase Pristine TiO$_2$ Thin Films

The growth procedure of the pristine TiO$_2$ thin films was divided into three steps: substrates cleaning, deposition by magnetron sputtering, and subsequent heat treatment. Details on each of these steps are detailed below.

4.1.1   Substrates Cleaning

Before the deposition step, glass substrates were cleaned using a routine used in the LPP-ITA. First, the substrates were washed with the aid of Extran detergent and sponge in order to remove coarse dirt and grease residues. After this stage, the substrates were submitted to three ultrasonic baths, each lasting 8 min with different solvents: ethyl alcohol, acetone, and isopropyl alcohol. After bathing, the substrates were dried with the aid of a thermal blower. The entire cleaning process was carried out using gloves.

The c-Si substrates were cleaned by a solution of sulfuric acid with hydrogen peroxide (H$_2$SO$_4$/H$_2$O$_2$, 4:1) for 10 min; then, they were washed with deionized water and subjected to a solution of hydrofluoric acid with deionized water (HF/H$_2$O, 1:10) for 1 min and, finally, the substrates were again washed with deionized water.

4.1.2   Pristine TiO$_2$ Thin Films Deposition by Magnetron Sputtering

After being cleaned, the substrates (glass and c-Si) were submitted to the deposition procedure using a magnetron sputtering system. This system belongs to the LPP-ITA. **Figure 4.1** presents a photograph and **Figure 4.2** a schematic diagram of this magnetron sputtering system.
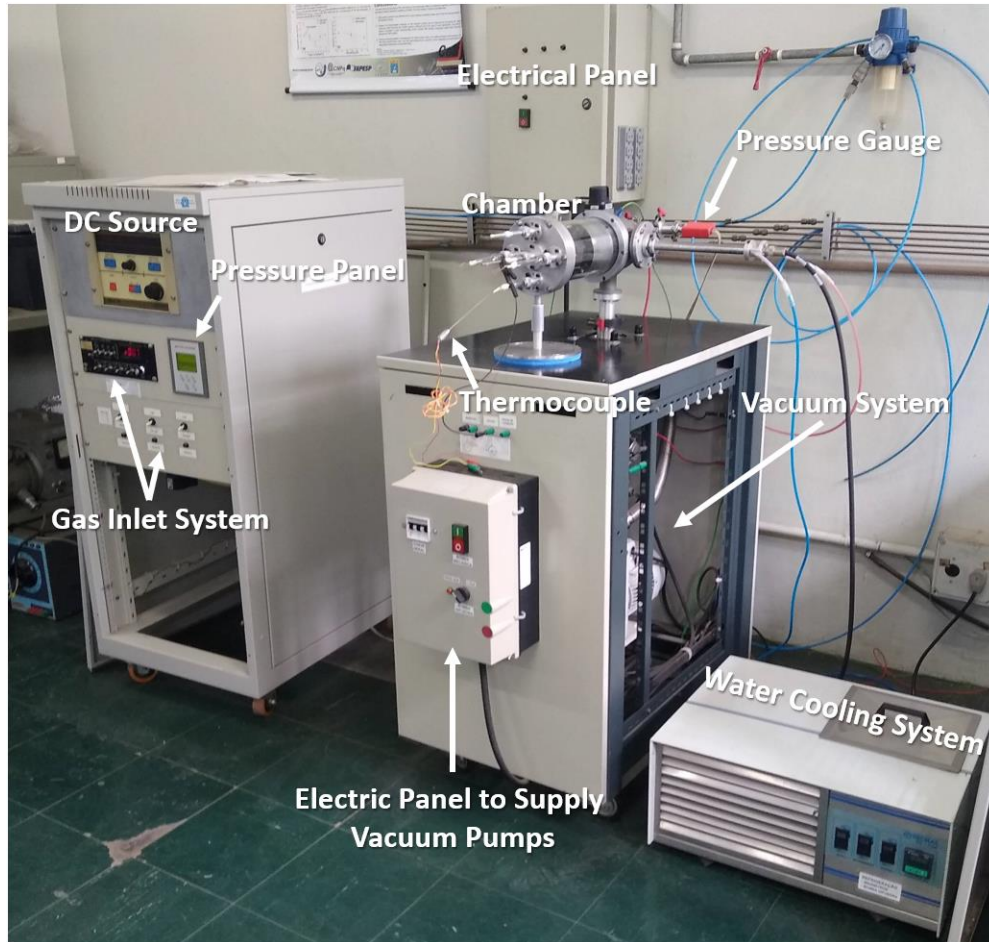
Figure 4.1. Photograph of the magnetron sputtering deposition system.
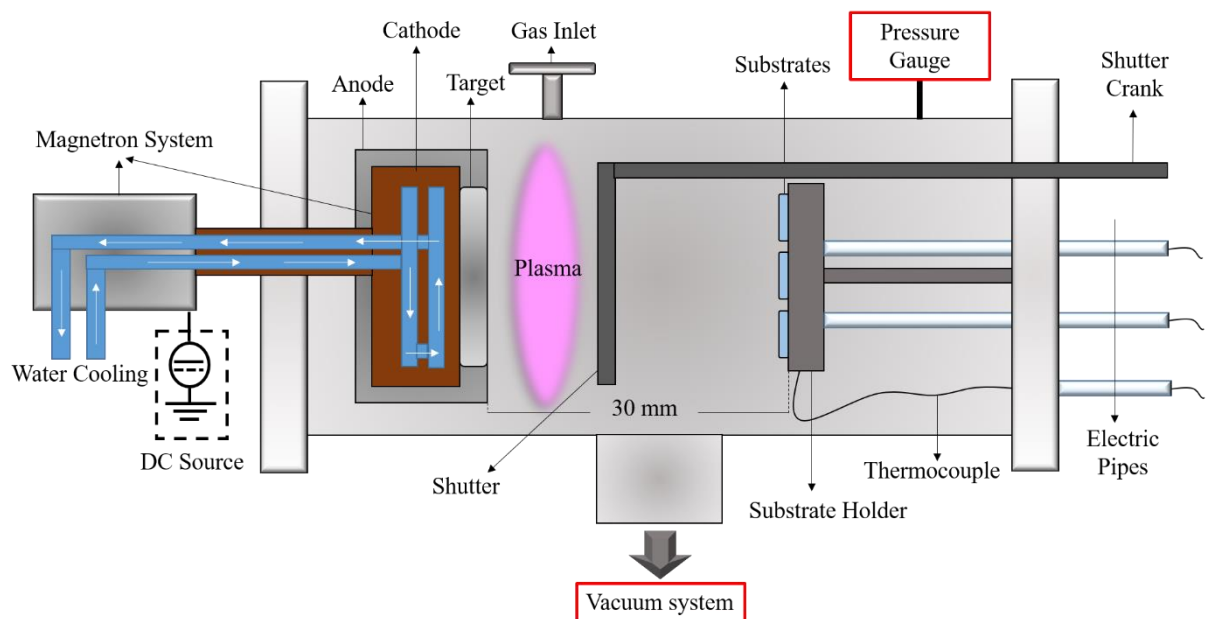
Figure 4.2. Schematic diagram of the magnetron sputtering deposition system.

The process chamber is made of Pyrex glass measuring 300 mm in length and 110 mm in diameter. The magnetron cathode used is positioned on one of the bases of the chamber. The titanium target is fixed on the cathode which is surrounded by the shield. The arrangement of permanent magnets existing in the cathode creates a preferential circular erosion zone, which can be seen in **Figure 4.3**.
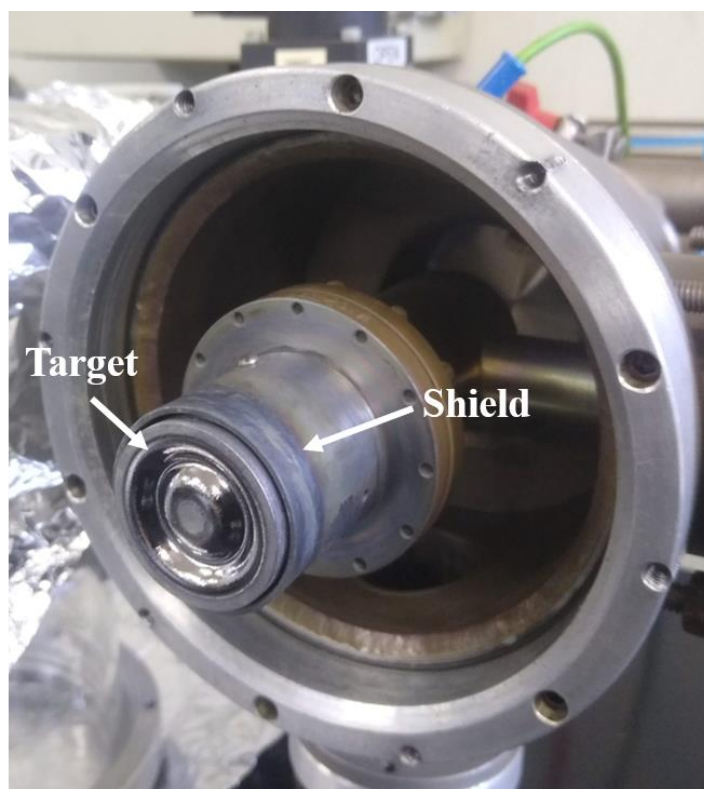
Figure 4.3. Photograph of the titanium target showing the circular erosion zone.

The vacuum system used is formed by a mechanical pump (E2M-18-Edwards) connected in series with a diffuser pump (CR 63/150 Diffstak-230 1/s-Edwards) and allows the system to reach a residual pressure in the order of 10^{-5} Torr after approximately 90 minutes. The diffuser pump is cooled with the aid of a fan and a closed water-cooling system.

The pressure inside the chamber was monitored using pressure sensors Pirani-type (p > 10^{-3} Torr) and ion gauge (p < 10^{-3} Torr), both from Edwards models APG100-XM and AIGX-S, respectively. The pressure values were monitored by a pressure panel also from the Edwards, TIC model.

The argon and oxygen gas injection system consist of a maximum flow rate controller of 50 sccm (MKS model 1159B), which is controlled by a control center with four channels, also MKS, model 247C.

The substrate's temperature was monitored through a thermocouple inserted in the side of the substrate holder, as shown in **Figure 4.4**.

The plasma is generated by a direct current (DC) source (Advanced Energy, model MDX 1K) that allows varying the output power from 0 V to 1000 V. The target used was a titanium disc, 33 mm in diameter, 3 mm thick, and 99.999% purity. The already cleaned substrates were positioned on the substrate holder at a distance of 30 mm from the target. **Figure 4.4** presents a photograph of the substrate holder used.
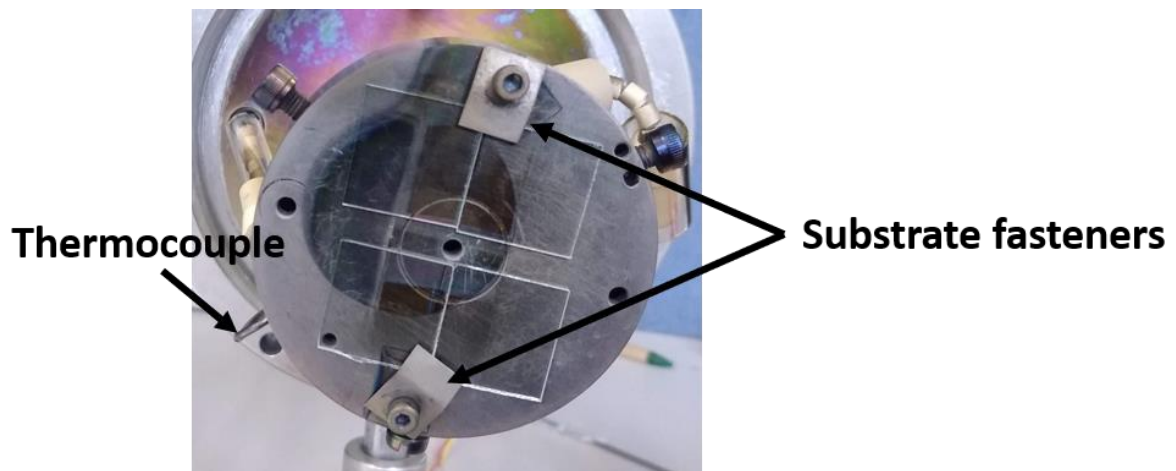
Figure 4.4. Photograph of the substrate holder highlighting details of the thermocouple and substrate fasteners.

The parameters used in this stage were based on previous studies carried out at LPP [170]. This care was important once, taking into account that it is a reactive sputtering process, a target poisoning phenomenon can occur. This happens when, in our case, the oxygen species in the plasma bind to the target, decreasing the deposition rate. **Table 4.1** shows the parameters that were used for the deposition.

Table 4.1. Deposition parameters of pristine TiO_2 films.

Parameter	Value
Ar flow (sccm)	15
O_2 flow(sccm)	3
Work Pressure (Torr)	1.0×10^{-3}
Residual Pressure (Torr)	3.0×10^{-5}
Deposition time (min)	30
DC Power (W)	150
Thin-film thickness (nm)	300 – 400

Before starting the deposition process, the target was cleaned (pre-sputtering) for 3 minutes in order to eliminate impurities from the surface due to the manipulation and exposure to the atmosphere. In this procedure, the substrate is protected by a shutter that prevents the sprayed material from the target from being deposited on it. During the deposition process of the films, the working pressure was maintained at $1,0 \times 10^{-3}$ Torr and the source power was adjusted to 150 W. The deposition time lasted 30 minutes.

The TiO$_2$ thin films were deposited at room temperature but, at the end of the process, the substrates reached a temperature of approximately 100 °C due to the kinetic energy of the particles ejected from the target. **Figure 4.5** shows the evolution of the substrate temperature as a function of the deposition time.
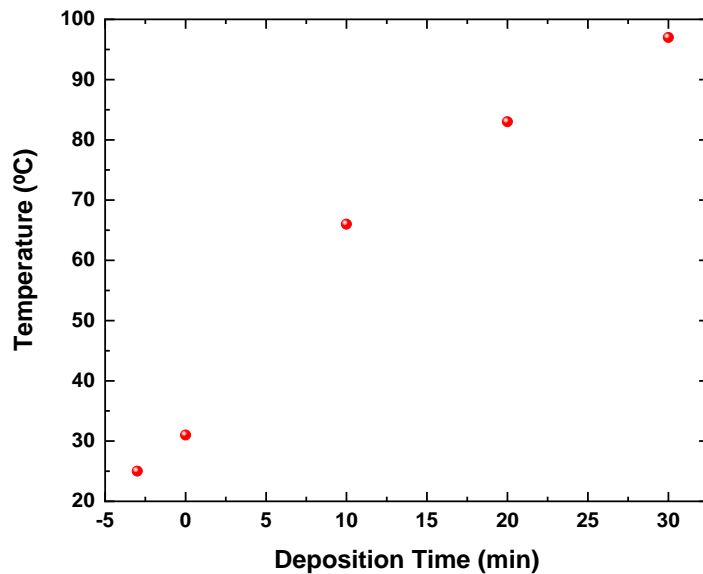
Figure 4.5. Variation of substrate temperature as a function of deposition time (T$_0$ = 25 °C). The dashed line is only a guide for the eyes.

The films were deposited on glass slides with dimensions of 20 mm × 20 mm and on ¼ of a 4-inch disk of Si wafers. After deposition, this Si was cleaved into small parts of approximately 5 mm × 5 mm. **Figure 4.6** shows the arrangement of each type of substrate placed in the substrate holder with a diameter of 40 mm.
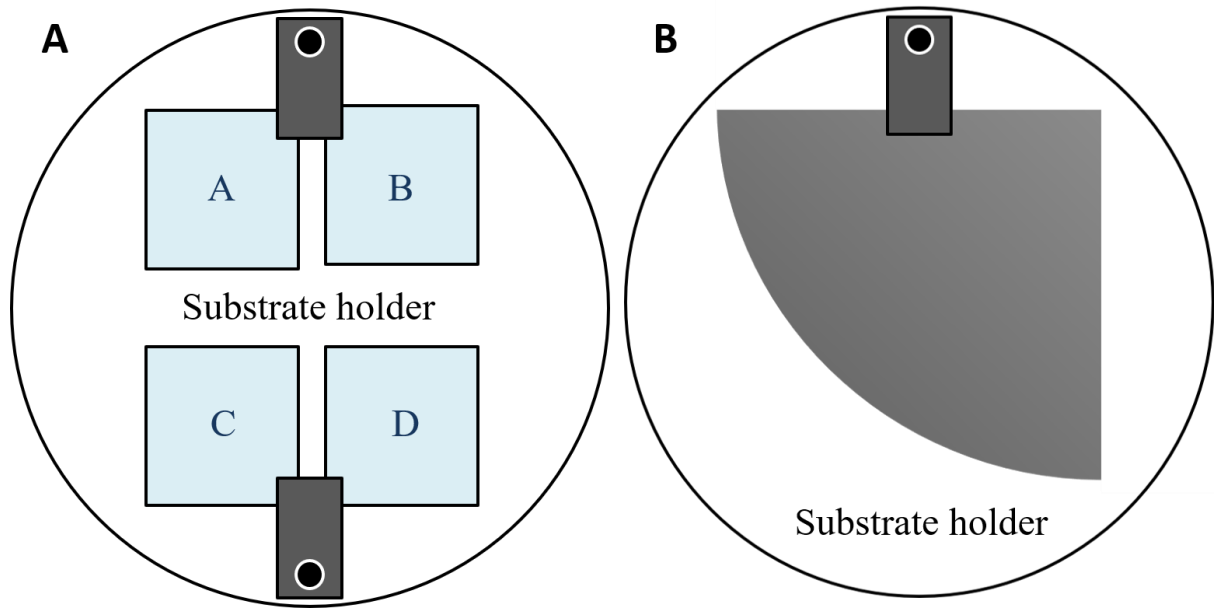
Figure 4.6. Representation of the arrangement of a) glass and b) silicon substrates on the substrate holder.

The A-D identification allowed a strict control and better criterion for comparing the analyzes of each sample concerning their position in the substrate holder because there is a small difference in the thickness values of the films produced according to their position in the substrate holder. Thus, comparisons between samples have always been made for samples deposited in the same position.

4.1.3 Heat Treatment

After the deposition process, to ensure the predominance of the anatase phase, the TiO_2 thin films were submitted to an annealing treatment at 450 °C using a tubular oven (INTI FT-1200) under atmosphere pressure for 120 min. The heating and cooling rates were 10 °C/min and -2 °C/min, respectively. **Figure 4.7** shows photos from the furnace used for the heat treatment.
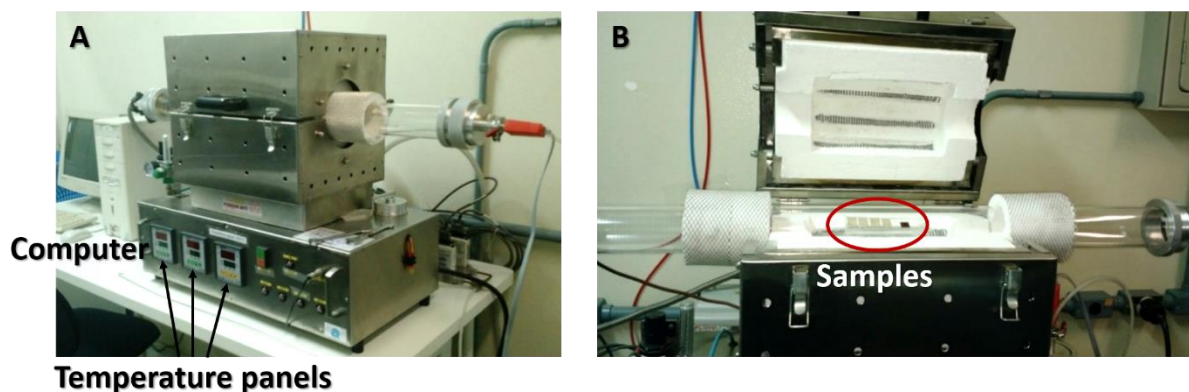
Figure 4.7. Photographs of the (a) furnace used for the heat treatment of pristine TiO$_2$ films and (b) the furnace opened showing the positioning of the samples inside it on a quartz sample-holder.

4.2   Hollow Cathode Plasma Hydrogenation System

This section presents some details concerning the experimental setup used for hydrogenating the pristine anatase TiO$_2$ thin films deposited, as described above. Also, details concerning the techniques used to characterize the H$_2$ plasma are described.

The hollow cathode hydrogen plasma was generated by a capacitive plasma system using a 13.56 MHz Kurt J. Lesker model R601 radio frequency (RF) power source. Details concerning the electrical circuit are schematized in **Figure 4.9b**. In this figure, can be seen the presence of a capacitor connected to the RF power and to the reactor electrode, through which the V$_{bias}$ can be measured. That system belongs to LPP-ITA and the photography and schematic diagram can be seen in **Figure 4.8** and **Figure 4.9**, respectively.
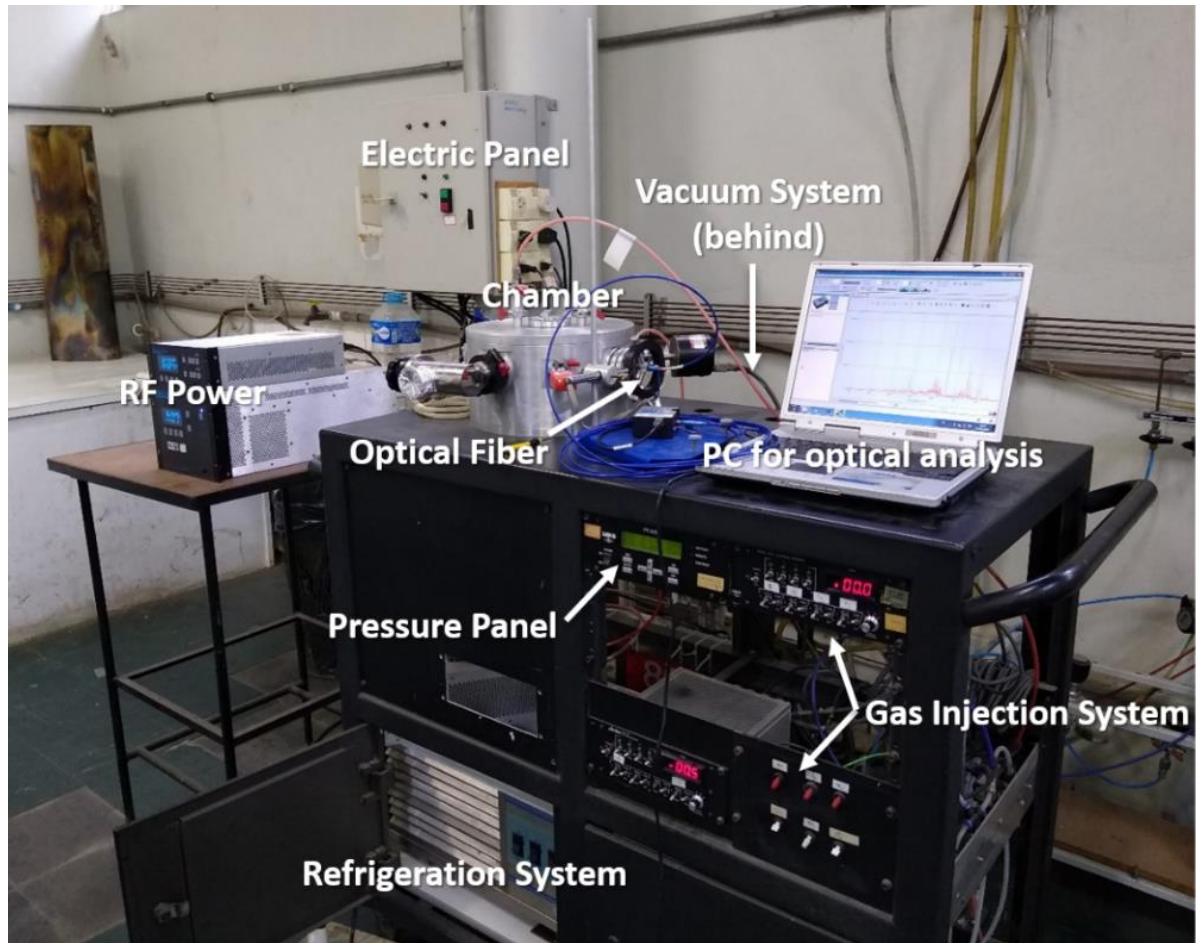
Figure 4.8. Photograph of the plasma hydrogenation system used.
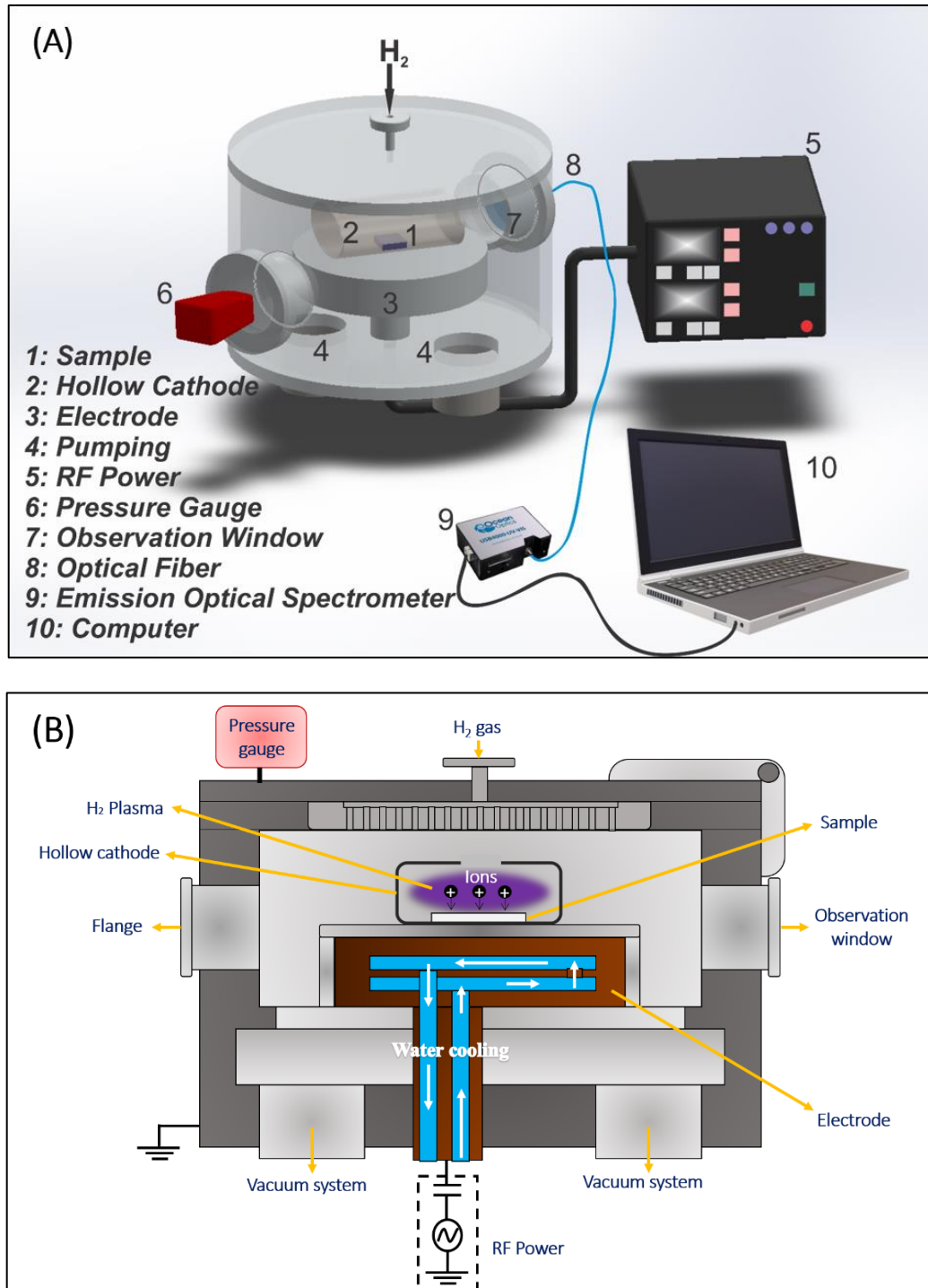
Figure 4.9. a) Schematic diagram of the setup used for the hydrogenation of TiO$_2$ thin films and the acquisition of optical emission spectra. Figure b) is a cross-section highlighting details of the electrode cooling and the electrical circuit of the system.

The lower electrode is 150 mm in diameter and made of copper with the surface in contact with the plasma covered by a 2 mm thick aluminum plate. The hollow cathode (diameter

= 30 mm, length = 120 mm) is positioned over this electrode, as shown in the photograph in **Figure 4.10.**

Figure 4.10. Photograph of the interior of the hydrogenation chamber with the hollow cathode positioned.

The TiO$_2$ samples were placed inside the hollow cathode (HC), as schematized in **Figure 4.9**. To avoid undesired contamination, the hollow cathode is entirely titanium-built (99.99%).

The electrode is cooled by an autonomous system (Tecnal, model TE184), which allows the variation of the temperature from -10 °C to 40 °C using water as a coolant (see **Figure 4.9b**). For this work, during all studies and processes, the water was maintained at a temperature of approximately 20 °C. The process chamber owns five flanges around it that can be used to connect pressure gauges, temperature sensors, plasma diagnostic tools, optical windows, etc.

The chamber was evacuated using a roots plus mechanical pump system (Edwards), reaching the residual pressure of 3.0×10^{-3} Torr. The pressure in the chamber was monitored through a Pirani-type sensor (Edwards, model APG100-XM). The pressure values were monitored by a pressure panel also from Edwards model TIC. The H$_2$ gas injection system is similar to that used in the deposition system (see **section 4.1**). It is worth noting here that tests were carried out with H$_2$ mixed with argon (Ar) in order to obtain an even more energetic plasma than with pure H$_2$. However, it was found that using this combination of gases the sputtering effect was very pronounced since the Ar atom is relatively much heavier than hydrogen. As a result, occurred pronounced flaking of the TiO$_2$ film during the hydrogenation process. This effect was not advantageous for our process as we wanted to prioritize the

chemical interactions of the reactive hydrogen species with our samples rather than sputtering, which is explained in more detail in **section 5.1**. Because of that, we use a plasma atmosphere composed of only H_2 gas.

The parameters used for hydrogenating the anatase TiO_2 thin films during different times are summarized in **Table 4.2**. The samples were named according to the duration that they were exposed to the H_2 plasma; e.g., "B-15" corresponds to the sample treated in the hydrogen plasma for 15 min. The non-hydrogenated (pristine TiO_2) film is named P-TiO_2.

Table 4.2. Parameters used for the plasma hydrogenation process.

Parameter	Value
H_2 flow (sccm)	45
Work pressure (Torr)	1.0×10^{-1}
Residual pressure (Torr)	3.0×10^{-3}
RF power (W)	200
V_{bias} (V)	380
Hydrogenation times (min)	0; 15; 30; 45 e 60

Is important to highlight that, using an optical pyrometer (Raytek, Raynger 3I), the interior of the hollow cathode wall reaches a temperature of about 256 ℃ after 8 min and maintains this temperature up to the end of the treatment.

4.2.1 Curves $P \times V_{bias}$ Acquisition

$P \times V_{bias}$ curves were obtained by applying different values of RF power. These values ranged from 0 W to 300 W (in increments of 5 W) and, for each RF power, the V_{bias} was acquired. This procedure was performed for different work pressure, ranging from 10 mTorr to 100 mTorr (in increments of 10 mTorr).

4.2.2 Optical Emission Spectroscopy (OES)

For the acquisition of optical spectra, an OCEAN OPTICS USB 4000 UV-VIS emission optical spectrometer with a resolution of 1.5 nm was used, operating in the ultraviolet and visible ranges. The radiation was captured by an optical fiber located perpendicularly to the quartz window positioned on the side (with the conventional geometry) and at the top (with the HC geometry) of the reactor. The spectrum is obtained through the OOIBase32 program.

4.3   Pristine and Black TiO$_2$ Thin Films Characterization

The thickness measurements of the films before and after the deposition and hydrogenation process were obtained using the mechanical profilometry technique. The morphological properties were analyzed by scanning electron microscopy by field emission (SEM-FEG) and atomic force (AFM). The microstructural properties were analyzed using X-ray diffraction (XRD) and Raman spectroscopy. Information regarding the chemical composition and chemical bonds were analyzed by X-ray excited photoelectron spectroscopy (XPS) and the optical properties were analyzed by spectrophotometry. Also, the wettability behavior and surface energy of the samples were evaluated by goniometry using deionized water and diiodomethane as polar and apolar liquids, respectively. Finally, the evaluation of the electrical resistance of the films was performed by measuring the sheet resistance using a four-point probe.

Table 4.3 briefly summarizes all the techniques used, with their respective equipment information (brand and model), the characteristics investigated by each technique, and the location where the measurements were performed. **Table 4.4**, on the other hand, presents the parameters/methodology used for the operation of the equipment and also presents the substrates that were used for the characterization of the samples.

Table 4.3. Description of the characterization techniques of pristine and hydrogenated TiO_2 thin films.

Technique	Equipment	Analysis Objective	Laboratory
Mechanical profilometry	KLA Tencor P-7	Thickness measurement	LPP-ITA
FEG-SEM	Mira 3 Tescan	Morphology	LABAS - INPE
AFM	Shimadzu SPM 9500	Morphology, topography e surface area	LPP-ITA
XRD	PANalytical Empyrean	Microstructural characteristics	LPP-ITA
Raman Spectroscopy	Horiba Evolution	Microstructural/vibrational characteristics	LPP-ITA
XPS	Kratos Axis Ultra	Chemical composition	LABAS - INPE
Spectrophotometry	Jasco V-570	Optical properties	IEAV
Four-point probe	JANDEL model RM3000	Electric resistance	LPP-ITA
Goniometry	Ramé-Hard model 500 – Advanced Goniometer	Wettability and surface energy	LPP-ITA

Table 4.4. Operation modes from the utilized equipment for the characterizations.

Technique	Operation mode	Substrate
Mechanical profilometry	Scan speed: 50 µm/s. Sample rate: 200 Hz. Applied force: 2 mg. Resolution:13µm/0,0078Å. Measurements were carried out through steps produced in the samples.	Silicon
FEG-SEM	Magnification: 100kx; beam intensity: 10 eV; secundar electrons mode detector.	Silicon
AFM	Intermittent contact mode.	Silicon
XRD	Cu K_α (1.5405 Å for $K_{\alpha 1}$) as an incident radiation source using 40 kV and 40 mA. The measurements were performed in the range from 20° to 80° (Bragg-Brentano) with a scan speed of 3.2°/min using step size and time per step of 0.013° and 60 s/step. The mean crystallite size was calculated using the Scherrer equation.	Glass
Raman Spectroscopy	Range: 100 – 700 cm^{-1}. Spectral resolution lower than 1 cm^{-1}. Laser: 532 nm (power < 10mV). Diffraction grade: 600 lines/mm. Acquisition time: 30 segs. Accumulation: 2.	Glass
XPS	Excitation source: Al Kα ($hv = 1486,69$ eV). Operating with 120W.	Silicon
Spectrophotometry	Range: 190 - 2500 nm in normal incidence with integration sphere of 150 mm.	Glass
Four-point probe	It was adjusted the function "auto current". Thus, the equipment set the most appropriate current value for the analyzed film.	Glass
Goniometry	Was measured the contact angles between the sample's surface and the droplets. Both contact angle and surface energy values were determined/calculated by the software DROPimage Advanced, version 2.4.	Glass

4.4 Photocatalytic Activity Evaluation

In order to evaluate the photocatalytic properties of the black TiO_2 thin films, a qualitative experiment was carried out using the films deposited on glass substrate by detecting the degradation rate of methylene blue-dye (MB) using a homemade reactor (see **Figure 4.11**)

equipped with 6 UV-visible germicide lamps with 15 W (Osram, model HNS G13 - G15T8/OF), that mainly emits radiation at 250 nm (4.95 eV).
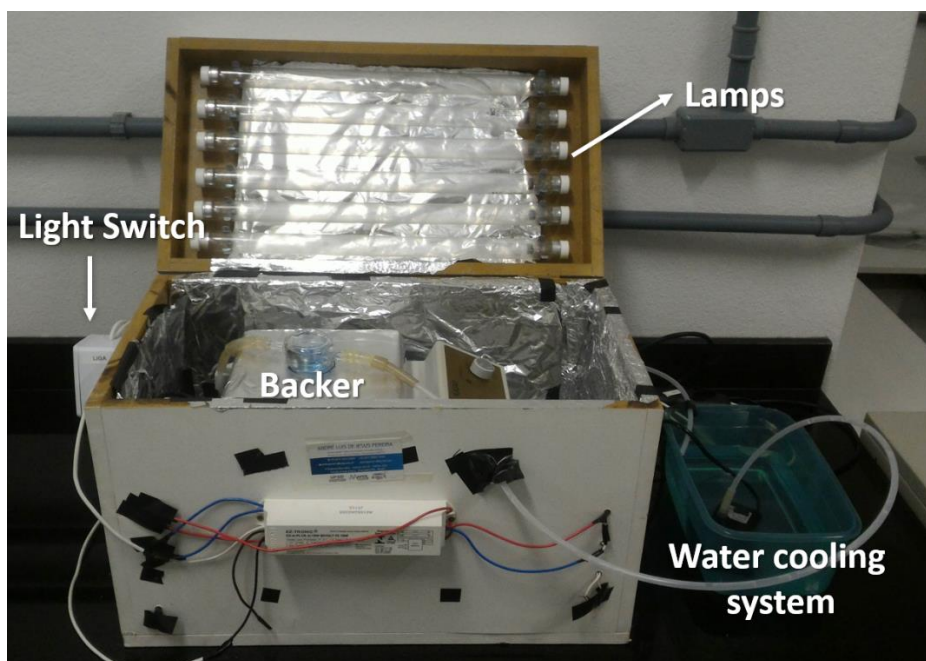
Figure 4.11. Photo of the photocatalysis homemade system used for the photocatalytic activity evaluation.

The lamps were fixed at a distance of 70 mm from the sample, which has an active area of 2×2 cm^2 (see **Figure 4.12**), delivering an irradiance of 2.2 mW.cm^{-2} at the sample position which was measured using a calibration cell (Abet Tech, model 15151), as reported elsewhere [171,172]. Is important to note that the main emission peak of the lamp (250 nm) is not detected by this reference cell who operates between ~300–1100 nm and, therefore, the irradiance can be slightly higher than the value herein reported.
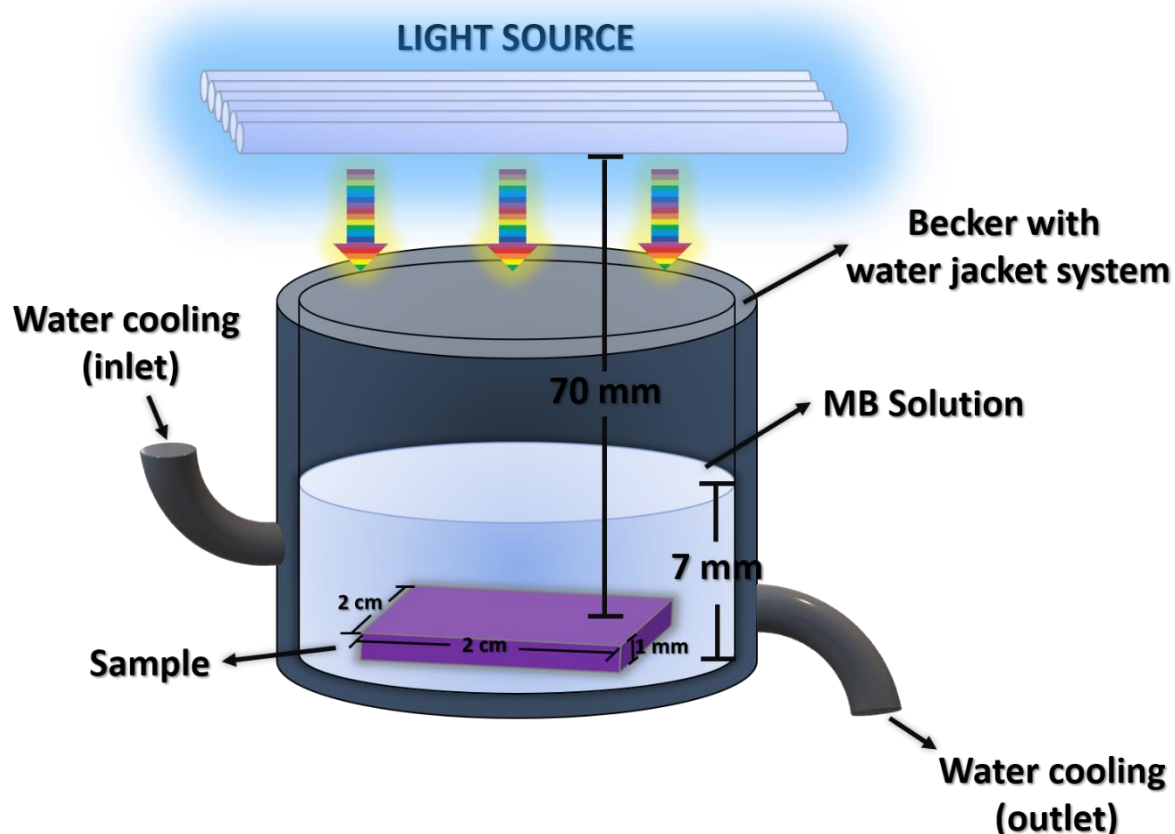
Figure 4.12. Schematic diagram of the photocatalysis homemade system used for the photocatalytic activity evaluation.

The samples were displaced in 6 mL of deionized water mixed with 10 mg/L of MB inside a backer equipped with a water jacket system, which maintained the solution at room temperature.

First, the solution was maintained for 1 h in the dark, and only after that were the lamps turned on. The MB degradation was inferred by the UV−Vis spectrophotometer (Thermo Fischer Scientific, model Evolution 220) every 10 min. The solution was stirred constantly during all the processes described above.

5 Results and Discussion

This chapter presents the results regarding the hydrogenation of the thin films of TiO_2 anatase produced through the methodology exposed in **Chapter 4**. The parameters used during hydrogenation were chosen from the plasma study carried out. Therefore, this chapter presents at the beginning the results and discussions related to the H_2 plasma characterization.

5.1 Hollow Cathode Hydrogen Plasma Characteristics

A brief description of the characteristics of the hollow cathode hydrogen plasma proposed in this thesis is presented. The discussions are focused on the source power (P) against V_{bias} curves (P × V_{bias}) for different pressure values, ranging from 10 mTorr to 100 mTorr. These curves were obtained using both a hollow cathode and conventional configurations. The purpose is to evaluate how the ion current increases/decreases with the variations of the parameters and at what moment the plasma enters the hollow cathode regime.

Furthermore, optical emission spectroscopy (OES) analyzes are also performed in order to observe which are the main chemical species present in the plasma. For this analysis, measurements were also performed with a conventional and hollow cathode geometry.

Before presenting the results related to this section, it is worth emphasizing here that hydrogen plasmas are a very relevant topic in the literature and, more than that, in the technological sector. Recent studies report the possibility of using this type of plasma both for the corrosion of silicon dioxide and other materials and for the production of hydrogen from natural gas [146,151]. Hydrogen plasma draws a lot of attention for purposes like those mainly because it is extremely reactive, due to the production of atomic hydrogen. Furthermore, the vibration of excited neutral H_2 molecules itself can contribute to the chemical composition and also energetic properties of the plasma [146].

5.1.1 $P \times V_{bias}$ Curves

The V_{bias} variation as the RF power applied to the plasma was increased (for different values of working pressure) can be observed in **Figure 5.1a** and **Figure 5.1b**, operating without and with the hollow cathode, respectively.
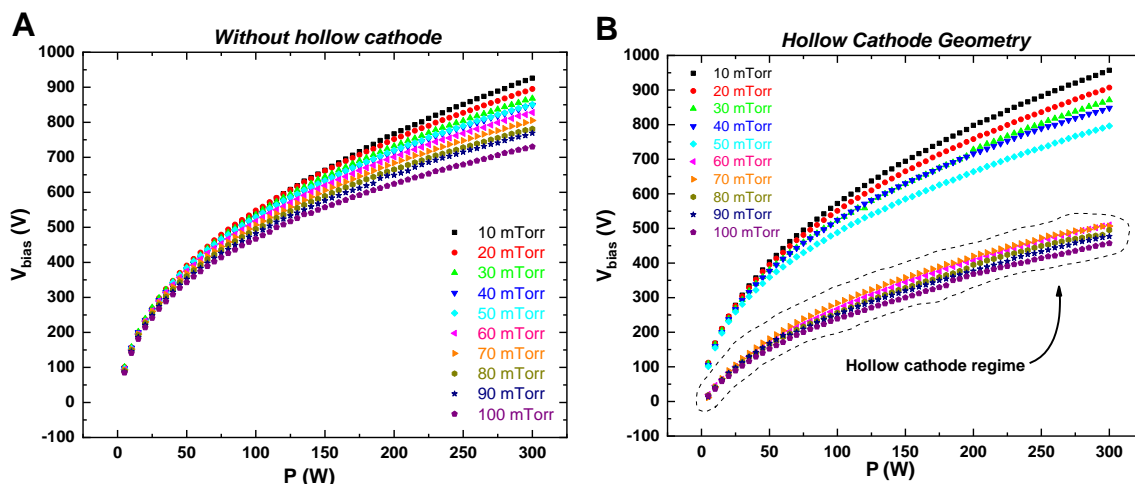
Figure 5.1. $P \times V_{bias}$ curves for different values of pressure (varying from 10 to 100 mTorr) using a) conventional geometry and b) hollow cathode geometry. All experiments were performed under H_2 atmosphere.

First, we can observe that, as the RF power applied to the plasma increases, the V_{bias} also increases. This was observed for both geometries, without and with the hollow cathode. Furthermore, for a fixed power value, there is a decrease in V_{bias} when the pressure is increased, which also occurs for both geometries. Besides, for pressures greater than 50 mTorr the V_{bias} is higher in the conventional than in the hollow cathode configuration.

Finally, it is also possible to notice that when the hollow cathode geometry was used, the system only actually entered this regime at pressures higher than 60 mTorr. We can also observe that there is an abrupt decrease in V_{bias}, which is directly related to the fact that in this regime there is a significant increase in the current of ions [143,144]. This increase is attributed to the significant increase in the plasma ionization degree, i.e., in the plasma density.

Considering what was discussed above and that this previous study of the characteristics of the hollow cathode hydrogen plasma was carried out in order to choose ideal conditions that would allow hydrogenation in mild but, at the same time, efficient conditions, the pressure of 100 mTorr and 200 W of RF power were chosen to be the parameters used for the hydrogenation. This is because, at these conditions, the system is in a hollow cathode regime, but with an intermediate V_{bias} value, if compared to the other conditions. It is known that the V_{bias} is directly related to the energy with which the plasma ions reach the walls of the cathode, in one of which the TiO_2 films will be placed. Therefore, operating the system with higher V_{bias} values, the physical interaction (etching) of the plasma with the films would be higher than the chemical interaction, which is more important for this work.

5.1.2   Optical Emission Spectroscopy (OES) Characterization

In **Figure 5.2**, the OES spectra collected using conventional and hollow cathode geometry are presented. For these analyses, an RF power of 200 W and a pressure of 100 mTorr was used. The spectrum in **Figure 5.2b** was performed with the TiO_2 film sample inside the hollow cathode.
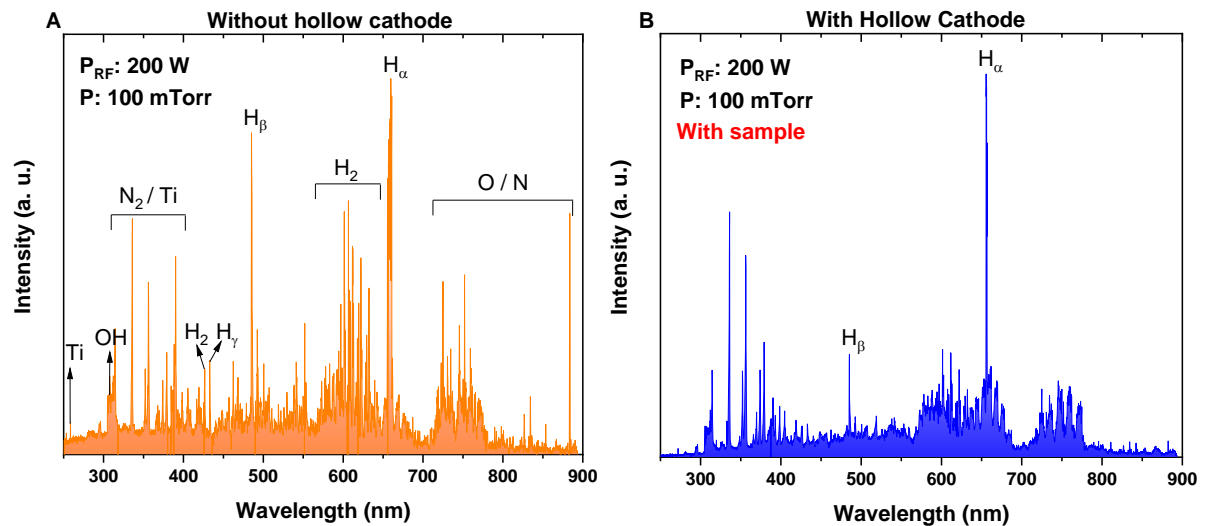
Figure 5.2. OES spectra of the hydrogen plasma generated using a) conventional and b) hollow cathode setups.

As can be observed, both configurations present similar OES peaks. The main peaks can be assigned to titanium (Ti) (258.45 nm); hydroxyl groups (OH) (306.31 nm); nitrogen (N_2) and Ti in the range of 310.16 nm - 402.2 nm; hydrogen (H_2) (426.2 nm and 564.9 nm - 646.87 nm); exited H_γ (432.4 nm), H_β (485.5 nm) and H_α (659.4 nm); oxygen (O) and nitrogen (N) (712.4 nm – 887.7 nm), which are species expected to be detected in these conditions [173–179]. Even though the spectra of the two situations are very similar, some interesting points can be discussed.

We can observe that the peaks are more intense in the spectrum without the cathode, which occurred due to the region from the chamber where the spectrum was collected. As the analysis was performed on the side flange where there is a plasma region very close to the quartz window, the peaks became more intense.

The OH species possibly come from H_2O molecules that are part of the residual contamination [180]. Besides, most of the peaks observed from 300 nm to 400 nm are related

to nitrogen species also from residual contamination of the chamber since these peaks also appeared in the spectrum without the hollow cathode (which is made of titanium). Although there is a chance of titanium atoms being ejected from the cathode walls, this possibility is very low, considering the mild conditions used. Furthermore, it is possible to infer this here quite properly, since in the XPS analyzes presented in the next section the presence of metallic Ti on the surface of the samples was not verified.

However, possibly there is a contribution of Ti species in the condition with the hollow cathode, which would come from the anatase TiO_2 sample. In order to confirm this possibility, an OES spectrum was acquired from the hollow cathode hydrogen plasma setup without the TiO_2 sample inside the cathode, as shown in **Figure 5.3**.
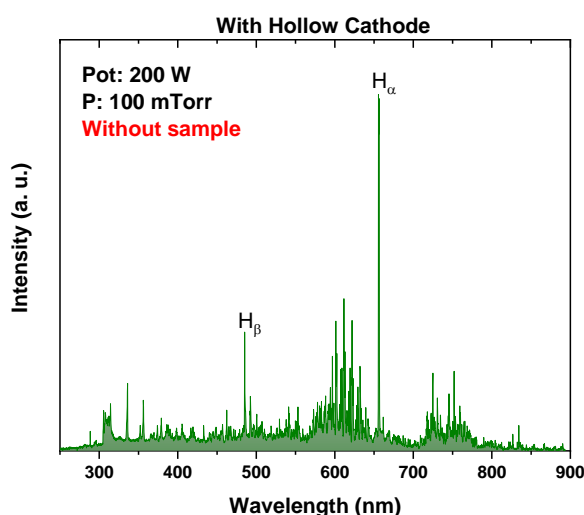
Figure 5.3. OES spectrum of the hydrogen plasma generated using hollow cathode setup without sample inside.

We can observe quite clearly that the relative peak intensities of the 300-400 nm region decrease a lot, which is a strong indication that for the condition presented in **Figure 5.2b** there are chemical species of Ti being ejected from the sample. Indeed, this is confirmed through analyzes that are best presented in the next section.

In this sense, we can highlight here the importance of using the hollow cathode effect for the synthesis of black TiO_2: the same treatment performed with the parameters presented above (100 mTorr and 200 W) for 240 min without the hollow cathode showed no significant change in the properties of the TiO_2 film when compared to the use of the same parameters using the hollow cathode configuration (see **Figure 5.4**). This observation can be a consequence

of the most intense plasma processes that occur inside a hollow cathode [158], which increase the efficiency of the incorporation of hydrogen in the films. In synthesis, this is a consequence of the high-energy electrons oscillating motion between repelling potentials of the walls in the cathode [157,158], as already explained in **Chapter 3**. This phenomenon can increases 10-100 orders of magnitude the plasma density inside the hollow cathode, that is, under these conditions we have 10 to 100 times more chemical species that can react with the sample. This explains the fact that we have obtained in **Figure 5.4** a black sample using a processing time at least 10 times shorter compared to the conventional method.
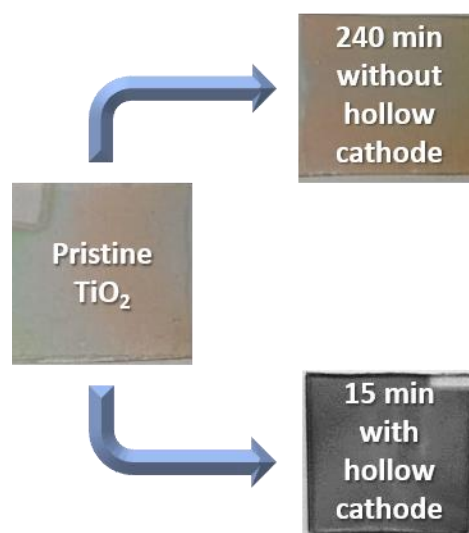
Figure 5.4. Photograph of TiO$_2$ films treated in H$_2$ plasma using the hollow cathode for 15 min and without using the hollow cathode for 240 min.

Therefore, the use of a hollow cathode geometry is necessary to reach a fast and efficient hydrogenation route. Also, it was verified that the pressure of 100 mTorr presented better operation conditions to favor the higher ion current between the parameters' values studied above. For these reasons, the hydrogenated anatase TiO$_2$ thin films presented in the next section were produced using the hollow cathode H$_2$ plasma setup described above.

5.2   Thin-film Characteristics

5.2.1   Morphological Characteristics

The morphological aspects of produced pristine and black TiO$_2$ thin films were characterized by FEG-SEM and AFM techniques. The acquired images (**Figure 5.5**) showed

that the pristine TiO_2 film presents round-shaped grains with approx. 70 nm average diameter whereas the B-15 sample presents smaller grains with approx. 40 nm average diameter. A subtle change was observed on the morphological aspects for samples with treatment time higher than 15 min, with the appearance of some valleys and the decrease of the grains size diameter.
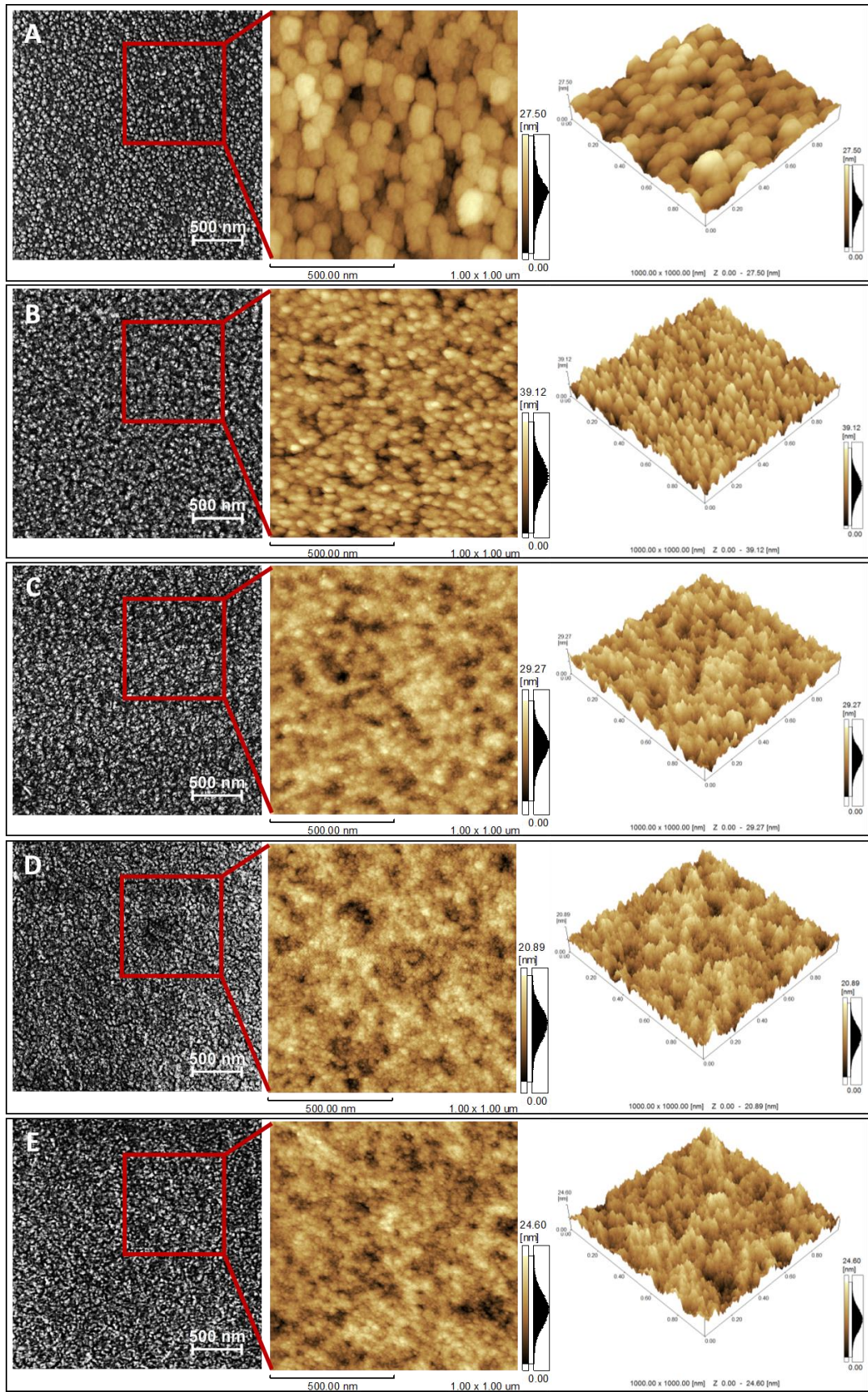
Figure 5.5. SEM-FEG, AFM 2D and 3D images of (a) pristine TiO$_2$ and the black TiO$_2$ thin films treated in the HCHP process during (b) 15, (c) 30, (d) 45, and (e) 60 min.

The measured surface area for all samples is shown in **Figure 5.6a**. Short treatment time (15 min) has produced significant changes on the TiO_2 surface, reaching the higher surface area value of ~1.3 μm^2. This effect is reduced and presents a slow decrease for longer treatment times. This is an indication that, up to 15 min, the hydrogen plasma etches the borders of the large grains presented in the pristine film leading to a rougher surface. As the treatment time increases, the etching process causes a smoothening on the film surface. Indeed, the black TiO_2 thin film thickness decreases as the HCHP treatment time increases at a rate of about -2.3 nm/min (see **Figure 5.6b**) due to the etch process.
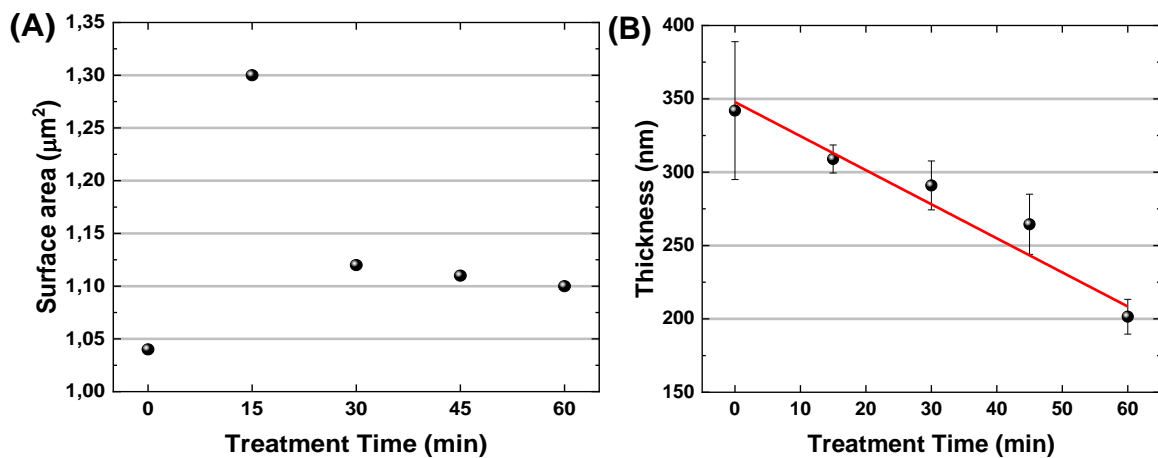
Figure 5.6. Graphs presenting the (a) surface area and (b) thickness values of the thin films as the HCHP treatment time increases. The red line corresponds to a linear fit.

The etching caused by the hydrogen plasma species has already been observed in other similar works [45,181]. The authors also observed the appearance of valleys and holes caused by the hydrogen radicals etching effect, which can be explained by the desorption of oxygen atoms that reacted with hydrogen radicals. Additionally, from the oxygen desorption, some Ti atoms can volatilize after absorbing energy provided by the activated hydrogen radicals from the plasma [45]. This is even more pronounced in this present work, mainly regarding treatment times superior to 15 min. This happens due to the use of the hollow cathode, which makes the hydrogen plasma denser than a conventional geometry, resulting in more reactive species interacting with the TiO_2 surface [182].

5.2.2   Microstructural Characteristics

The crystalline microstructure was determined by XRD analysis. Anatase TiO_2 patterns (ICOD 01-089-4921) were observed in both pristine and black TiO_2 samples, as can be observed in **Figure 5.7a**. This indicates that neither the incorporation of hydrogen on the TiO_2 microstructure or the temperature of the hydrogen plasma treatment (~260 °C) was enough to significantly change the original TiO_2 anatase tetragonal microstructure. However, slight changes could be observed in the main anatase peak (101) as the treatment time increases: (i) a shift of approx. 1° to lower angles; (ii) a decrease of its relative intensity; and (iii) an increase of the FWHM. These results can be an indicator of an increase in the structural disorder of the films, due to the treatment in hydrogen plasma. This can be attributed to a lattice disorder induced by the creation of V_o, mainly due to the chemical interaction between the reactive species (H^+ and OH^- mainly) formed in the hydrogen plasma with the TiO_2 thin film surface, which results in volatiles water molecules [42,182], and also due to the high kinetic energy that the hydrogen ions from the plasma reach the film surface [26]. Correlating to that, we can observe in **Figure 5.7b** that the average crystallite size decreases only to the sample B-60.
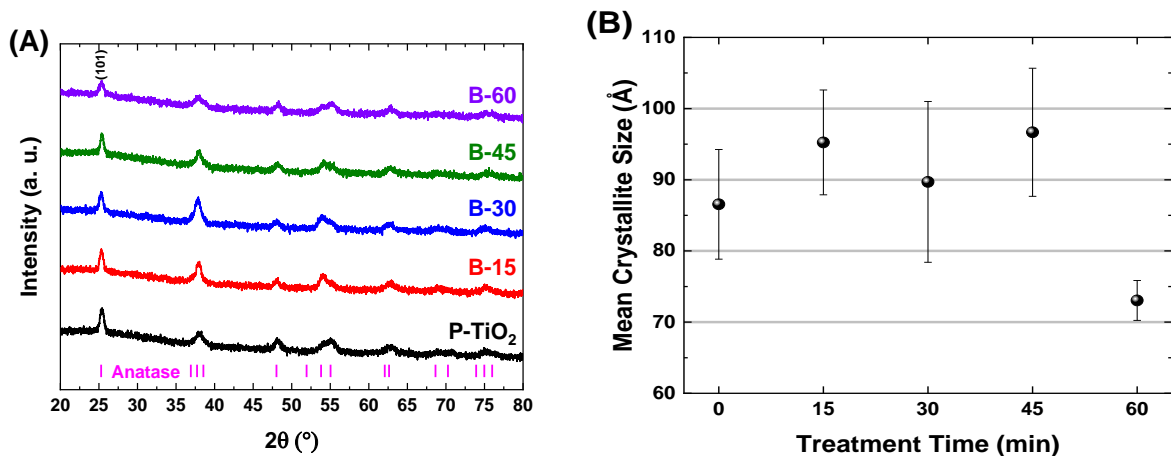
Figure 5.7. (a) TiO_2 anatase XRD patterns and (b) mean crystallite size values as the HCHP treatment time increases.

Liu et al and Panomsuwan et al. also observed a slight reduction in the average crystallite size after the hydrogenation process and attributed this reduction to the increase of V_o, and, consequently, to the lattice disorder created [121,183]. Although in the present work we observe that the crystallite size decreases only after 60 min of hydrogenation (**Figure 5.7b**), we cannot ensure that did not happen changes in the other samples, once possibly the HCHP treatment can

hydrogenate only the surface of the film [182]. Therefore, considering that the Cu-K$_\alpha$'s X-rays might penetrate ~15 µm depth in the samples, the changes that occurred on the hydrogenated layer on the surface of the black TiO_2 thin films are covered up by the higher counts detected by the diffraction of the plans referring to the pristine TiO_2 crystalline layer located below the hydrogenated layer, as outlined in **Figure 5.8**. Hence, as the B-60 possibly obtained the thicker hydrogenated layer, the average crystallite size change was sharply observed only in this sample.
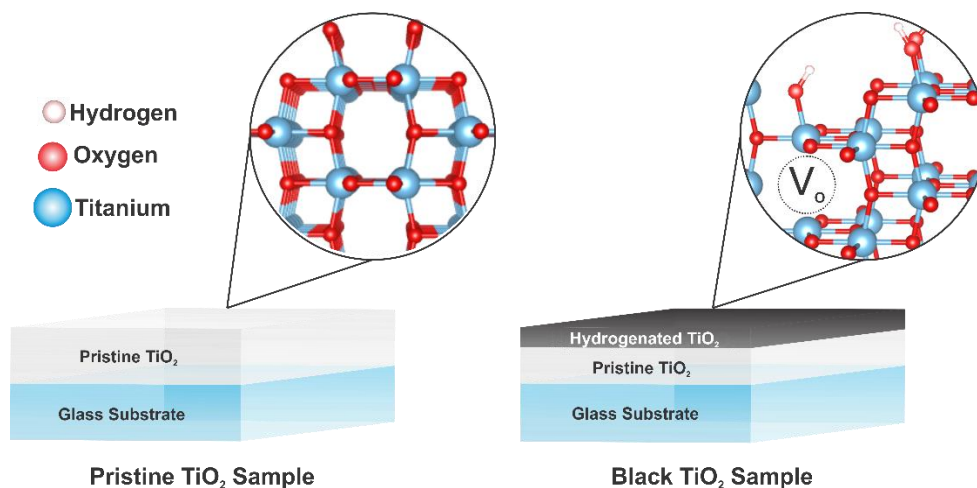
Figure 5.8. Schematic illustration of the pristine and black TiO_2 thin films highlighting its microstructures and the hydrogenated layer after HCHP treatment.

Therefore, in order to obtain more structural information of the film surface, we performed micro-Raman spectroscopy analysis. As can be observed in **Figure 5.9a**, all samples present peaks related to the anatase TiO_2 vibrational modes, confirming the XRD results, which also shown that the HCHP treatment did not modify the film structural phase. However, analyzing the position and the profile of the main E_g anatase vibrational mode (~140 cm^{-1}) is possible to observe some interesting behaviors. **Figure 5.9b** shows that this peak presents a blue-shift of 0.04 cm^{-1}/min as the hydrogen treatment time increases. Is already established that the blue-shift of Raman peaks is attributed to a lattice distortion by compressive strain, whereas a red-shit is attributed to a tensile strain [184]. Moreover, the FWHM of this peak also presented the same increase tendency, but in a ratio of ~0.1 cm^{-1}/min, as we increase the HCHP treatment time.

Both blue-shift and FWHM increase of the main E_g vibrational mode detected after TiO_2 hydrogenation was also observed in previous works and is attributed to the structural changes

that the TiO$_2$ suffers by the induced lattice defects, i.e., structural disorder promoted by the creation of V$_o$ [73,185].
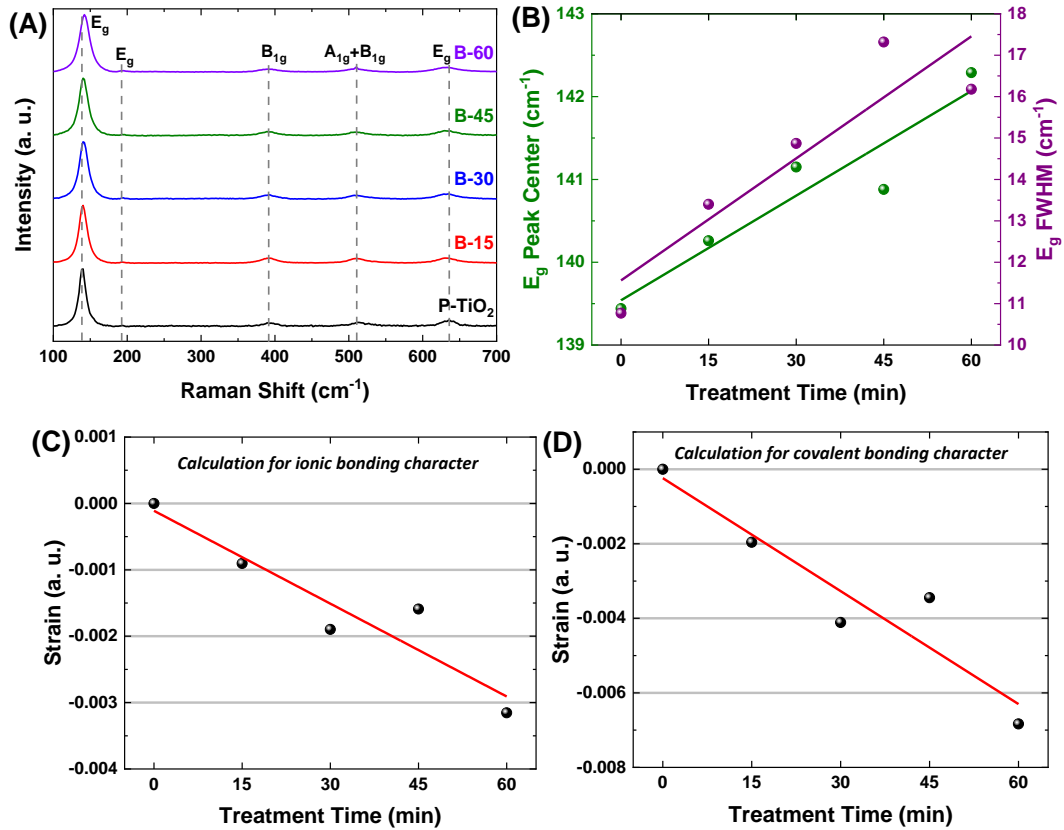
Figure 5.9. (a) Raman spectra with the main anatase vibrational modes indicated; (b) peak center and FWHM of the main E$_g$ anatase vibrational mode values; (c) strain variation for the ionic bonding character and for (d) covalent bonding character as the HCHP treatment time increases. The linear lines in graphs (b), (c) and, (d) are a linear fit.

From the blue-shift of the main E$_g$ mode, is possible to calculate the strain (ε_R) of the black TiO$_2$ films using the following equation:

$$\omega = \omega_0 \left(1 - \frac{a + r + 3}{2} \varepsilon_R \right) \tag{5.1}$$

where the constants "a" and "r" are related to the attractive and repulsive potential of each bond [184,186]. The constants a and r correspond to different values according to the bonding type

presenting in the material structure, being respectively 6 and 12 for van der Waal's bonding, 1 and 9 for ionic bonding, and 3 as a result of the sum ($a + r$) for covalent bonding [184,186]. Although the authors of the reference "[184]" have considered that the TiO_2 molecule owns 100% of the covalent bonding type, this statement is not considered in this current study, since we hardly have molecules with 100% of covalent or ionic bonding character type. In almost all molecules there is a certain amount of bonding with ionic character and the remainder with covalent character, which is precisely the case of TiO_2. Therefore, is necessary to calculate the bonding type character percentage of each of these two bonding types present in the TiO_2 molecule, which can be determined by the following expression:

$$\% \, \boldsymbol{ionic \, character} = \{\mathbf{1} - \boldsymbol{exp}[-(\mathbf{0.25})(X_A - X_B)^2]\} \times \mathbf{100} \qquad (5.2)$$

where X_A and X_B are the electronegativities of each element (A and B), being A the most electronegative element [187].

Thus, from **Eq. 5.2**, we obtain that the TiO_2 owns 64% of ionic bonding character and, consequently, 36% of covalent bonding character. Therefore, even the portion of the covalent bond being small than the ionic bond, this portion exerts a significant influence on the TiO_2 structure and cannot be ignored. Hence, the strain was calculated for both situations, which is plotted in **Figure 5.9c** and **Figure 5.9d**. Considering the pristine sample as a starting point and, therefore, with a strain value of zero, and considering that positive values are attributed to tensile strain whereas the negative ones refer to compressive strain, we can observe a compressive strain ratio increase for both figures (-4.66×10^{-5}/min of HCHP and -1.01×10^{-4}/min of HCHP for ionic and covalent bonding character, respectively) as longer is the exposure of the TiO_2 thin films to the hydrogen plasma.

This increase in the compressive strain behavior was expected, once it is a direct consequence of the increase of defects in the black TiO_2 lattice, which was also reported in previous studies [188,189]. Moreover, Naldoni et al explained that the structural defects founded in the black TiO_2 can be classified in linear 1D (i), 2D (ii), and 3D (iii) defects, being assigned to (i) dislocations caused by the plastic deformation of crystal lattice; (ii) uncoordinated atoms in the surface and also grain boundaries; and (iii) atoms vacancies in the lattice [190]. All these defect types are possible in the samples studied in this work, however, considering the hydrogenation process performed and the acquired results from the produced

samples, we consider the defects caused by the creation of V_o more determinant to the structural changes build in the black TiO_2 thin films, which will be better discussed in the next section.

5.2.3   Chemical Characteristics

Surface chemical states and compositions relating to each sample were investigated by XPS analysis. **Figure 5.10** shows the survey spectra of each sample and **Figure 5.11a** and **Figure 5.11b** show the deconvolution of the Ti $2p_{3/2}$ and O $1s$ high-resolution spectra, respectively.
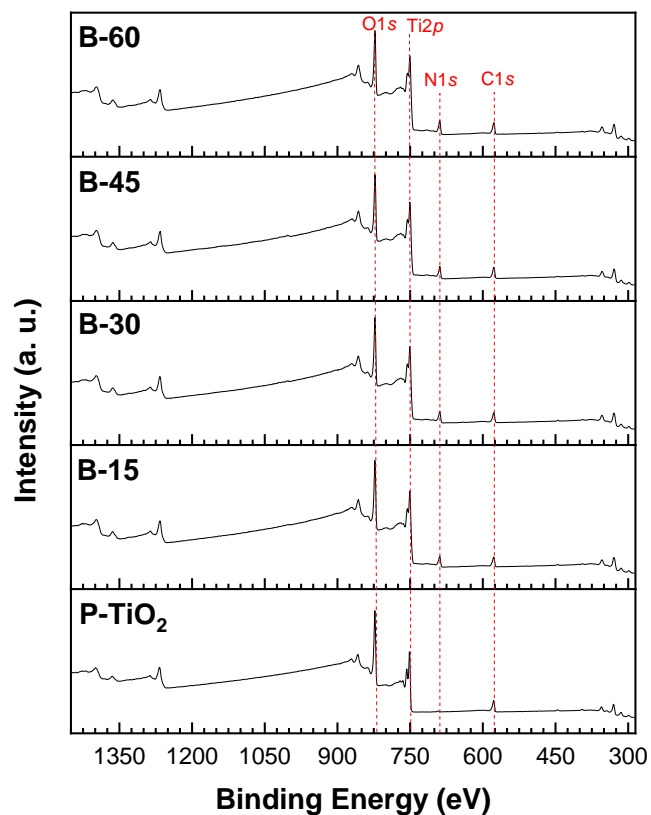
Figure 5.10. Survey spectra of each sample before and after the HCHP process during 15, 30, 45, and 60 min.

It is possible to observe that, in addition to the expected O1s, Ti2p, and C1s peaks, we also can observe peaks assigned to N1s peaks. This corroborates the results of OES (see **section 5.1.2**) through which we could observe nitrogen species in the plasma.
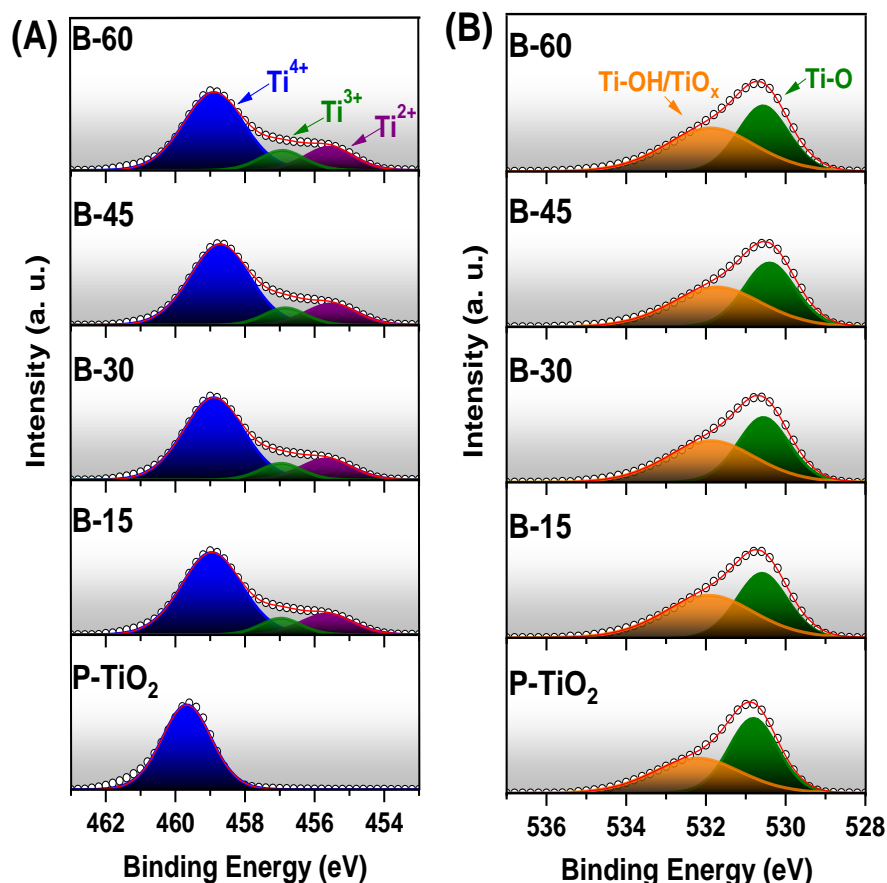
Figure 5.11. High-Resolution XPS spectra of (a) Ti $2p_{3/2}$ and (b) O $1s$ peaks of each sample before and after the HCHP process during 15, 30, 45, and 60 min. Open circles and lines represent the experimental data and the fit, respectively.

The Ti $2p_{3/2}$ curve of the pristine sample can be deconvoluted in only one peak centered at ~459.7 eV, which is related to the Ti^{4+} oxidation state [42]. The same Ti $2p_{3/2}$ peak undergoes a redshift of ~0.8 eV after the hydrogen treatment (precisely to the B-60 sample), which is related to an electron density decrease around Ti atoms, which is a strong indication that the HCHP treatment induces a Ti reduction reaction [191]. Indeed, the Ti $2p_{3/2}$ curves acquired from the black TiO_2 samples can be deconvoluted in three peaks centered at ~458.88 eV, ~456.91 eV, and ~455.54 eV, which is assigned to Ti^{4+}, Ti^{3+}, and Ti^{2+} oxidation states, respectively [42,106]. The reduction of Ti^{4+} to $Ti^{3+/2+}$ species is a consequence of the hydrogenation process through the formation of V_o [189], which were formed mainly by the removal of oxygen atoms from the TiO_2 lattice by the formation of H_2O volatiles molecules resulted from the interaction between hydrogen ions, from the plasma, with the oxygen atoms from the film [42,182]. The Ti atoms with 3+ and 2+ oxidation states, created after the hydrogenation process, were also detected in previous studies and attributed to Ti^{3+} ions in

Ti_2O_3 and Ti^{2+} ions in TiO [192]. Hereupon, two chemical reactions are possible to occur as a result of the interaction between the reactive species generated in the hydrogen plasma and the TiO_2 thin films during the HCHP treatment [182]:

$$2TiO_2 \xrightarrow[+2H]{Hydrogen\ Plasma} Ti_2O_3 + H_2O \uparrow$$

and

$$TiO_2 \xrightarrow[+H]{Hydrogen\ Plasma} TiO + H_2O \uparrow$$
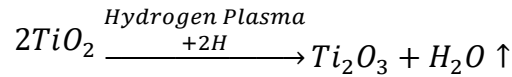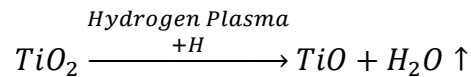
We can also observe that in the presence of hydrogen plasma, TiO_2 molecules might interact with H atoms resulting in both Ti_2O_3 and/or TiO and H_2O volatile molecules.

It is important to highlight that several authors attributed the oxidation state reduction of titanium atoms only to Ti^{3+} species, after the hydrogenation process [10]. However, previous studies reported the Ti^{4+} reduction to Ti^{2+}, besides the Ti^{3+} [42,106,183]. In general, these works reported the presence of Ti^{2+} species in the produced black TiO_2 mainly due to the direct reduction of Ti^{4+} oxidation states to Ti^{2+} induced by the efficient/assertive method used to induce structural defects in TiO_2. In our case, the presence of Ti^{2+} species can be related to the high density and energy of the hydrogen plasma generated through the use of a hollow cathode geometry, which was able to accelerate hydrogen ions with high energy (~380 eV) against the TiO_2 thin films, improving the capability to promote the direct reduction of Ti^{4+} to Ti^{2+}.

Moreover, considering the percentage area under each curve, we can note in **Figure 5.12a** a significant increase (~26.41%) of $Ti^{3+/2+}$ species after 15 min of treatment. However, above 15 min, the black TiO_2 films achieve a slight increase of $Ti^{3+/2+}$ species concentration, reaching an increase of ~30% for the sample B-60.

Concerning the O 1*s* high-resolution curve (**Figure 5.11b**), both pristine and black TiO_2 thin films can be deconvoluted into two peaks centered at around 532.1 eV and 530.8 eV, which might be assigned to hydroxyl groups bonded to Ti atoms (Ti-OH) or/and V_o (TiO_x) neighboring the Ti atoms with 3+/2+ oxidation state, and Ti-O bindings, respectively [65,121,183]. From the acquired percentage area under each deconvoluted curve, it can be observed in **Figure 5.12b** expressive concentration increase (from ~45% to ~53%) of hydroxyl groups/V_o on the sample B-15, and a slight variation around this value to superior treatment times, reaching an enhancement of 53% for the sample B-60. The acquired 45% concentration to the peak centered at 532.1 eV for the pristine TiO_2 thin film can be assigned mainly to OH

species from the atmosphere adsorbed on the film surface or even to intrinsic structural defects on the thin film [42]. At the same time, in **Figure 5.12c**, is possible to observe an opposite behavior for the Ti-O bonding concentration, reaching a significant decrease for the sample B-15 (from 54.5% to 47.0%), and a slight variation around 47% for superior times, reaching 46.7% for the B-60 sample. This means evidently that our black TiO_2 thin film surface contains less Ti bonded to oxygen atoms as the HCHP treatment time increases.

Finally, in **Figure 5.12d**, is possible to observe a linear increase behavior, at a ratio of 0.25%, of hydroxyl groups/oxygen vacancies and $Ti^{3+/2+}$ species concentration on the black TiO_2 thin film surface as a function of hydrogenation process time. These results are in agreement with the literature that has shown that the appearance of $Ti^{3+/2+}$ could be a consequence of the creation of V_o, as previously mentioned [42,189].

Therefore, the results obtained from the Ti $2p_{3/2}$ and O $1s$ deconvoluted spectra indicate that the HCHP treatment was effective to promote both V_o and $Ti^{3+/2+}$ defects, which can narrow the bandgap of TiO_2 [6], as will be discussed later.
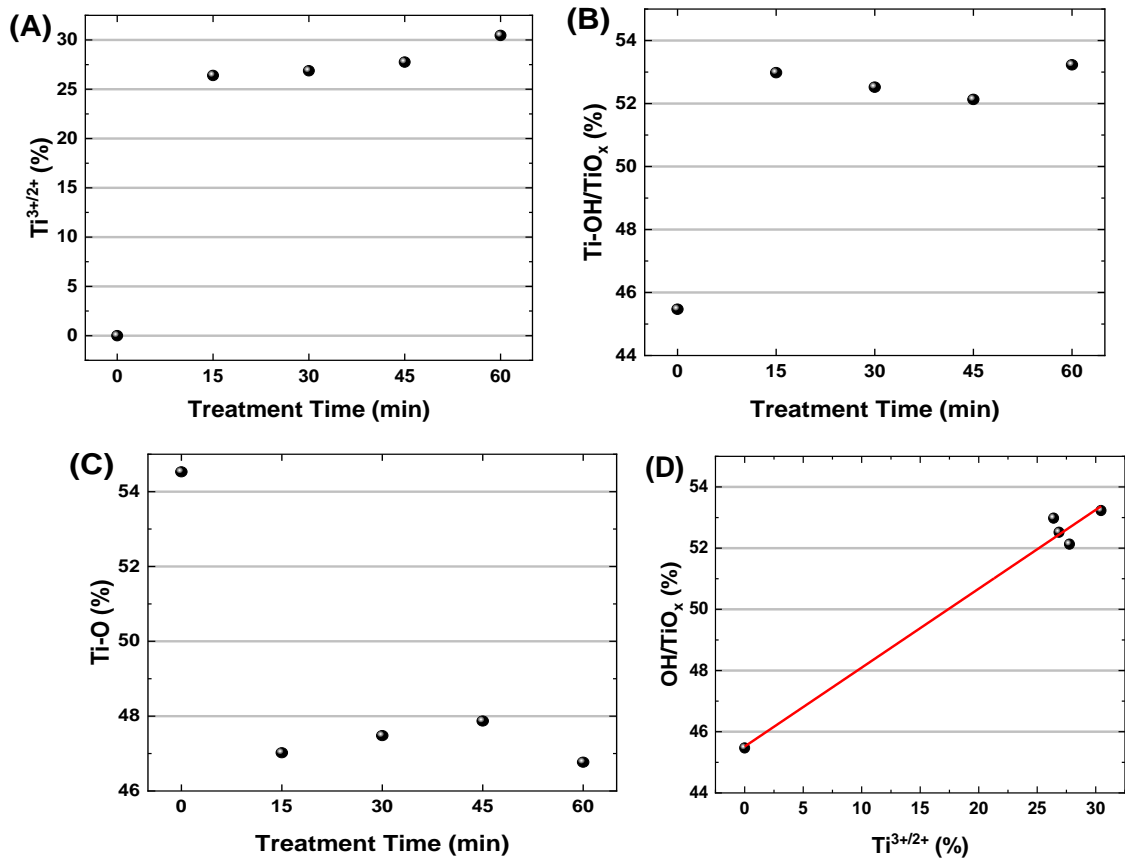
Figure 5.12. (a) Percentage of $Ti^{3+/2+}$ species, (b) Ti-OH/TiO$_x$ chemical groups, and (c) Ti-O bonds as the HCHP treatment time increase; (d) dependence relation between the percentage variation of $Ti^{3+/2+}$ species and Ti-OH/TiO$_x$ chemical groups. The red line is a linear fit.

5.2.4 Optical and Electric Characteristics

The optical characteristics of the produced black TiO₂ thin films were investigated by transmittance measurements, as shown in **Figure 5.13**. The dashed line represents the glass substrate. As expected, all the films present a well-defined band-gap energy E_g of ~3.2 eV at ~390 nm (UV), where the transmittance goes rapidly from zero to some value above 30%, depending on the HCHP treatment time. The oscillations observed above 400 nm are due to the well-known interference effect caused by the multiple reflections on the film/substrate and film/air interfaces [193,194].
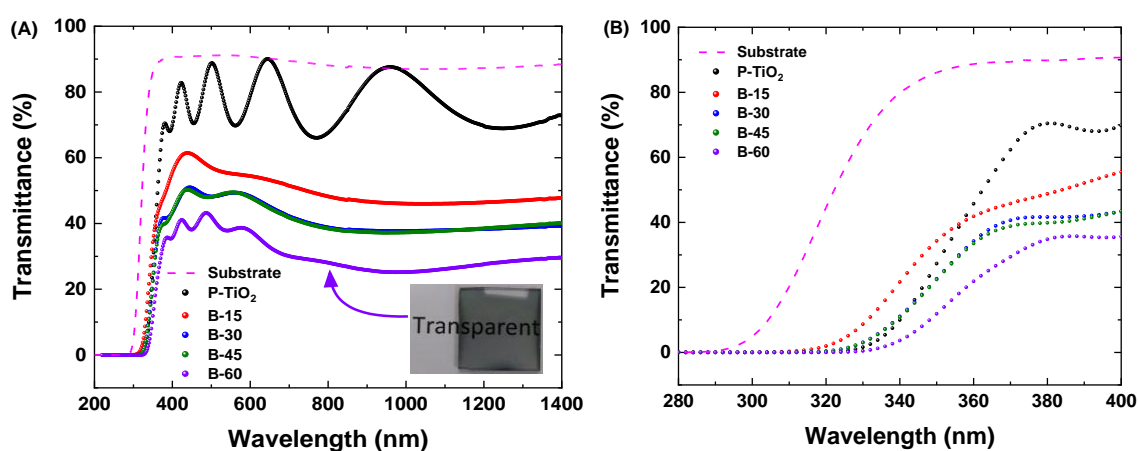
Figure 5.13. a) UV-Vis-NIR transmittance spectra of the glass substrate, pristine and black TiO₂ thin films hydrogenated by the HCHP process during 15, 30, 45, and 60 minutes. Figure b) is a zoom highlighting the transmittance decrease in the gap region.

From **Figure 5.13**, is possible to observe that the absorption in the visible and NIR regions increases proportionally to the hydrogen plasma exposition time. Additionally, is important to highlight that even for the longest treatment time (sample B-60) the black TiO₂ thin films continue translucent, as shown by the inset of **Figure 5.13**.

The optical changes verified above are a direct result of a significant increase of $Ti^{3+/2+}$ band states defect density and the increase of tail states (TS) among the valance (VB) and conduction (CB) bands for the black TiO₂ [6]. Indeed, the presence of both phenomena was confirmed by the XPS valance band spectra, as shown in **Figure 5.14**, and schematically represented in **Figure 5.15a**.
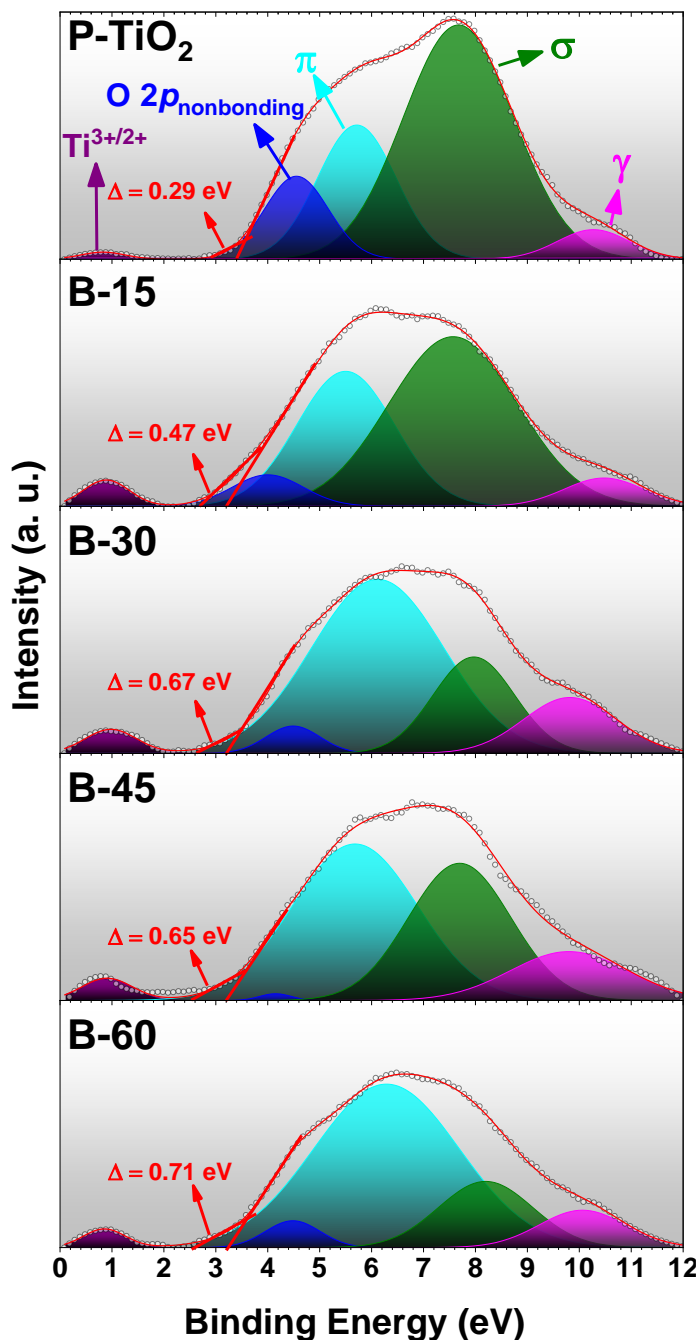
Figure 5.14. XPS valance band spectra of pristine and black TiO₂ thin films treated by the HCHP process during 15, 30, 45, and 60 min.

We can observe that all samples display TS, which are represented as Δ in **Figure 5.14**. As the HCHP treatment time increases, the TS also tends to increase, presenting a quasi-linear tendency with a ratio of 6.8×10^{-3} eV/min of HCHP, as shown in **Figure 5.15b**. From **Figure 5.14**, it is also possible to note an important increase of the $Ti^{3+/2+}$ defect band states from pristine to 15 min HCHP treated sample, confirming the results from **Figure 5.12a**. Besides,

the close values obtained for both Δ (TS of 0.67 and 0.65 eV, respectively) and $Ti^{3+/2+}$ states percentage (**Figure 5.12a**) from samples B-30 and B-45 can explain the similar light absorption performance observed by the spectrophotometry results (**Figure 5.13**).

Fan et al also reported similar changes concerning the TS in the valance band after the hydrogenation process and attributed the presence of these TS as a result of the structural disorder induced on the TiO_2 structure, mainly through the creation of V_o [43], which is therefore in line with the results presented in the above sections. Besides, we can highlight that the existence of a TS of 0.29 eV in the $P-TiO_2$ is due to intrinsic structural defects, as was previously mentioned.
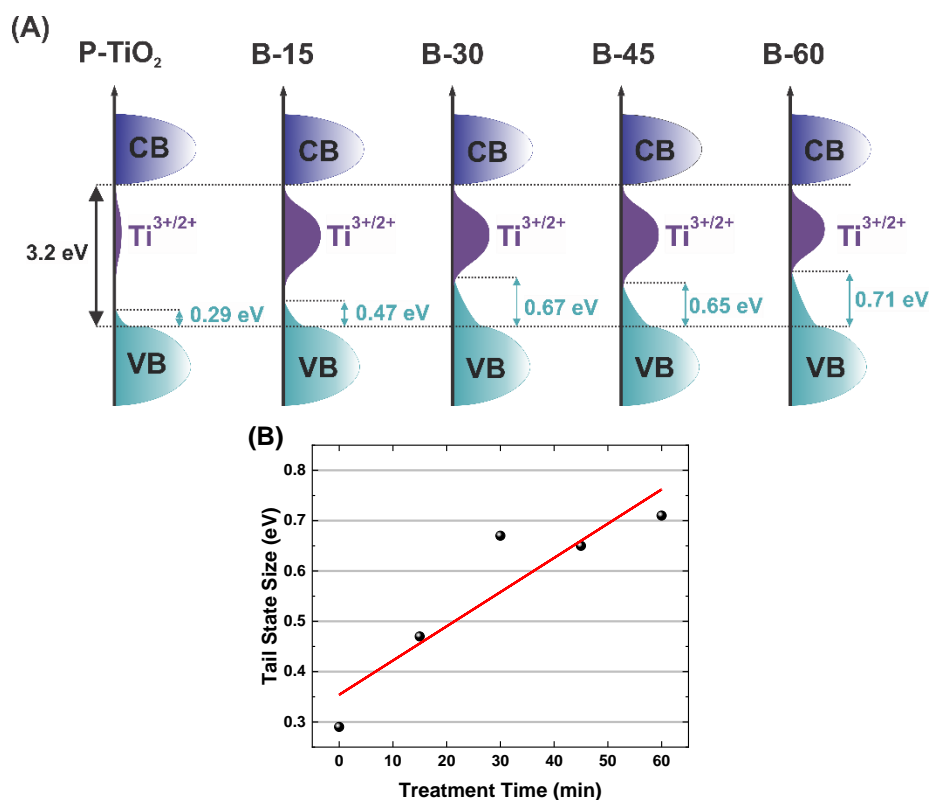
Figure 5.15. (a) Schematic of the defect $Ti^{3+/2+}$ and tail states between the valence and conduction bands; (b) tail state as the HCHP treatment time increase. The red line is a linear fit.

Furthermore, the valance band (**Figure 5.14**) can be deconvoluted into four curves centered at 10.3 eV (γ), 7.7 eV (σ), 5.7 eV (π), and 4.5 eV (for the pristine sample), which are assigned to OH groups, σ-type molecular orbital, π-type molecular orbital, , and nonbonding O $2p$ orbitals, respectively [42]. Besides, another curve centered in 0.8 eV (for the pristine TiO_2) can also be fitted in the acquired spectra and is related to the $Ti^{3+/2+}$ $3d$ states. These in-gap

states, as well as the TS, are responsible to narrow the bandgap and consequently increase the light absorption [195], which is consistent with the spectrophotometry results.

From the areas of the deconvoluted fitted curves, we can analyze quantitatively the progress composition concerning each species and orbitals as we increase the hydrogenation treatment time. The percentage area of the γ curve increases at a ratio of 0.11 %/min, indicating an increase of the OH groups' concentration on black TiO_2 thin film as the HCHP process increase. At the same time, while the concentration of π-type molecular orbitals increases, the σ-type molecular orbitals decrease at the same ratio (~0.7 %/min of HCHP). We can observe, in **Figure 5.14**, that the increase of the π-type molecular orbitals curve contribution was the main factor that results in the TS size increase. Moreover, the nonbonding O $2p$ orbitals concentration presents a decreasing behavior at a ratio of -0.14 %/min as the exposition of the TiO_2 thin films to the hydrogen plasma increases, which is consistent with the XPS results presented previously. These nonbonding O $2p$ orbitals are related to the removal of oxygen atoms from the TiO_2 structure [42].

Furthermore, the modifications inside the bandgap of the produced black TiO_2 thin films influenced the changes in electric properties. **Figure 5.16** shows a meaningful sheet resistance decrease of 99.98% after 15 min of hydrogenation, and for longer times the sheet resistance of the samples continues to decrease but with a slightly lower rate of -20 $\Omega/\square.min^{-1}$. This conductivity improvement can be a consequence of the increase of Ti suboxides ($Ti^{3+/2+}$) in the black TiO_2 thin films, once these species are responsible to increase the excess of electrons on the electronic states neighboring the Fermi edge [42,44].
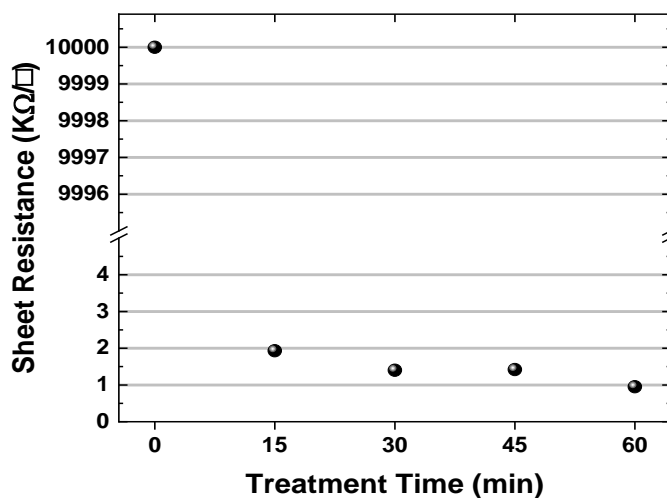
Figure 5.16. Sheet resistance as the HCHP treatment time increases. The deviation bars are covered by the ball symbols.

5.2.5   Wettability and Surface Energy Characteristics

The contact angles measured for all samples (using water) are presented in **Figure 5.17**. All samples presented a hydrophilic behavior with contact angle values smaller than 90°. The contact angle values decreased from 49° (pristine TiO_2) to 33° for short exposition to the HCHP treatment (15 min) and start to increase with the increase of treatment time, achieving 69° for the sample B-60. This is an indication that the exposure to the HCHP treatment for times longer than 15 min decreases the film surface energy turning the surface more hydrophobic.
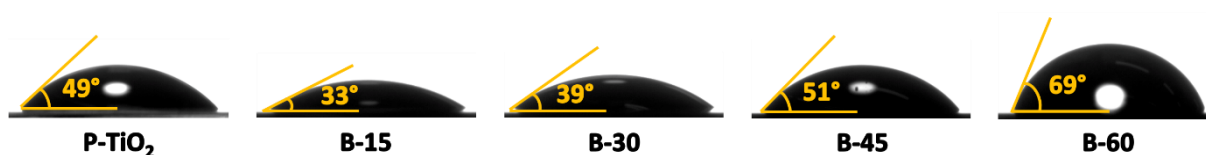
Figure 5.17. Photos of the water droplets showing the contact angles formed with the thin film surface of each sample.

As presented in **Figure 5.18**, the surface energy of the treated samples follows the same tendency of the water contact angles. Is already known that wettability, and consequently the surface energy, depends on the chemical surface composition, as well as the morphological pattern of the film surface [106,196].
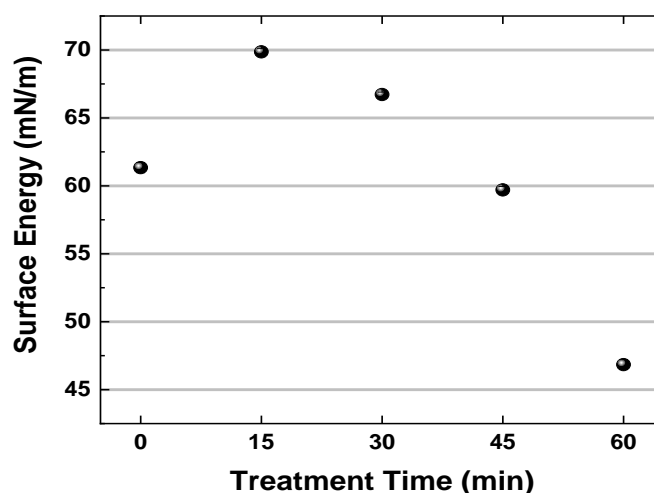
Figure 5.18. Surface energy values as the HCHP treatment time increases. The deviation bars are covered by the ball symbols.

Then, the acquired results can be attributed to the morphological pattern change achieved to the sample B-15 and the significative enhancement of OH species concentration on its surface, as presented previously. Han et al. obtained similar results and attributed the hydrophilicity enhance to the presence of OH radicals that can form hydrogen bindings with water molecules [106]. However, for HCHP treatment times longer than 15 min, we believe that the morphological changes were the preponderant factor for decreasing the surface energy, once we acquired approx. similar content of OH groups to the samples B-15, B-30, B-45, and B-60, but different morphological patterns and surface area decrease after 15 min of hydrogenation. Then, we propose that the changes observed in B-15 (the emergence of more pronounce valleys among the minor grains, as well described in **section 5.2.1**), were the main factor for the decreasing tendency of the hydrophilic behavior, i.e, for the decrease of the surface energy after 15 min of HCHP treatment.

5.3   Photocatalytic Activity Evaluation

The photocatalytic activity (PA) of pristine and hydrogenated TiO_2 at different times are compared from the photodegradation rate of MB under UV-Vis irradiation, as presented in **Figure 5.19a**. The PA was evaluated by measuring the MB optical absorption using a UV-Vis spectrophotometer. Prior to exposing the samples to the UV-visible light source, they were kept in the MB solution for 1 h to reach the adsorption/desorption stability. Then, the first absorbance measurement (C_0) was performed. Finally, the light source was turned on and measurements were taken every 10 min.

As is readily observed, MB pure solution did not exhibit any significant photocatalytic activity under light exposure. In contrast, the photocatalytic activity of the films under the test conditions was substantially increased because of hydrogenation treatment in comparison to pristine one, as can be seen, by the concentration ratio (C_0/C) of MB plotted against light irradiation time in the presence of the photocatalysts.

Figure 5.19a shows that B-15 and B-30 samples presented higher photodegradation rates, where around 60% of MB dye was decomposed, while B-45 and B-60 presented photodegradation performance at around 45%. Even so, all-black TiO$_2$ samples showed better photocatalytic performance than pristine TiO$_2$ film, which after 90 min of reaction, decomposed only ~25% of MB. This enhancement in the photocatalytic activities of the black TiO$_2$ films may be due to the concentration of Ti$^{3+/2+}$ interstitials, V$_o$, and hydroxyl radicals (OH) onto the film surface [98,197], which is in accordance with the XPS results. Although Ti$^{3+/2+}$ and V$_o$ species present an important role in improving the PA, the formed OH groups are the principal oxidative species in photocatalysis reactions, once they have a great performance on the photodecomposition of organic molecules [198,199]. Besides, the increase of the film's surface areas may also improve the PA, once it is a determining factor in increasing dye degradation, which can be seen by AFM results [168].
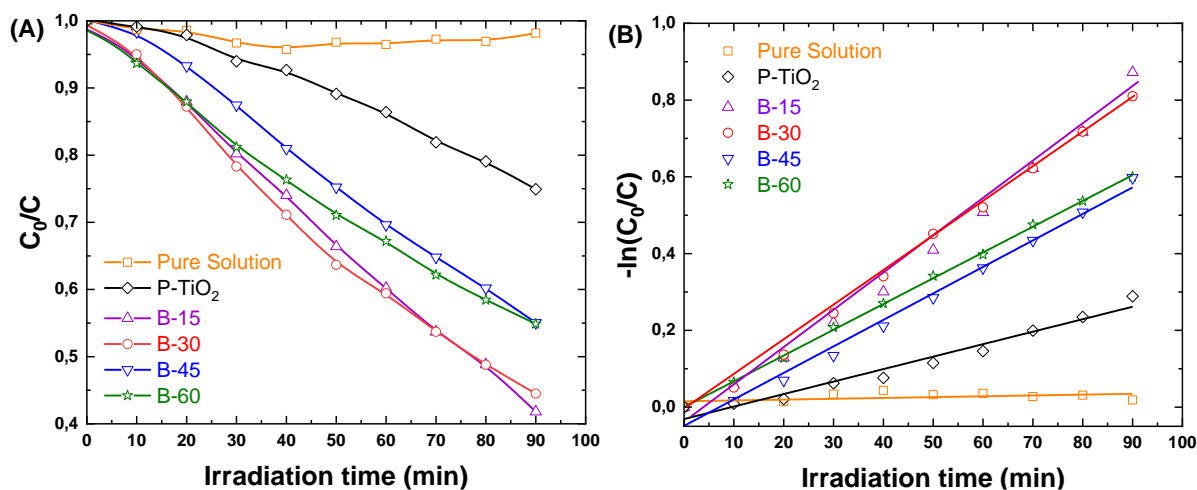
Figure 5.19. a) MB photodegradation comparison over pristine TiO$_2$ and black TiO$_2$ hydrogenated by different conditions under UV light; b) -ln(C$_o$/C) vs. time plot for photocatalytic degradation of MB system under UV light.

The photodegradation reaction rates of pristine TiO$_2$, pure solution, and all-black TiO$_2$ films are compared with each other by the kinetic plot, as shown in **Figure 5.19b**. A linear behavior can be observed for all samples. This behavior allowed us to use the equation below:

$$-\ln\frac{C_0}{C} = kt, \qquad (5.3)$$

where C is the concentration after a determined period of UV-visible light irradiation, t represents the irradiation time, and k is the apparent rate constant (min^{-1}) [200,201]. The constant k is known to be independent of the dye concentration or temperature, whereas photodegradation is a function that depends only on the irradiation flux and light source spectrum [201,202]. The k values from each sample are presented in **Table 5.1**.

Table 5.1. Apparent rate constant k of each sample.

Sample	k ($\times 10^{-3}$ min^{-1})
P-TiO$_2$	2.5
B-15	9.6
B-30	7.1
B-45	5.1
B-60	6.7

Is possible to observe that the photoactivity of black TiO$_2$ varies depending on the hydrogenation time and the PA did not increase as the time extended. Compared with the PA of pristine TiO$_2$ ($k = 2.5 \times 10^{-3}$ min^{-1}), black TiO$_2$ films had their photoactivity increased at a minimum by a factor of 2 after the hydrogen treatment. **Figure 5.19b** shows that black TiO$_2$ hydrogenated for 45, 60, 30, and 15 min presented significant improvement in their photoactivity, in this order. The k values were 5.1×10^{-3} min^{-1}, 6.7×10^{-3} min^{-1}, 7.1×10^{-3} min^{-1}, and 9.6×10^{-3} min^{-1}, respectively. Long periods of hydrogenation may generate a high concentration of V$_o$ located at the TiO$_2$ bulk, inducing charge annihilation centers, and may also increase the electron-hole recombination rate [203–205]. These factors combined with the reduction of the thin film surface suggest some reasons for the efficiency of photocatalytic degradation have been impaired [206]. This can cause an improvement in the visible light absorption combined with a negative effect in the photocatalytic activity of black TiO$_2$ nanomaterials which may be the reason for the B-15 and B-30 samples have been shown better results than the others.

6 Conclusion and Recommendations for Future Works

6.1   Conclusion

Black TiO_2 thin films hydrogenated during different times by an RF-CVD system using a hollow cathode geometry were successfully produced by the methodology proposed in **Chapter 4**. The results show that the HCHP hydrogenation treatment used was effective to create $Ti^{3+/2+}$ species and oxygen vacancies on the TiO_2 structure. These achievements were determinant to the light absorption increase and conductivity improvement, reaching ~30% and ~99.98% of improvement, respectively, after 60 min of treatment. The results indicate that these optical and electrical improvements occur mainly due to in-gap states created by the presence of $Ti^{3+/2+}$ species and V_o in the black TiO_2 thin film structure, with such species showing a quasi-linear increase ratio behavior with the hydrogenation treatment time.

The investigation of morphological properties evidenced that the surface area increases by 24% after 15 min of HCHP, but starts to decrease for longer treatment times, in addition to obtaining different morphological patterns with the increase of hydrogenation process time. This non-linear behavior was also observed in the wettability and surface energy results, indicating that the morphological aspects were the main characteristic response to the best hydrophilicity of the sample hydrogenated for 15 min, and the decrease of this characteristic for longer times. Moreover, it was found that even the longest treatment time (60 min), which created more structural disorder in the TiO_2 thin film, was not enough to alter the TiO_2 phase, which was confirmed as anatase in all samples by the acquired diffractograms.

In general, considering our sample set, the results showed that the modifications produced by the HCHP treatment are more pronounced after just 15 min, although the changes continue to occur at longer times, but at a slight rate. Therefore, the present study brought insights into the role of the hydrogenation time using the HCHP treatment route on the anatase TiO_2 thin films. Besides, it was possible to show that the produced black TiO_2 thin films own the potential to be tested in photovoltaic and photocatalytic applications.

Furthermore, this study allows a consistent comprehension concerning the characteristics of the hollow cathode hydrogen plasma generated for the hydrogenation of the anatase TiO_2 thin films. At this point, it was found that the hollow cathode geometry allowed much faster hydrogenation compared with a conventional geometry and, at the same time, without harming the bulk structure of the film.

In this sense, this doctoral thesis, based on the studies carried out, might pave the way for further studies concerning the use of plasma processes to produce black TiO_2-based materials suitable for photocatalytic and photovoltaic applications. Hence, as a means of disseminating the results obtained here, some scientific work was published, which is presented in **Chapter 8**.

Even having achieved the objectives proposed in **Chapter 1**, there are still important points to be explored regarding the theme of this thesis. These points are highlighted in the next section.

6.2   Recommendations for Future Works

Considering that the use of the methodology proposed in this thesis for the production of black TiO_2-based materials has not yet been reported in the literature, except for our works, there are still many points to be explored. These points can be divided into four study sections: (i) hollow cathode hydrogen plasma (HCHP) study; (ii) production of black TiO_2-based materials by HCHP; application of these materials in (iii) photocatalysis and (iv) solar cells. In this way, the main points to be developed within each of these study sections are point out below:

(i) Perform a characterization/quantitative study of the plasma properties through theoretical calculations and simulations, through which it would be possible to determine physical and chemical characteristics of the plasma in a more complete and in-depth way. This could be done by combining the analyzes already performed (see **Chapter 5**) in combination with Langmuir probe analyzes and simulations using the Global Model as a theoretical model.

(ii) In order to better understand the properties of the black TiO_2 produced, some more characterizations can be performed. Three are considered very important: Rutherford backscattering spectrometry (RBS), high-resolution transmission electron microscopy (HRTEM), and photoluminescence spectroscopy. The first one could favor the investigation with more precision of the hydrogenated layer (thickness, composition, etc); the second one will allow a better understanding of black TiO_2 microstructure; the third will enable to measure the electron-hole pairs recombination rate. In addition, it would be important to perform the XPS analysis for the N1s peak at high resolution to see how the nitrogen species are affecting the structure of black TiO_2.

(iii) For a more complete analysis, it would be interesting to evaluate the photocatalytic performance of the black TiO_2 thin films produced in the degradation of other types of dyes and even drugs. Furthermore, it would also be interesting to carry out this evaluation under different sources of light irradiation, e. g., solar simulator, and also in isolated ranges, only UV and then only visible.

(iv) Finally, it would be interesting developing a study focused on the application of these black TiO_2 thin films as an absorber layer in a heterojunction solar cell.

7 References

[1]   M. Grätzel, Dye-sensitized solid-state heterojunction solar cells, MRS Bull. 30 (2005) 23–27. doi:10.1557/mrs2005.4.

[2]   J. Liqiang, Q. Yichun, W. Baiqi, L. Shudan, J. Baojiang, Y. Libin, F. Wei, F. Honggang, S. Jiazhong, Review of photoluminescence performance of nano-sized semiconductor materials and its relationships with photocatalytic activity, Sol. Energy Mater. Sol. Cells. (2006). doi:10.1016/j.solmat.2005.11.007.

[3]   Y. Wang, H. Suzuki, J. Xie, O. Tomita, D.J. Martin, M. Higashi, D. Kong, R. Abe, J. Tang, Mimicking Natural Photosynthesis: Solar to Renewable H_2 Fuel Synthesis by Z-Scheme Water Splitting Systems, Chem. Rev. 118 (2018) 5201–5241. doi:10.1021/acs.chemrev.7b00286.

[4]   R.S. Pessoa, M.A. Fraga, L.V. Santos, M. Massi, H.S. Maciel, Nanostructured thin films based on TiO_2 and/or SiC for use in photoelectrochemical cells: A review of the material characteristics, synthesis and recent applications, Mater. Sci. Semicond. Process. 29 (2015) 56–68. doi:10.1016/j.mssp.2014.05.053.

[5]   X. Zhang, J. Xiao, C. Peng, Y. Xiang, H. Chen, Enhanced photocatalytic hydrogen production over conjugated polymer/black TiO_2 hybrid: The impact of constructing active defect states, Appl. Surf. Sci. 465 (2019) 288–296. doi:10.1016/j.apsusc.2018.09.105.

[6]   X. Chen, L. Liu, P.Y. Yu, S.S. Mao, Increasing solar absorption for photocatalysis with black hydrogenated titanium dioxide nanocrystals, Science (80-.). 331 (2011) 746–750. doi:10.1126/science.1200448.

[7]   G. Liu, L. Wang, H.G. Yang, H.M. Cheng, G.Q. Lu, Titania-based photocatalysts - Crystal growth, doping and heterostructuring, J. Mater. Chem. 20 (2010) 831–843. doi:10.1039/b909930a.

[8]   R. V. Nair, P.K. Gayathri, V.S. Gummaluri, P.M.G. Nambissan, C. Vijayan, Large bandgap narrowing in rutile TiO_2 aimed towards visible light applications and its correlation with vacancy-type defects history and transformation, J. Phys. D. Appl. Phys. 51 (2018). doi:10.1088/1361-6463/aaa187.

[9]   J. Xu, J. Huang, S. Zhang, Z. Hong, F. Huang, Understanding the surface reduction of nano rutile and anatase: Selective breaking of Ti-O bonds, Mater. Res. Bull. 121 (2020) 110617. doi:10.1016/j.materresbull.2019.110617.

[10]   S.G. Ullattil, S.B. Narendranath, S.C. Pillai, P. Periyat, Black TiO$_2$ Nanomaterials: A Review of Recent Advances, Chem. Eng. J. 343 (2018) 708–736. doi:10.1016/j.cej.2018.01.069.

[11]   X. Chen, D. Zhao, K. Liu, C. Wang, L. Liu, B. Li, Z. Zhang, D. Shen, Laser-Modified Black Titanium Oxide Nanospheres and Their Photocatalytic Activities under Visible Light, ACS Appl. Mater. Interfaces. (2015). doi:10.1021/acsami.5b04568.

[12]   B. Hu, C. hui Liang, F. Yang, J. Chen, W. Jin, H. Xing, L. Cai, S. Yang, K. zhao Liu, A.W. Kleyn, C. an Chen, TiO$_2$ powder modified by plasma afterglow: A correlation between active species, microstructure, and optical properties, Mater. Lett. 268 (2020) 127577. doi:10.1016/j.matlet.2020.127577.

[13]   T. Lin, C. Yang, Z. Wang, H. Yin, X. Lü, F. Huang, J. Lin, X. Xie, M. Jiang, Effective nonmetal incorporation in black titania with enhanced solar energy utilization, Energy Environ. Sci. 7 (2014) 967. doi:10.1039/c3ee42708k.

[14]   J. Jian, Y. Sun, F. Chen, R. Wu, S. Wei, Black and yellow anatase titania formed by (H,N)-doping: strong visible-light absorption and enhanced visible-light photocatalysis, Dalt. Trans. 44 (2014) 1534–1538. doi:10.1039/c4dt02984d.

[15]   A. Naldoni, M. Allieta, S. Santangelo, M. Marelli, F. Fabbri, S. Cappelli, C.L. Bianchi, R. Psaro, V. Dal Santo, Effect of nature and location of defects on bandgap narrowing in black TiO$_2$ nanoparticles, J. Am. Chem. Soc. (2012). doi:10.1021/ja3012676.

[16]   D. Zhao, B. Xu, J. Yang, J. Wu, W. Zhai, B. Yang, M. Liu, Rapid Preparation of TiO$_{2-x}$ and Its Photocatalytic Oxidation for Arsenic Adsorption under Visible Light, Langmuir. 36 (2020) 3853–3861. doi:10.1021/acs.langmuir.9b02444.

[17]   Z. Wang, C. Yang, T. Lin, H. Yin, P. Chen, D. Wan, F. Xu, F. Huang, J. Lin, X. Xie, M. Jiang, H-doped black titania with very high solar absorption and excellent photocatalysis enhanced by localized surface plasmon resonance, Adv. Funct. Mater. 23 (2013) 5444–5450. doi:10.1002/adfm.201300486.

[18]   B. Li, Z. Zhao, Q. Zhou, B. Meng, X. Meng, J. Qiu, Highly Efficient Low-Temperature Plasma-Assisted Modification of TiO$_2$ Nanosheets with Exposed {001} Facets for Enhanced Visible-Light Photocatalytic Activity, Chem. - A Eur. J. 20 (2014) 14763–14770. doi:10.1002/chem.201402664.

[19]   L. Hu, X. Song, X. Shan, X. Zhao, F. Guo, P. Xiao, Visible Light-Activated Self-Recovery Hydrophobic CeO$_2$/Black TiO$_2$ Coating Prepared Using Air Plasma Spraying, ACS Appl. Mater. Interfaces. 11 (2019) 37209–37215. doi:10.1021/acsami.9b10675.

[20]   M. Zhai, Y. Liu, J. Huang, Y. Wang, K. Chen, Y. Fu, H. Li, Efficient suspension plasma

spray fabrication of black titanium dioxide coatings with visible light absorption performances, Ceram. Int. 45 (2019) 930–935. doi:10.1016/j.ceramint.2018.09.268.

[21] M. Pylnev, M.S. Wong, Comparative study of photocatalytic deactivation of pure and black titania thin films, J. Photochem. Photobiol. A Chem. 378 (2019) 125–130. doi:10.1016/j.jphotochem.2019.04.020.

[22] S.Z. Islam, A. Reed, S. Nagpure, N. Wanninayake, J.F. Browning, J. Strzalka, D.Y. Kim, S.E. Rankin, Hydrogen incorporation by plasma treatment gives mesoporous black TiO$_2$ thin films with visible photoelectrochemical water oxidation activity, Microporous Mesoporous Mater. 261 (2018) 35–43. doi:10.1016/j.micromeso.2017.10.036.

[23] W. Zhang, J. Gu, K. Li, J. Zhao, H. Ma, C. Wu, C. Zhang, Y. Xie, F. Yang, X. Zheng, A hydrogenated black TiO$_2$ coating with excellent effects for photothermal therapy of bone tumor and bone regeneration, Mater. Sci. Eng. C. 102 (2019) 458–470. doi:10.1016/j.msec.2019.04.025.

[24] Y. Yan, B. Hao, D. Wang, G. Chen, E. Markweg, A. Albrecht, P. Schaaf, Understanding the fast lithium storage performance of hydrogenated TiO$_2$ nanoparticles, J. Mater. Chem. A. 1 (2013) 14507. doi:10.1039/c3ta13491a.

[25] F. Teng, M. Li, C. Gao, G. Zhang, P. Zhang, Y. Wang, L. Chen, E. Xie, Preparation of black TiO$_2$ by hydrogen plasma assisted chemical vapor deposition and its photocatalytic activity, Appl. Catal. B Environ. 148–149 (2014) 339–343. doi:10.1016/j.apcatb.2013.11.015.

[26] A. Lepcha, C. Maccato, A. Mettenbörger, T. Andreu, L. Mayrhofer, M. Walter, S. Olthof, T.-P. Ruoko, A. Klein, M. Moseler, K. Meerholz, J.R. Morante, D. Barreca, S. Mathur, Electrospun Black Titania Nanofibers: Influence of Hydrogen Plasma-Induced Disorder on the Electronic Structure and Photoelectrochemical Performance, J. Phys. Chem. C. 119 (2015) 18835–18842. doi:10.1021/acs.jpcc.5b02767.

[27] W. Ren, Y. Yan, L. Zeng, Z. Shi, A. Gong, P. Schaaf, D. Wang, J. Zhao, B. Zou, H. Yu, G. Chen, E.M.B. Brown, A. Wu, A Near Infrared Light Triggered Hydrogenated Black TiO$_2$ for Cancer Photothermal Therapy, Adv. Healthc. Mater. 4 (2015) 1526–1536. doi:10.1002/adhm.201500273.

[28] O. Carp, C.L. Huisman, A. Reller, Photoinduced reactivity of titanium dioxide, Prog. Solid State Chem. (2004). doi:10.1016/j.progsolidstchem.2004.08.001.

[29] M. Malekshahi Byranvand, A. Nemati Kharat, L. Fatholahi, Z. Malekshahi Beiranvand, A Review on Synthesis of Nano-TiO$_2$ via Different Methods, J. Nanostructures. 3 (2013) 1–9. doi:10.7508/jns.2013.01.001.

[30] J. Tian, Z. Zhao, A. Kumar, R.I. Boughton, H. Liu, Recent progress in design, synthesis, and applications of one-dimensional TiO₂ nanostructured surface heterostructures: A review, Chem. Soc. Rev. 43 (2014) 6920–6937. doi:10.1039/c4cs00180j.

[31] C. Dette, M.A. Pérez-Osorio, C.S. Kley, P. Punke, C.E. Patrick, P. Jacobson, F. Giustino, S.J. Jung, K. Kern, TiO₂ Anatase with a Bandgap in the Visible Region, Nano Lett. 14 (2014) 6533–6538. doi:10.1021/nl503131s.

[32] Y. Liu, L. Tian, X. Tan, X. Li, X. Chen, Synthesis, properties, and applications of black titanium dioxide nanomaterials, Sci. Bull. 62 (2017) 431–441. doi:10.1016/j.scib.2017.01.034.

[33] G. Wang, J. Zheng, H. Bi, S. Wang, J. Wang, J. Sun, Y. Guo, C. Wang, Ti^{3+} self-doping in bulk of rutile TiO₂ for enhanced photocatalysis, Scr. Mater. 162 (2019) 28–32. doi:10.1016/j.scriptamat.2018.10.025.

[34] D.A. Duarte, J.C. Sagás, A.S. da Silva Sobrinho, M. Massi, Modeling the reactive sputter deposition of N-doped TiO₂ for application in dye-sensitized solar cells: Effect of the O₂ flow rate on the substitutional N concentration, Appl. Surf. Sci. 269 (2013) 55–59. doi:10.1016/j.apsusc.2012.10.048.

[35] R. Marschall, L. Wang, Non-metal doping of transition metal oxides for visible-light photocatalysis, Catal. Today. (2014). doi:10.1016/j.cattod.2013.10.088.

[36] P. Koshy, W.-F. Chen, E. Adabifiroozjaei, Y. Yao, C.C. Sorrell, Y. Huang, Effects of precipitation, liquid formation, and intervalence charge transfer on the properties and photocatalytic performance of cobalt- or vanadium-doped TiO₂ thin films, Int. J. Hydrogen Energy. 41 (2016) 19025–19056. doi:10.1016/j.ijhydene.2016.08.115.

[37] J. Chen, X. Li, B. Lei, L. Zhou, S. Wang, Visible light photocatalysis of pristine anatase TiO₂ mesocrystals induced by largely exposed and stepped {001} surface, Green Chem. 21 (2019) 483–490. doi:10.1039/c8gc03300e.

[38] H. Han, X. Wang, C. Li, Y. Ma, X. Chen, Y. Jia, Titanium Dioxide-Based Nanomaterials for Photocatalytic Fuel Generations, Chem. Rev. 114 (2014) 9987–10043. doi:10.1021/cr500008u.

[39] Z. Xiu, M. Guo, T. Zhao, K. Pan, Z. Xing, Z. Li, W. Zhou, Recent advances in Ti^{3+} self-doped nanostructured TiO₂ visible light photocatalysts for environmental and energy applications, Chem. Eng. J. 382 (2020) 123011. doi:10.1016/j.cej.2019.123011.

[40] T.S. Rajaraman, S.P. Parikh, V.G. Gandhi, Black TiO₂: A review of its properties and conflicting trends, Chem. Eng. J. 389 (2020) 123918. doi:10.1016/j.cej.2019.123918.

[41] S.G. Ullattil, S.B. Narendranath, S.C. Pillai, P. Periyat, Black TiO₂ Nanomaterials: A

Review of Recent Advances, Chem. Eng. J. 343 (2018) 708–736. doi:10.1016/j.cej.2018.01.069.

[42] M. Hannula, H. Ali-Löytty, K. Lahtonen, E. Sarlin, J. Saari, M. Valden, Improved Stability of Atomic Layer Deposited Amorphous TiO_2 Photoelectrode Coatings by Thermally Induced Oxygen Defects, Chem. Mater. 30 (2018) 1199–1208. doi:10.1021/acs.chemmater.7b02938.

[43] C. Fan, C. Chen, J. Wang, X. Fu, Z. Ren, G. Qian, Z. Wang, Black Hydroxylated Titanium Dioxide Prepared via Ultrasonication with Enhanced Photocatalytic Activity, Sci. Rep. (2015). doi:10.1038/srep11712.

[44] C. Di Valentin, G. Pacchioni, A. Selloni, Reduced and n-type doped TiO_2: Nature of Ti^{3+} species, J. Phys. Chem. C. 113 (2009) 20543–20552. doi:10.1021/jp9061797.

[45] S.J. Baik, J.H. Jang, C.H. Lee, W.Y. Cho, K.S. Lim, Highly textured and conductive undoped ZnO film using hydrogen post-treatment, Appl. Phys. Lett. 70 (1997) 3516–3518. doi:10.1063/1.119218.

[46] M. Wajid Shah, Y. Zhu, X. Fan, J. Zhao, Y. Li, S. Asim, C. Wang, Facile Synthesis of Defective TiO_{2-x} Nanocrystals with High Surface Area and Tailoring Bandgap for Visible-light Photocatalysis, Sci. Rep. 5 (2015) 1–8. doi:10.1038/srep15804.

[47] T. Wang, W. Li, D. Xu, X. Wu, L. Cao, J. Meng, A novel and facile synthesis of black TiO_2 with improved visible-light photocatalytic H_2 generation: Impact of surface modification with CTAB on morphology, structure and property, Appl. Surf. Sci. 426 (2017) 325–332. doi:10.1016/j.apsusc.2017.07.153.

[48] Y. Fang, Y. Li, F. Zhou, P. Gu, J. Liu, D. Chen, N. Li, Q. Xu, J. Lu, An Efficient Photocatalyst Based on Black TiO_2 Nanoparticles and Porous Carbon with High Surface Area: Degradation of Antibiotics and Organic Pollutants in Water, Chempluschem. 84 (2019) 474–480. doi:10.1002/cplu.201900103.

[49] L. Wang, D. Wu, Z. Guo, J. Yan, Y. Hu, Z. Chang, Q. Yuan, H. Ming, J. Wang, Ultra-thin TiO_2 sheets with rich surface disorders for enhanced photocatalytic performance under simulated sunlight, J. Alloys Compd. 745 (2018) 26–32. doi:10.1016/j.jallcom.2018.02.070.

[50] P. Qiao, B. Sun, H. Li, K. Pan, G. Tian, L. Wang, W. Zhou, Surface Plasmon Resonance-Enhanced Visible-NIR-Driven Photocatalytic and Photothermal Catalytic Performance by Ag/Mesoporous Black TiO_2 Nanotube Heterojunctions, Chem. - An Asian J. 14 (2019) 177–186. doi:10.1002/asia.201801428.

[51] K. Zhang, W. Zhou, X. Zhang, Y. Qu, L. Wang, W. Hu, K. Pan, M. Li, Y. Xie, B. Jiang,

G. Tian, Large-scale synthesis of stable mesoporous black TiO$_2$ nanosheets for efficient solar-driven photocatalytic hydrogen evolution: Via an earth-abundant low-cost biotemplate, RSC Adv. 6 (2016) 50506–50512. doi:10.1039/c6ra06751d.

[52] N. Liu, C. Schneider, D. Freitag, M. Hartmann, U. Venkatesan, J. Müller, E. Spiecker, P. Schmuki, Black TiO$_2$ Nanotubes: Cocatalyst-Free Open-Circuit Hydrogen Generation, Nano Lett. 14 (2014) 3309–3313. doi:10.1021/nl500710j.

[53] T. Leshuk, S. Linley, F. Gu, Hydrogenation processing of TiO$_2$ nanoparticles, Can. J. Chem. Eng. 91 (2013) 799–807. doi:10.1002/cjce.21745.

[54] Z. Lu, C.T. Yip, L. Wang, H. Huang, L. Zhou, Hydrogenated TiO$_2$ nanotube arrays as high-rate anodes for lithium-ion microbatteries, Chempluschem. (2012). doi:10.1002/cplu.201200104.

[55] M. Ge, C. Cao, J. Huang, S. Li, Z. Chen, K.Q. Zhang, S.S. Al-Deyab, Y. Lai, A review of one-dimensional TiO$_2$ nanostructured materials for environmental and energy applications, J. Mater. Chem. A. (2016). doi:10.1039/c5ta09323f.

[56] S. Wei, R. Wu, X. Xu, J. Jian, H. Wang, Y. Sun, One-step synthetic approach for core-shelled black anatase titania with high visible light photocatalytic performance, Chem. Eng. J. 299 (2016) 120–125. doi:10.1016/j.cej.2016.04.067.

[57] Y. Zhu, D. Liu, M. Meng, H$_2$ spillover enhanced hydrogenation capability of TiO$_2$ used for photocatalytic splitting of water: A traditional phenomenon for new applications, Chem. Commun. 50 (2014) 6049–6051. doi:10.1039/c4cc01667j.

[58] M.C. Wu, I.C. Chang, K.C. Hsiao, W.K. Huang, Highly visible-light absorbing black TiO$_2$ nanocrystals synthesized by sol-gel method and subsequent heat treatment in low partial pressure H$_2$, J. Taiwan Inst. Chem. Eng. 63 (2016) 430–435. doi:10.1016/j.jtice.2016.02.026.

[59] L. Han, Z. Ma, Z. Luo, G. Liu, J. Ma, X. An, Enhanced visible light and photocatalytic performance of TiO$_2$ nanotubes by hydrogenation at lower temperature, RSC Adv. (2016). doi:10.1039/c5ra11616c.

[60] X. Liu, Z. Xing, H. Zhang, W. Wang, Y. Zhang, Z. Li, X. Wu, X. Yu, W. Zhou, Fabrication of 3D Mesoporous Black TiO$_2$/MoS$_2$/TiO$_2$ Nanosheets for Visible-Light-Driven Photocatalysis, ChemSusChem. 9 (2016) 1118–1124. doi:10.1002/cssc.201600170.

[61] L. Liu, P.Y. Yu, X. Chen, S.S. Mao, D.Z. Shen, Hydrogenation and disorder in engineered black TiO$_2$, Phys. Rev. Lett. 111 (2013) 1–5. doi:10.1103/PhysRevLett.111.065505.

[62] L.R. Grabstanowicz, S. Gao, T. Li, R.M. Rickard, T. Rajh, D.J. Liu, T. Xu, Facile oxidative conversion of TiH_2 to high-concentration Ti^{3+}-self-doped rutile TiO_2 with visible-light photoactivity, Inorg. Chem. 52 (2013) 3884–3890. doi:10.1021/ic3026182.

[63] S.T. Myung, M. Kikuchi, C.S. Yoon, H. Yashiro, S.J. Kim, Y.K. Sun, B. Scrosati, Black anatase titania enabling ultra high cycling rates for rechargeable lithium batteries, Energy Environ. Sci. (2013). doi:10.1039/c3ee41960f.

[64] S.G. Ullattil, S.B. Narendranath, S.C. Pillai, P. Periyat, Black TiO_2 Nanomaterials: A Review of Recent Advances, Chem. Eng. J. 343 (2018) 708–736. doi:10.1016/j.cej.2018.01.069.

[65] G. Wang, H. Wang, Y. Ling, Y. Tang, X. Yang, R.C. Fitzmorris, C. Wang, J.Z. Zhang, Y. Li, Hydrogen-Treated TiO_2 Nanowire Arrays for Photoelectrochemical Water Splitting, Nano Lett. 11 (2011) 3026–3033. doi:10.1021/nl201766h.

[66] C. Sun, Y. Jia, X.H. Yang, H.G. Yang, X. Yao, G.Q. Lu, A. Selloni, S.C. Smith, Hydrogen incorporation and storage in well-defined nanocrystals of anatase titanium dioxide, J. Phys. Chem. C. 115 (2011) 25590–25594. doi:10.1021/jp210472p.

[67] X. Chen, L. Liu, F. Huang, Black titanium dioxide (TiO_2) nanomaterials, Chem. Soc. Rev. 44 (2015) 1861–1885. doi:10.1039/c4cs00330f.

[68] M. Kapilashrami, Y. Zhang, Y.S. Liu, A. Hagfeldt, J. Guo, Probing the optical property and electronic structure of TiO_2 nanomaterials for renewable energy applications, Chem. Rev. (2014). doi:10.1021/cr5000893.

[69] M. Dahl, Y. Liu, Y. Yin, Composite Titanium Dioxide Nanomaterials, Chem. Rev. 114 (2014) 9853–9889. doi:10.1021/cr400634p.

[70] X. Jiang, Y. Zhang, J. Jiang, Y. Rong, Y. Wang, Y. Wu, C. Pan, Characterization of oxygen vacancy associates within hydrogenated TiO_2: A positron annihilation study, J. Phys. Chem. C. 116 (2012) 22619–22624. doi:10.1021/jp307573c.

[71] T. Leshuk, R. Parviz, P. Everett, H. Krishnakumar, R.A. Varin, F. Gu, Photocatalytic activity of hydrogenated TiO_2, ACS Appl. Mater. Interfaces. 5 (2013) 1892–1895. doi:10.1021/am302903n.

[72] A. Sinhamahapatra, J.P. Jeon, J.S. Yu, A new approach to prepare highly active and stable black titania for visible light-assisted hydrogen production, Energy Environ. Sci. 8 (2015) 3539–3544. doi:10.1039/c5ee02443a.

[73] A. Naldoni, M. Allieta, S. Santangelo, M. Marelli, F. Fabbri, S. Cappelli, C.L. Bianchi, R. Psaro, V. Dal Santo, Effect of Nature and Location of Defects on Bandgap Narrowing in Black TiO_2 Nanoparticles, J. Am. Chem. Soc. 134 (2012) 7600–7603.

doi:10.1021/ja3012676.

[74] Q. Kang, J. Cao, Y. Zhang, L. Liu, H. Xu, J. Ye, Reduced TiO_2 nanotube arrays for photoelectrochemical water splitting, J. Mater. Chem. A. 1 (2013) 5766–5774. doi:10.1039/c3ta10689f.

[75] H. Tan, Z. Zhao, M. Niu, C. Mao, D. Cao, D. Cheng, P. Feng, Z. Sun, A facile and versatile method for preparation of colored TiO_2 with enhanced solar-driven photocatalytic activity, Nanoscale. 6 (2014) 10216–10223. doi:10.1039/c4nr02677b.

[76] Z. Wang, C. Yang, T. Lin, H. Yin, P. Chen, D. Wan, F. Xu, F. Huang, J. Lin, X. Xie, M. Jiang, Visible-light photocatalytic, solar thermal and photoelectrochemical properties of aluminium-reduced black titania, Energy Environ. Sci. (2013). doi:10.1039/c3ee41817k.

[77] T. Lin, C. Yang, Z. Wang, H. Yin, X. Lü, F. Huang, J. Lin, X. Xie, M. Jiang, Effective nonmetal incorporation in black titania with enhanced solar energy utilization, Energy Environ. Sci. 7 (2014) 967–972. doi:10.1039/c3ee42708k.

[78] S.G. Ullattil, P. Periyat, Green microwave switching from oxygen rich yellow anatase to oxygen vacancy rich black anatase TiO_2 solar photocatalyst using Mn(II) as "anatase phase purifier," Nanoscale. (2015). doi:10.1039/c5nr05975e.

[79] K. Li, J. Xu, X. Yan, L. Liu, X. Chen, Y. Luo, J. He, D.Z. Shen, The origin of the strong microwave absorption in black TiO_2, Appl. Phys. Lett. 108 (2016). doi:10.1063/1.4948456.

[80] T. Nakajima, T. Nakamura, K. Shinoda, T. Tsuchiya, Rapid formation of black titania photoanodes: Pulsed laser-induced oxygen release and enhanced solar water splitting efficiency, J. Mater. Chem. A. 2 (2014) 6762–6771. doi:10.1039/c4ta00557k.

[81] M. Yao, J. Zhao, S. Lv, K. Lu, Preparation and hydrogenation of urchin-like titania using a one-step hydrothermal method, Ceram. Int. 43 (2017) 6925–6931. doi:10.1016/j.ceramint.2017.02.115.

[82] Y. Yan, B. Hao, D. Wang, G. Chen, E. Markweg, A. Albrecht, P. Schaaf, Understanding the fast lithium storage performance of hydrogenated TiO_2 nanoparticles, J. Mater. Chem. A. (2013). doi:10.1039/c3ta13491a.

[83] Y. Yan, M. Han, A. Konkin, T. Koppe, D. Wang, T. Andreu, G. Chen, U. Vetter, J.R. Morante, P. Schaaf, Slightly hydrogenated TiO_2 with enhanced photocatalytic performance, J. Mater. Chem. A. 2 (2014) 12708–12716. doi:10.1039/c4ta02192d.

[84] G. Panomsuwan, A. Watthanaphanit, T. Ishizaki, N. Saito, Water-plasma-assisted synthesis of black titania spheres with efficient visible-light photocatalytic activity, Phys. Chem. Chem. Phys. 17 (2015) 13794–13799. doi:10.1039/C5CP00171D.

[85] Y. Ishida, W. Doshin, H. Tsukamoto, T. Yonezawa, Black TiO_2 Nanoparticles by a Microwave-induced Plasma over Titanium Complex Aqueous Solution, Chem. Lett. 44 (2015) 1327–1329. doi:10.1246/cl.150531.

[86] T. Nakano, R. Ito, S. Kogoshi, N. Katayama, Optimal levels of oxygen deficiency in the visible light photocatalyst TiO_{2-x} and long-term stability of catalytic performance, J. Phys. Chem. Solids. (2016). doi:10.1016/j.jpcs.2016.06.017.

[87] G.S. Kim, J.K. Kim, S.H. Kim, J. Jo, C. Shin, J.H. Park, K.C. Saraswat, H.Y. Yu, Specific contact resistivity reduction through Ar plasma-treated TiO_{2-x} interfacial layer to metal/Ge contact, IEEE Electron Device Lett. (2014). doi:10.1109/LED.2014.2354679.

[88] Z. Zhang, M.N. Hedhili, H. Zhu, P. Wang, Electrochemical reduction induced self-doping of Ti^{3+} for efficient water splitting performance on TiO_2 based photoelectrodes, Phys. Chem. Chem. Phys. 15 (2013) 15637–15644. doi:10.1039/c3cp52759j.

[89] H. Zhou, Y. Zhang, Electrochemically self-doped TiO_2 nanotube arrays for supercapacitors, J. Phys. Chem. C. (2014). doi:10.1021/jp4082883.

[90] L. Zheng, H. Cheng, F. Liang, S. Shu, C.K. Tsang, H. Li, S.T. Lee, Y.Y. Li, Porous TiO_2 photonic band gap materials by anodization, J. Phys. Chem. C. 116 (2012) 5509–5515. doi:10.1021/jp212416c.

[91] B. Chen, J.A. Beach, D. Maurya, R.B. Moore, S. Priya, Fabrication of black hierarchical TiO_2 nanostructures with enhanced photocatalytic activity, RSC Adv. 4 (2014) 29443–29449. doi:10.1039/c4ra04260c.

[92] J. Dong, J. Han, Y. Liu, A. Nakajima, S. Matsushita, S. Wei, W. Gao, Defective black TiO_2 synthesized via anodization for visible-light photocatalysis, ACS Appl. Mater. Interfaces. 6 (2014) 1385–1388. doi:10.1021/am405549p.

[93] J. Xu, G. Zhu, W. Zhao, T. Lin, Z. Tian, F. Huang, Y. Shan, H. Zhang, C. Zheng, Hydrogenated blue titania with high solar absorption and greatly improved photocatalysis, Nanoscale. 8 (2016) 4705–4712. doi:10.1039/c5nr07953e.

[94] H. Huang, H. Zhang, Z. Ma, Y. Liu, X. Zhang, Y. Han, Z. Kang, Si quantum dot-assisted synthesis of mesoporous black TiO_2 nanocrystals with high photocatalytic activity, J. Mater. Chem. A. 1 (2013) 4162–4166. doi:10.1039/c3ta10206h.

[95] S.G. Ullattil, P. Periyat, A "one pot" gel combustion strategy towards Ti^{3+} self-doped "black" anatase TiO_{2-x} solar photocatalyst, J. Mater. Chem. A. 4 (2016) 5854–5858. doi:10.1039/c6ta01993e.

[96] Z. Wang, C. Yang, T. Lin, H. Yin, P. Chen, D. Wan, F. Xu, F. Huang, J. Lin, X. Xie, M.

Jiang, H-Doped Black Titania with Very High Solar Absorption and Excellent Photocatalysis Enhanced by Localized Surface Plasmon Resonance, Adv. Funct. Mater. 23 (2013) 5444–5450. doi:10.1002/adfm.201300486.

[97]   H. Wu, C. Xu, J. Xu, L. Lu, Z. Fan, X. Chen, Y. Song, D. Li, Enhanced supercapacitance in anodic TiO_2 nanotube films by hydrogen plasma treatment, Nanotechnology. 24 (2013) 455401. doi:10.1088/0957-4484/24/45/455401.

[98]   Y. Yan, M. Han, A. Konkin, T. Koppe, D. Wang, T. Andreu, G. Chen, U. Vetter, J.R. Morante, P. Schaaf, Slightly hydrogenated TiO_2 with enhanced photocatalytic performance, J. Mater. Chem. A. 2 (2014) 12708–12716. doi:10.1039/c4ta02192d.

[99]   Z. Tian, H. Cui, G. Zhu, W. Zhao, J. Xu, F. Shao, J. He, F. Huang, Hydrogen plasma reduced black TiO_2-B nanowires for enhanced photoelectrochemical water-splitting, J. Power Sources. 325 (2016) 697–705. doi:10.1016/j.jpowsour.2016.06.074.

[100] J. Xu, W. Dong, C. Song, Y. Tang, W. Zhao, Z. Hong, F. Huang, Black rutile (Sn, Ti)O_2 initializing electrochemically reversible Sn nanodots embedded in amorphous lithiated titania matrix for efficient lithium storage, J. Mater. Chem. A. 4 (2016) 15698–15704. doi:10.1039/C6TA05645H.

[101] A.P. Singh, N. Kodan, B.R. Mehta, A. Dey, S. Krishnamurthy, In-situ plasma hydrogenated TiO_2 thin films for enhanced photoelectrochemical properties, Mater. Res. Bull. 76 (2016) 284–291. doi:10.1016/j.materresbull.2015.12.015.

[102] J. Liang, N. Wang, Q. Zhang, B. Liu, X. Kong, C. Wei, D. Zhang, B. Yan, Y. Zhao, X. Zhang, Exploring the mechanism of a pure and amorphous black-blue TiO_2:H thin film as a photoanode in water splitting, Nano Energy. 42 (2017) 151–156. doi:10.1016/j.nanoen.2017.10.062.

[103] M. Pylnev, W.-H. Chang, M.-S. Wong, Shell of black titania prepared by sputtering TiO_2 target in H_2 + Ar plasma, Appl. Surf. Sci. 462 (2018) 285–290. doi:10.1016/j.apsusc.2018.08.103.

[104] T. Jedsukontorn, T. Ueno, N. Saito, M. Hunsom, Facile preparation of defective black TiO_2 through the solution plasma process: Effect of parametric changes for plasma discharge on its structural and optical properties, J. Alloys Compd. 726 (2017) 567–577. doi:10.1016/j.jallcom.2017.08.028.

[105] H.R. An, Y.C. Hong, H. Kim, J.Y. Huh, E.C. Park, S.Y. Park, Y. Jeong, J.I. Park, J.P. Kim, Y.C. Lee, W.K. Hong, Y.K. Oh, Y.J. Kim, M.H. Yang, H.U. Lee, Studies on mass production and highly solar light photocatalytic properties of gray hydrogenated-TiO_2 sphere photocatalysts, J. Hazard. Mater. 358 (2018) 222–233.

doi:10.1016/j.jhazmat.2018.06.055.

[106] J. Han, Y. Cheng, W. Tu, T.-Y. Zhan, Y. Cheng, The black and white coatings on Ti-6Al-4V alloy or pure titanium by plasma electrolytic oxidation in concentrated silicate electrolyte, Appl. Surf. Sci. 428 (2018) 684–697. doi:10.1016/j.apsusc.2017.09.109.

[107] M. Li, G. Zhang, E. Xie, F. Teng, Y. Wang, L. Chen, P. Zhang, C. Gao, Preparation of black TiO_2 by hydrogen plasma assisted chemical vapor deposition and its photocatalytic activity, Appl. Catal. B Environ. 148–149 (2013) 339–343. doi:10.1016/j.apcatb.2013.11.015.

[108] B. Bharti, S. Kumar, H.N. Lee, R. Kumar, Formation of oxygen vacancies and Ti^{3+} state in TiO_2 thin film and enhanced optical properties by air plasma treatment, Sci. Rep. 6 (2016) 1–12. doi:10.1038/srep32355.

[109] W. Wei, N. Yaru, L. Chunhua, X. Zhongzi, Hydrogenation of TiO_2 nanosheets with exposed {001} facets for enhanced photocatalytc activity, RSC Adv. 2 (2012) 8286–8288. doi:10.1039/c2ra21049e.

[110] X. Yu, B. Kim, Y.K. Kim, Highly enhanced photoactivity of anatase TiO_2 nanocrystals by controlled hydrogenation-induced surface defects, ACS Catal. (2013). doi:10.1021/cs4005776.

[111] S. Wei, R. Wu, J. Jian, F. Chen, Y. Sun, Black and yellow anatase titania formed by (H,N)-doping: Strong visible-light absorption and enhanced visible-light photocatalysis, Dalt. Trans. (2015). doi:10.1039/c4dt02984d.

[112] J.W. Chen, J.W. Shi, M.L. Fu, Nitrogen-doped anatase titania nanorods with reactive {101} + {010} facets exposure produced from ultrathin titania nanosheets for high photocatalytic performance, Catal. Commun. 76 (2016) 82–86. doi:10.1016/j.catcom.2016.01.001.

[113] Q. Bi, X. Huang, Y. Dong, F. Huang, Conductive Black Titania Nanomaterials for Efficient Photocatalytic Degradation of Organic Pollutants, Catal. Letters. 150 (2020) 1346–1354. doi:10.1007/s10562-019-02941-1.

[114] S. Kang, S. Li, T. Pu, X. Fang, C. Yin, M. Dong, L. Cui, Mesoporous black TiO_2 array employing sputtered Au cocatalyst exhibiting efficient charge separation and high H_2 evolution activity, Int. J. Hydrogen Energy. (2018) 22265–22272. doi:10.1016/j.ijhydene.2018.10.067.

[115] P. Qiao, J. Wu, H. Li, Y. Xu, B. Sun, L. Ren, K. Pan, L. Wang, W. Zhou, Improved charge separation of NiS nanoparticles modified defect-engineered black TiO_2 hollow nanotubes for boosting solar-driven photocatalytic H_2 evolution, Nanotechnology. 30

(2019). doi:10.1088/1361-6528/aafcee.

[116] J. Xu, J. Zhang, Z. Cai, H. Huang, T. Huang, P. Wang, X. Wang, Facile and large-scale synthesis of defective black TiO_{2-x} (B) nanosheets for efficient visible-light-driven photocatalytic hydrogen evolution, Catalysts. 9 (2019) 2–9. doi:10.3390/catal9121048.

[117] X. Chen, L. Liu, P.Y. Yu, S.S. Mao, Increasing Solar Absorption for Photocatalysis with Black Hydrogenated Titanium Dioxide Nanocrystals, Science (80-.). 331 (2011) 746–750. doi:10.1126/science.1200448.

[118] C. Yang, Z. Wang, T. Lin, H. Yin, X. Lü, D. Wan, T. Xu, C. Zheng, J. Lin, F. Huang, X. Xie, M. Jiang, Core-shell nanostructured "black" Rutile Titania as excellent catalyst for hydrogen production enhanced by sulfur doping, J. Am. Chem. Soc. 135 (2013) 17831–17838. doi:10.1021/ja4076748.

[119] W. Zhou, W. Li, J.-Q. Wang, Y. Qu, Y. Yang, Y. Xie, K. Zhang, L. Wang, H. Fu, D. Zhao, Ordered Mesoporous Black TiO_2 as Highly Efficient Hydrogen Evolution Photocatalyst, J. Am. Chem. Soc. 136 (2014) 9280–9283. doi:10.1021/ja504802q.

[120] A. Sinhamahapatra, J.P. Jeon, J.S. Yu, A new approach to prepare highly active and stable black titania for visible light-assisted hydrogen production, Energy Environ. Sci. 8 (2015) 3539–3544. doi:10.1039/c5ee02443a.

[121] X. Liu, Z. Xing, H. Zhang, W. Wang, Y. Zhang, Z. Li, X. Wu, X. Yu, W. Zhou, Fabrication of 3D Mesoporous Black TiO_2/MoS_2/TiO_2 Nanosheets for Visible-Light-Driven Photocatalysis, ChemSusChem. 9 (2016) 1118–1124. doi:10.1002/cssc.201600170.

[122] G. Zhou, L. Shen, Z. Xing, X. Kou, S. Duan, L. Fan, H. Meng, Q. Xu, X. Zhang, L. Li, M. Zhao, J. Mi, Z. Li, Ti^{3+} self-doped mesoporous black TiO_2/graphene assemblies for unpredicted-high solar-driven photocatalytic hydrogen evolution, J. Colloid Interface Sci. 505 (2017) 1031–1038. doi:10.1016/j.jcis.2017.06.097.

[123] C. Zhang, Y. Xie, J. Ma, J. Hu, C. Zhang, A composite catalyst of reduced black TiO_{2-x}/CNT: A highly efficient counter electrode for ZnO-based dye-sensitized solar cells, Chem. Commun. 51 (2015) 17459–17462. doi:10.1039/c5cc07284k.

[124] S.G. Ullattil, A.V. Thelappurath, S.N. Tadka, J. Kavil, B.K. Vijayan, P. Periyat, A Sol-solvothermal Processed 'Black TiO_2' as Photoanode Material in Dye Sensitized Solar Cells, Sol. Energy. 155 (2017) 490–495. doi:10.1016/j.solener.2017.06.059.

[125] C. Kim, S. Kim, J. Lee, J. Kim, J. Yoon, Capacitive and oxidant generating properties of black-colored TiO_2 nanotube array fabricated by electrochemical self-doping, ACS Appl. Mater. Interfaces. (2015). doi:10.1021/acsami.5b00123.

[126] J. Zhi, C. Yang, T. Lin, H. Cui, Z. Wang, H. Zhang, F. Huang, Flexible all solid state supercapacitor with high energy density employing black titania nanoparticles as a conductive agent, Nanoscale. (2016). doi:10.1039/c5nr08136j.

[127] T. Xia, W. Zhang, W. Li, N.A. Oyler, G. Liu, X. Chen, Hydrogenated surface disorder enhances lithium ion battery performance, Nano Energy. (2013). doi:10.1016/j.nanoen.2013.02.005.

[128] T. Xia, W. Zhang, J. Murowchick, G. Liu, X. Chen, Built-in electric field-assisted surface-amorphized nanocrystals for high-rate lithium-ion battery, Nano Lett. (2013). doi:10.1021/nl402810d.

[129] T. Xia, W. Zhang, Z. Wang, Y. Zhang, X. Song, J. Murowchick, V. Battaglia, G. Liu, X. Chen, Amorphous carbon-coated TiO_2 nanocrystals for improved lithium-ion battery and photocatalytic performance, Nano Energy. (2014). doi:10.1016/j.nanoen.2014.03.012.

[130] Z. Lu, C.T. Yip, L. Wang, H. Huang, L. Zhou, Hydrogenated TiO_2 nanotube arrays as high-rate anodes for lithium-ion microbatteries, Chempluschem. (2012). doi:10.1002/cplu.201200104.

[131] J. Bae, D.S. Kim, H. Yoo, E. Park, Y.G. Lim, M.S. Park, Y.J. Kim, H. Kim, High-Performance Si/SiO_x Nanosphere Anode Material by Multipurpose Interfacial Engineering with Black TiO_{2-x}, ACS Appl. Mater. Interfaces. (2016). doi:10.1021/acsami.5b10707.

[132] J.Y. Eom, S.J. Lim, S.M. Lee, W.H. Ryu, H.S. Kwon, Black titanium oxide nanoarray electrodes for high rate Li-ion microbatteries, J. Mater. Chem. A. (2015). doi:10.1039/c5ta01718a.

[133] Y.J. He, J.F. Peng, W. Chu, Y.Z. Li, D.G. Tong, Black mesoporous anatase TiO_2 nanoleaves: A high capacity and high rate anode for aqueous Al-ion batteries, J. Mater. Chem. A. (2014). doi:10.1039/c3ta13906a.

[134] J. Chen, Z. Ding, C. Wang, H. Hou, Y. Zhang, C. Wang, G. Zou, X. Ji, Black Anatase Titania with Ultrafast Sodium-Storage Performances Stimulated by Oxygen Vacancies, ACS Appl. Mater. Interfaces. 8 (2016) 9142–9151. doi:10.1021/acsami.6b01183.

[135] X. Hou, S. Jiang, Y. Li, A two-anode reduction technique to monitor the defect and dope the surface of TiO_2 nanotube array as photo-anode for water splitting, Appl. Catal. B Environ. 258 (2019) 117949. doi:10.1016/j.apcatb.2019.117949.

[136] Q. Liu, D. Ding, C. Ning, X. Wang, Black Ni-doped TiO_2 photoanodes for high-efficiency photoelectrochemical water-splitting, Int. J. Hydrogen Energy. 40 (2015) 2107–2114. doi:10.1016/j.ijhydene.2014.12.064.

[137] G. Zhu, H. Yin, C. Yang, H. Cui, Z. Wang, J. Xu, T. Lin, F. Huang, Black Titania for Superior Photocatalytic Hydrogen Production and Photoelectrochemical Water Splitting, ChemCatChem. 7 (2015) 2614–2619. doi:10.1002/cctc.201500488.

[138] H. Cui, W. Zhao, C. Yang, H. Yin, T. Lin, Y. Shan, Y. Xie, H. Gu, F. Huang, Black TiO_2 nanotube arrays for high-efficiency photoelectrochemical water-splitting, J. Mater. Chem. A. 2 (2014) 8612–8616. doi:10.1039/c4ta00176a.

[139] W. Qingli, Z. Zhaoguo, C. Xudong, H. Zhengfeng, D. Peimei, C. Yi, Z. Xiwen, Photoreduction of CO_2 using black TiO_2 films under solar light, J. CO2 Util. 12 (2015) 7–11. doi:10.1016/j.jcou.2015.09.001.

[140] X. Xin, T. Xu, L. Wang, C. Wang, Ti^{3+}-self doped brookite TiO_2 single-crystalline nanosheets with high solar absorption and excellent photocatalytic CO_2 reduction, Sci. Rep. 6 (2016) 1–8. doi:10.1038/srep23684.

[141] G. Zhu, J. Xu, W. Zhao, F. Huang, Constructing black titania with unique nanocage structure for solar desalination, ACS Appl. Mater. Interfaces. (2016). doi:10.1021/acsami.6b11466.

[142] J. Mou, T. Lin, F. Huang, H. Chen, J. Shi, Black titania-based theranostic nanoplatform for single NIR laser induced dual-modal imaging-guided PTT/PDT, Biomaterials. (2016). doi:10.1016/j.biomaterials.2016.01.009.

[143] X. Pang, H. Peng, H. Yang, K. Gao, X. Wu, A.A. Volinsky, Fast deposition of diamond-like carbon films by radio frequency hollow cathode method, Thin Solid Films. 534 (2013) 226–230. doi:10.1016/j.tsf.2013.02.123.

[144] C. Lejeune, J. Grandchamp, O. Kessi, J. Gilles, Rf multipolar plasma for broad and reactive ion beams, Vacuum. 36 (1986) 837–840. doi:10.1016/0042-207X(86)90122-3.

[145] C.M. Horwitz, Hollow cathode reactive sputter etching - A new high-rate process, Appl. Phys. Lett. 43 (1983) 977–979. doi:10.1063/1.94172.

[146] G.L. Majstorović, N.M. Iović, N. Konjević, Rotational and vibrational temperatures of molecular hydrogen in a hollow cathode glow discharge, Plasma Sources Sci. Technol. 16 (2007) 750–756. doi:10.1088/0963-0252/16/4/009.

[147] L. Bárdoš, Radio frequency hollow cathodes for the plasma processing technology, Surf. Coatings Technol. 86–87 (1996) 648–656. doi:10.1016/S0257-8972(96)03056-3.

[148] A.D. White, New hollow cathode glow discharge, J. Appl. Phys. 30 (1959) 711–719. doi:10.1063/1.1735220.

[149] C.M. Horwitz, D.R. McKenzie, High-rate hollow-cathode amorphous silicon deposition, Appl. Surf. Sci. 22–23 (1985) 925–929. doi:10.1016/0378-5963(85)90225-9.

[150] B.B. Sahu, S.H. Kim, J.S. Lee, J.G. Han, Comparison of plasma properties in normal and multiple holes hollow cathode RF PECVD and their utility in a-SiNx:H thin film deposition, Vacuum. 160 (2019) 316–324. doi:10.1016/j.vacuum.2018.11.034.

[151] O. Peña, S. Muhl, W. López, L. Rodríguez-Fernández, J.L. Ruvalcaba-Sil, Hydrogen plasma etching of silicon dioxide in a hollow cathode system, Thin Solid Films. 518 (2010) 3156–3159. doi:10.1016/j.tsf.2009.08.042.

[152] T.R. Society, The hollow-cathode effect and the theory of glow discharges, Proc. R. Soc. London. Ser. A. Math. Phys. Sci. 224 (1954) 209–227. doi:10.1098/rspa.1954.0152.

[153] D.J. Sturges, H.J. Oskam, Hollow-cathode glow discharge in hydrogen and the noble gases, J. Appl. Phys. 37 (1966) 2405–2412. doi:10.1063/1.1708828.

[154] M. Fitzgerald, J. Khachan, S. Bosi, Relative densities of hydrogen ion species in a hollow cathode glow discharge, Eur. Phys. J. D. 39 (2006) 35–39. doi:10.1140/epjd/e2006-00070-x.

[155] R. Mavrodineanu, Hollow Cathode Discharges: Analytical Applications., J. Res. Natl. Bur. Stand. (United States). 89 (1984) 143–185. doi:10.6028/jres.089.009.

[156] C.M. Horwitz, S. Boronkay, M. Gross, K. Davies, Hollow cathode etching and deposition, J. Vac. Sci. Technol. A Vacuum, Surfaces, Film. 6 (1988) 1837–1844. doi:10.1116/1.575265.

[157] P.F. Little, The Hollow-Cathode Effect and the Theory of Glow Discharges, Proc. R. Soc. A Math. Phys. Eng. Sci. (1954). doi:10.1098/rspa.1954.0152.

[158] L. Bárdoš, Radio frequency hollow cathodes for the plasma processing technology, Surf. Coatings Technol. (1996). doi:10.1016/S0257-8972(96)03056-3.

[159] S. Berardi, S. Drouet, L. Francàs, C. Gimbert-Suriñach, M. Guttentag, C. Richmond, T. Stoll, A. Llobet, Molecular artificial photosynthesis, Chem. Soc. Rev. 43 (2014) 7501–7519. doi:10.1039/c3cs60405e.

[160] X. Yang, D. Wang, Photocatalysis: From Fundamental Principles to Materials and Applications, ACS Appl. Energy Mater. 1 (2018) 6657–6693. doi:10.1021/acsaem.8b01345.

[161] P. Zhou, J. Yu, M. Jaroniec, All-Solid-State Z-Scheme Photocatalytic Systems, Adv. Mater. 26 (2014) 4920–4935. doi:10.1002/adma.201400288.

[162] A. Fujishima, K. Honda, Electrochemical Photolysis of Water at a Semiconductor Electrode, Nature. 238 (1972) 37–38. doi:10.1038/238037a0.

[163] W. Zhao, I.W. Chen, F. Huang, Toward large-scale water treatment using nanomaterials, Nano Today. 27 (2019) 11–27. doi:10.1016/j.nantod.2019.05.003.

[164] W. Choi, A. Termin, M.R. Hoffmann, The Role of Metal Ion Dopants in Quantum-Sized TiO$_2$: Correlation between Photoreactivity and Charge Carrier Recombination Dynamics, J. Phys. Chem. 98 (1994) 13669–13679. doi:10.1021/j100102a038.

[165] L.E. Oi, M.Y. Choo, H.V. Lee, H.C. Ong, S.B.A. Hamid, J.C. Juan, Recent advances of titanium dioxide (TiO$_2$) for green organic synthesis, RSC Adv. 6 (2016) 108741–108754. doi:10.1039/c6ra22894a.

[166] W. Chiappim Junior, Deposição por Camada Atômica de TiO$_2$: Estudo Morfológico, Estrutural, Óptico e Comparação entre os Modos de Deposição Plasma e Térmico, Instituto Tecnológico de Aeronáutica, 2016.

[167] C. Di Valentin, A. Selloni, Bulk and surface polarons in photoexcited anatase TiO$_2$, J. Phys. Chem. Lett. 2 (2011) 2223–2228. doi:10.1021/jz2009874.

[168] J. Schneider, M. Matsuoka, M. Takeuchi, J. Zhang, Y. Horiuchi, M. Anpo, D.W. Bahnemann, Understanding TiO$_2$ Photocatalysis: Mechanisms and Materials, Chem. Rev. 114 (2014) 9919–9986. doi:10.1021/cr5001892.

[169] X. Yan, Y. Li, T. Xia, Black Titanium Dioxide Nanomaterials in Photocatalysis, Int. J. Photoenergy. 2017 (2017). doi:10.1155/2017/8529851.

[170] H. Toku, R.S. Pessoa, H.S. Maciel, M. Massi, U.A. Mengui, The effect of oxygen concentration on the low temperature deposition of TiO$_2$ thin films, Surf. Coatings Technol. 202 (2008) 2126–2131. doi:10.1016/j.surfcoat.2007.08.075.

[171] L.E. Gomes, M.F. Da Silva, R. V. Gonçalves, G. MacHado, G.B. Alcantara, A.R.L. Caires, H. Wender, Synthesis and Visible-Light-Driven Photocatalytic Activity of Ta^{4+} Self-Doped Gray Ta$_2$O$_5$ Nanoparticles, J. Phys. Chem. C. 122 (2018) 6014–6025. doi:10.1021/acs.jpcc.7b11822.

[172] A.C. Nogueira, L.E. Gomes, J.A.P. Ferencz, J.E.F.S. Rodrigues, R. V. Gonçąlves, H. Wender, Improved Visible Light Photoactivity of CuBi$_2$O$_4$/CuO Heterojunctions for Photodegradation of Methylene Blue and Metronidazole, J. Phys. Chem. C. 123 (2019) 25680–25690. doi:10.1021/acs.jpcc.9b06907.

[173] S. Nur Abdulmadjid, Z.S. Lie, H. Niki, M. Pardede, R. Hedwig, T.J. Lie, E. Jobiliong, K.H. Kurniawan, K.I. Fukumoto, K. Kagawa, M.O.N. Tjia, Quantitative deuterium analysis of titanium samples in ultraviolet laser-induced low-pressure helium plasma, Appl. Spectrosc. 64 (2010) 365–369. doi:10.1366/000370210791114202.

[174] J. Iqbal, H. Asghar, S.K.H. Shah, M. Naeem, S.A. Abbasi, R. Ali, Elemental analysis of sage (herb) using calibration-free laser-induced breakdown spectroscopy, Appl. Opt. 59 (2020) 4927. doi:10.1364/ao.385932.

[175] R. Bogdanowicz, Investigation of $H_2:CH_4$ plasma composition by means of spatially resolved optical spectroscopy, Acta Phys. Pol. A. 114 (2008). doi:10.12693/aphyspola.114.a-33.

[176] J. Torres, P.G. Reyes, C. Torres, H. Martinez, J. Vergara, Optical Emission Spectroscopy of Hγ, Hα, and Hβ in a Glow Discharge Mixture of Ar/H_2, IEEE Trans. Plasma Sci. 43 (2015) 846–850. doi:10.1109/TPS.2015.2395141.

[177] F. Wu, G. Levitin, D.W. Hess, Temperature Effects and Optical Emission Spectroscopy Studies of Hydrogen-Based Plasma Etching of Copper, J. Electrochem. Soc. 159 (2011) H121–H124. doi:10.1149/2.015202jes.

[178] Y. Suda, A. Okita, J. Takayama, A. Oda, H. Sugawara, Carbon-Nanotube Growth in Alcohol-Vapor Plasma, 37 (2009) 1150–1155.

[179] H.W. Liu, T.H. Chen, C.H. Chang, S.K. Lu, Y.C. Lin, D.S. Liu, Impact on the gas barrier property of silicon oxide films prepared by tetramethylsilane-based PECVD incorporating with ammonia, Appl. Sci. 7 (2017). doi:10.3390/app7010056.

[180] V.-D. Hodoroaba, E.B.M. Steers, V. Hoffmann, W.E.S. Unger, W. Paatsch, K. Wetzig, Influence of hydrogen on the analytical figures of merit of glow discharge optical emission spectroscopy—friend or foe?, J. Anal. At. Spectrom. 18 (2003) 521–526. doi:10.1039/B301326J.

[181] F.-H. Wang, J.-C. Chao, H.-W. Liu, F.-J. Liu, Physical properties of TiO_2-doped zinc oxide thin films: Influence of plasma treatment in H_2 and/or Ar gas ambient, Vacuum. 140 (2017) 155–160. doi:10.1016/j.vacuum.2016.11.005.

[182] A. Godoy-Jr, A. Pereira, M. Gomes, M. Fraga, R. Pessoa, D. Leite, G. Petraconi, A. Nogueira, H. Wender, W. Miyakawa, M. Massi, A. da S. Sobrinho, Y. Wu, W. Yang, Y. Fan, Q. Song, S. Xiao, Black TiO_2 thin films production using hollow cathode hydrogen plasma treatment: Synthesis, material characteristics and photocatalytic activity, Catalysts. 5 (2020) 1–8. doi:10.3390/catal10030282.

[183] G. Panomsuwan, A. Watthanaphanit, T. Ishizaki, N. Saito, Water-plasma-assisted synthesis of black titania spheres with efficient visible-light photocatalytic activity, Phys. Chem. Chem. Phys. 17 (2015) 13794–13799. doi:10.1039/c5cp00171d.

[184] P.M. Kibasomba, S. Dhlamini, M. Maaza, C.P. Liu, M.M. Rashad, D.A. Rayan, B.W. Mwakikunga, Strain and grain size of TiO_2 nanoparticles from TEM, Raman spectroscopy and XRD: The revisiting of the Williamson-Hall plot method, Results Phys. 9 (2018) 628–635. doi:10.1016/j.rinp.2018.03.008.

[185] B.K. Tudu, V. Gupta, A. Kumar, A. Sinhamahapatra, Freshwater production via efficient

oil-water separation and solar-assisted water evaporation using black titanium oxide nanoparticles, J. Colloid Interface Sci. 566 (2020) 183–193. doi:10.1016/j.jcis.2020.01.079.

[186] G. Gouadec, P. Colomban, Raman Spectroscopy of nanomaterials: How spectra relate to disorder, particle size and mechanical properties, Prog. Cryst. Growth Charact. Mater. 53 (2007) 1–56. doi:10.1016/j.pcrysgrow.2007.01.001.

[187] J. William D. Callister, Materials Science and Engineering 7th Ed. : An Introduction, 2007. doi:10.1007/BF01184995.

[188] B. Leedahl, T. de Boer, X. Yuan, A. Moewes, Oxygen Vacancy Induced Structural Distortions in Black Titania: A Unique Approach using Soft X-ray EXAFS at the O–K Edge, Chem. - A Eur. J. 25 (2019) 3272–3278. doi:10.1002/chem.201805423.

[189] X. Wang, B. Ma, J. Xue, J. Wu, J. Chang, C. Wu, Defective Black Nano-Titania Thermogels for Cutaneous Tumor-Induced Therapy and Healing, Nano Lett. 19 (2019) 2138–2147. doi:10.1021/acs.nanolett.9b00367.

[190] A. Naldoni, M. Altomare, G. Zoppellaro, N. Liu, Š. Kment, R. Zbořil, P. Schmuki, Photocatalysis with Reduced TiO_2: From Black TiO_2 to Cocatalyst-Free Hydrogen Production, ACS Catal. 9 (2019) 345–364. doi:10.1021/acscatal.8b04068.

[191] X. Liu, B. Hou, G. Wang, Z. Cui, X. Zhu, X. Wang, Black titania/graphene oxide nanocomposite films with excellent photothermal property for solar steam generation, J. Mater. Res. 33 (2018) 674–684. doi:10.1557/jmr.2018.25.

[192] S. Saied, J. Sullivan, T. Choudhury, C. Pearce, A comparison of ion and fast atom beam reduction in TiO_2, Vacuum. 38 (1988) 917–922. doi:10.1016/0042-207X(88)90492-7.

[193] G. Xia, Q. Liu, H. Zhou, F. Yu, Thickness measurement of low reflectance optical thin film with transparent substrate, AOPC 2015 Opt. Test, Meas. Equip. 9677 (2015) 96770K. doi:10.1117/12.2197726.

[194] Q. Yang, X.A. Zhang, A. Bagal, W. Guo, C.H. Chang, Antireflection effects at nanostructured material interfaces and the suppression of thin-film interference, Nanotechnology. 24 (2013). doi:10.1088/0957-4484/24/23/235202.

[195] X. Chen, C. Burda, The electronic origin of the visible-light absorption properties of C-, N- and S-doped TiO_2 nanomaterials, J. Am. Chem. Soc. 130 (2008) 5018–5019. doi:10.1021/ja711023z.

[196] A. Godoy, F.G. Carlucci, D.M.G. Leite, W. Miyakawa, A.L.J. Pereira, M. Massi, A.S. da Silva Sobrinho, Plasma nanotexturing of amorphous carbon films by reactive ion etching, Surf. Coatings Technol. 354 (2018) 153–160.

doi:10.1016/j.surfcoat.2018.09.024.

[197] N. Kaur, A. Verma, I. Thakur, S. Basu, In-situ dual effect of Ag-Fe-TiO$_2$ composite for the photocatalytic degradation of Ciprofloxacin in aqueous solution, Chemosphere. 276 (2021) 130180. doi:10.1016/j.chemosphere.2021.130180.

[198] J. Wang, X. Liu, R. Li, P. Qiao, L. Xiao, J. Fan, TiO$_2$ nanoparticles with increased surface hydroxyl groups and their improved photocatalytic activity, Catal. Commun. 19 (2012) 96–99. doi:10.1016/j.catcom.2011.12.028.

[199] M.H. Baek, J.W. Yoon, J.S. Hong, J.K. Suh, Application of TiO$_2$-containing mesoporous spherical activated carbon in a fluidized bed photoreactor - Adsorption and photocatalytic activity, Appl. Catal. A Gen. 450 (2013) 222–229. doi:10.1016/j.apcata.2012.10.018.

[200] A. Lepcha, C. Maccato, T. Andreu, L. Mayrhofer, M. Walter, S. Olthof, M. Moseler, K. Meerholz, J.R. Morante, D. Barreca, P.O. Box, Electrospun Black Titania Nanofibres: Influence of Hydrogen Plasma Induced Disorder on the Electronic Structure and Photoelectrochemical Performance, (n.d.) 1–22.

[201] J. Wang, Y. Song, L. Liu, Q. Wu, Y. Chen, The fabrication of self-floating Ti^{3+}/N co-doped TiO$_2$/diatomite granule catalyst with enhanced photocatalytic performance under visible light irradiation, Appl. Surf. Sci. 467–468 (2018) 514–525. doi:10.1016/j.apsusc.2018.10.146.

[202] Y. Chen, K. Liu, Fabrication of magnetically recyclable Ce/N co-doped TiO$_2$/NiFe$_2$O$_4$/diatomite ternary hybrid: Improved photocatalytic efficiency under visible light irradiation, J. Alloys Compd. (2017). doi:10.1016/j.jallcom.2016.12.153.

[203] X. Zhang, X. Chang, M.A. Gondal, B. Zhang, Y. Liu, G. Ji, Synthesis and photocatalytic activity of graphene/BiOBr composites under visible light, Appl. Surf. Sci. 258 (2012) 7826–7832. doi:10.1016/j.apsusc.2012.04.049.

[204] A. Turki, C. Guillard, F. Dappozze, Z. Ksibi, G. Berhault, H. Kochkar, Phenol photocatalytic degradation over anisotropic TiO$_2$ nanomaterials: Kinetic study, adsorption isotherms and formal mechanisms, Appl. Catal. B Environ. 163 (2015) 404–414. doi:10.1016/j.apcatb.2014.08.010.

[205] T. Su, Y. Yang, Y. Na, R. Fan, L. Li, L. Wei, B. Yang, W. Cao, An Insight into the Role of Oxygen Vacancy in Hydrogenated TiO$_2$ Nanocrystals in the Performance of Dye-Sensitized Solar Cells, ACS Appl. Mater. Interfaces. 7 (2015) 3754–3763. doi:10.1021/am5085447.

[206] X. Liu, A. Jin, Y. Jia, T. Xia, C. Deng, M. Zhu, C. Chen, X. Chen, Synergy of adsorption

and visible-light photocatalytic degradation of methylene blue by a bifunctional Z-scheme heterojunction of WO_3/g-C_3N_4, Appl. Surf. Sci. 405 (2017) 359–371. doi:10.1016/j.apsusc.2017.02.025.

8 Annexes

8.1 Annex A – Published Papers

1. **Godoy-Jr**, A.; Pereira, A.; Gomes, M.; Fraga, M.; Pessoa, R.; Leite, D.; Petraconi, G.; Nogueira, A.; Wender, H.; Miyakawa, Walter; Massi, M.; da Silva Sobrinho, A. Black TiO_2 Thin Films Production Using Hollow Cathode Hydrogen Plasma Treatment: Synthesis, Material Characteristics, and Photocatalytic Activity. Catalysts, v.10, p. 282, 2020.

2. **Godoy-Jr**, A.; Pereira, A.; Gomes, M.; Pessoa, R.; Leite, D.; Petraconi, G.; Miyakawa, Walter; da Silva Sobrinho, A. New and Fast Route to Black TiO_2 Based on Hollow Cathode H_2 Plasma. arXiv, *preprint*, 1-30, 2019.

3. **Godoy-Jr**, A.; Pereira, A.; Gomes, M.; Fraga, M.; Pessoa, R.; Leite, D.; Petraconi, G.; Nogueira, A.; Wender, H.; Miyakawa, Walter; Massi, M.; Da Silva Sobrinho, A. Plasma Nanotexturing of Amorphous Carbon Films by Reactive Ion Etching. Surface & Coatings Technology, v. 354, p. 153-160, 2018.

4. Carlucci, F. G.; **Godoy-Jr**, A.; Moraes, R. S.; Saito, E.; da Silva Sobrinho, A.; Massi, M.; Leite, D. M. G. Plasma Processed Carbon Thin Films Applied to Dye-Sensitized Solar Cells. Journal of Solid State Electrochemistry, v. 22, p. 1331-1338, 2018.

8.2 Annex B – Papers in Progress

1. **Godoy-Jr**, A.; Pereira, A.; Gomes, M.; Leite, D.; Pessoa, R.; Petraconi, G.; Miyakawa, Walter; Baldan, M.; Massi, M.; da Silva Sobrinho, A. The Time Influence on Black TiO_2 Thin Films Properties Hydrogenated by Hollow Cathode Plasma. (Article).

2. **Godoy-Jr**, A.; Damasceno, B.; Miranda, F.; Marquesi, A.; Pereira, A.; Leite, D.; da Silva Sobrinho, A. A Review on Recent Advances of Nanostructured Black TiO_2 Photocatalysis: Pollutant Degradation and Hydrogen Production. (Review).

3. Pereira, A.; Sans, J.; Gomis, O; Santamaría-Pérez, D.; Ray, S.; **Godoy-Jr**, A.; da Silva Sobrinho; A. S. Rodríguez-Hernández, P; Muñoz, A; Popescu, C.; Manjón, F. Experimental and Theoretical Study of Bulk Y_2O_3 and Y_2O_3:Eu^{3+} Nanoparticles under High Pressure. (Article).

4. Pereira, A.; **Godoy-Jr**, A.; Damasceno, B.; Horta, I.; Leite, D.; da Silva Sobrinho, A. Metal Oxide-based Heterostructures / Development of Metal Oxide Heterostructures for Photovoltaic and Solar Cell Applications (Book chapter).

8.3 Annex B – Abstracts Presented/Published in Scientific Events

1. **TiO$_2$ Nanoparticles Deposition by Suspension Thermal Plasma Spray. GODOY-JR**; MIRANDA, F. S.; PEREIRA, A. L. J.; GOMES, M. C.; PETRACONI FILHO, G.; PESSOA, R. S.; LEITE, D. M. G.; DA SILVA SOBRINHO, A. S. *Poster presentation in the* XVIII Brazilian MRS meeting, 2019, Balneário Camboriú, Brazil. ISBN: 978-85-63273-40-6. Held by Brazilian Materials Research Society.

2. **Synthesis and Characterization of Pure and Mn Doped TiO$_2$ Nanoparticles Synthesized by a Modified Hydrothermal Method.** NORBERTO, A. G.; GOMES, M. C.; SCHIABER, Z. S.; SILVA, L. F.; **GODOY-JR, A.**; LEITE, D. M. G.; DA SILVA SOBRINHO, A. S.; PEREIRA, A. L. J. *Poster presentation (presented by A. Norberto) in the* XVIII Brazilian MRS meeting, 2019, Balneário Camboriú, Brazil. ISBN: 978-85-63273-40-6. Held by Brazilian Materials Research Society.

3. **The role of Citric Acid as Chelating Agent in the Synthesis of Mn Doped TiO$_2$ Nanoparticles by Modified Polymeric Precursor Method.** PEREIRA, A. L. J.; NORBERTO, A. G.; SCHIABER, Z. S.; **GODOY-JR, A.**; LEITE, D. M. G.; DA SILVA SOBRINHO, A. S. *Poster presentation (presented by A. Pereira) in the* XVIII Brazilian MRS meeting, 2019, Balneário Camboriú, Brazil. ISBN: 978-85-63273-40-6. Held by Brazilian Materials Research Society.

4. **Study of the Properties of V-doped TiO$_2$ Nanoparticles: Evaluation of the Photocatalytic Potential.** GOMES, M. C.; PEREIRA, A. L. J.; NORBERTO, A. G.; SCHIABER, Z. S.; SILVA, L. F.; **GODOY-JR, A.**; LEITE, D. M. G.; DA SILVA SOBRINHO, A. S. *Poster presentation (presented by M. Gomes) in the* XVIII Brazilian MRS meeting, 2019, Balneário Camboriú, Brazil. ISBN: 978-85-63273-40-6. Held by Brazilian Materials Research Society.

5. **Optical and Electronic Characteristics of Hydrogenated TiO$_2$ Thin Films Obtained by Radiofrequency Capacitive H$_2$ Plasma. GODOY-JR, A**; PEREIRA, A. L. J.; GOMES, M. C.; PESSOA, R. S.; LEITE, D. M. G.; PETRACONI FILHO, G.; MIYAKAWA, W.; DA SILVA SOBRINHO, A. S. *Poster presentation in the* XIII ITA Physics Meeting (XIII-EFITA), 2019, São José dos Campos, Brazil. Held by Technological Institute of Aeronautics (ITA).

6. **Hydrogenated Titania Nanoparticles Deposited by Suspension Thermal Plasma Spray. GODOY-JR, A.**; MIRANDA, F. S.; PEREIRA, A. L. J.; GOMES, M. C.; PETRACONI FILHO, G.; PESSOA, R. S.; LEITE, D. M. G.; DA SILVA SOBRINHO, A. S. *Poster presentation in the* XIII ITA Physics Meeting (XIII-EFITA), 2019, São José dos Campos, Brazil. Held by Technological Institute of Aeronautics (ITA).

7. **Influence Study of Calcination Temperature on the Synthesis of Bi$_2$O$_3$ Nanoparticles Obtained by Hydrothermal Method**. BARROS, H. C. S.; **GODOY-JR, A.**; PEREIRA, A. L. J.; DA SILVA SOBRINHO, A. S. *Poster presentation*

(presented by H. Barros) in the Congress of Innovation, Science and Technology, 2019. Held by Federal Institute of São Paulo (IFSP).

8. **Study of V-doped TiO₂ Nanoparticles Obtained by the Modified Pechini Method: Evaluation of the Photocatalytic Potential**. FERNANDES, G. L.; **GODOY-JR, A.**; PEREIRA, A. L. J.; PETRACONI FILHO, G. *Poster presentation (presented by G. Fernandes) in the* Congress of Innovation, Science and Technology, 2019. Held by Federal Institute of São Paulo (IFSP).

9. **The Effects of Sodium Content and Hydrogenation of TiO₂ Nanoparticles Doped with Manganese on Photocatalytic Activity.** FERNANDES, G. L.; BARROS, H. C. S.; OLIVEIRA, F. P.; GOMES, M. C.; **GODOY-JR, A.**; LEITE, D. M. G.; DA SILVA SOBRINHO, A. S.; PEREIRA, A. L. J. *Poster presentation (presented by G. Fernandes) in the* XIII ITA Physics Meeting (XIII-EFITA), 2019, São José dos Campos, Brazil. Held by Technological Institute of Aeronautics (ITA).

10. **Growth and Characterization of Pure and Mn Doped TiO₂ Thin Films by DC Magnetron Sputtering.** NORBERTO, A. G.; GOMES, M. C.; **GODOY-JR, A.**; LEITE, D. M. G.; DA SILVA SOBRINHO, A. S.; PEREIRA, A. L. J. *Poster presentation (presented by A. Norberto) in the* XIII ITA Physics Meeting (XIII-EFITA), 2019, São José dos Campos, Brazil. Held by Technological Institute of Aeronautics (ITA).

11. **Influence Study of the Synthesis Method on the Photocatalytic Properties of Pure and Mn-doped TiO₂ Nanoparticles.** FERNANDES, G. L.; BARROS, H. C. S.; OLIVEIRA, F. P.; BOTAN NETO, B. D.; GOMES, M. C.; **GODOY-JR, A.**; LEITE, D. M. G.; DA SILVA SOBRINHO, A. S.; PEREIRA, A. L. J. *Poster presentation (presented by G. Fernandes) in the* MetMat Symposium -USP, 2019, São Paulo, Brazil. Held by Dept. Of School Metallurgical and Materials Engineering Polytechnic of University of São Paulo (USP).

12. **Co-doped TiO₂: Effect of Calcination Temperature and Dopant Content on Vibrational and Structural Properties.** BOTAN NETO, B. D.; GOMES, M. C.; FERNANDES, G. L.; BARROS, H. C. S.; OLIVEIRA, F. P.; **GODOY-JR, A.**; LEITE, D. M. G.; DA SILVA SOBRINHO, A. S.; PEREIRA, A. L. J. *Poster presentation (presented by B. Botan Neto) in the* MetMat Symposium - USP, 2019, São Paulo, Brazil. Held by Dept. Of School Metallurgical and Materials Engineering Polytechnic of University of São Paulo (USP).

13. **Synthesis and Characterization of Black TiO₂ Obtained by Plasma Processes. GODOY-JR, A.**; PEREIRA, A. L. J.; GOMES, M. C.; LEITE, D. M. G.; MASSI, M.; DA SILVA SOBRINHO, A. S. *Oral presentation in the* XVII Brazilian MRS meeting, 2018, Natal, Brazil. ISBN: 978-85-63273-38-3. Held by Brazilian Materials Research Society.

14. **Effects of Mn on the Properties of TiO₂ Nanoparticles Prepared by the Polymeric Precursor Method.** PEREIRA, A. L. J.; GOMES, M. C.; SCHIABER, Z. S.; MARTINEZ, A. L.; BELTRAN, A.; NORBERTO, A. G.; SILVA, L. F.; LEITE, D. M. G.; **GODOY-JR**, A.; DA SILVA SOBRINHO, A. S. *Poster presentation (presented by*

A. Pereira) in the XVII Brazilian MRS meeting, 2018, Natal, Brazil. ISBN: 978-85-63273-38-3. Held by Brazilian Materials Research Society.

15. **Thin Carbon Films Processed by Plasma for Application in Grätzel Solar Cells. Caliari, F. R.**; CARLUCCI, F. G.; **GODOY-JR, A.**; DA SILVA SOBRINHO, A. S.; MASSI, M.; LEITE, D. M. G. *Poster presentation (presented by F. Carlucci) in the* XXI Brazilian Symposium on Electrochemistry and Electroanalysis, 2017, Natal, Brazil.

16. **Nanotexturing Amorphous Carbon Films by Reactive Ion Etching. GODOY-JR, A.**; CARLUCCI, F. G.; MIYAKAWA, W.; LEITE, D. M. G.; MASSI, M.; DA SILVA SOBRINHO, A. S. *Poster presentation in the* 28th International Conference on Diamond and Carbon Materials, 2017, Gothenburg, Sweden, Brazil. Held by Elsevier.

FOLHA DE REGISTRO DO DOCUMENTO

[1.] CLASSIFICAÇÃO/TIPO	[2.] DATA	[3.] REGISTRO N°	[4.] N° DE PÁGINAS
TD	05 de outubro de 2021	DCTA/ITA/TD-023/2021	105

[5.] TÍTULO E SUBTÍTULO:

Black TiO$_2$ Thin Films Production by Hollow Cathode Hydrogen Plasma for Photocatalytic Applications

[6.] AUTOR(ES):

Armstrong Godoy Junior

[7.] INSTITUIÇÃO(ÕES)/ÓRGÃO(S) INTERNO(S)/DIVISÃO(ÕES):

Instituto Tecnológico de Aeronáutica – ITA

[8.] PALAVRAS-CHAVE SUGERIDAS PELO AUTOR:

1. Black TiO$_2$. 2. Plasma Processes. 3. Photocatalysis

9. PALAVRAS-CHAVE RESULTANTES DE INDEXAÇÃO:

Catodos ocos; Processamento de materiais a plasma; Catálise; Filmes finos; Física.

[10.] APRESENTAÇÃO: (X) **Nacional**   ( ) **Internacional**

ITA, São José dos Campos. Curso de Doutorado. Programa de Pós-Graduação em Física. Área de Física de Plasmas. Orientador: Prof. Dr. Argemiro Soares da Silva Sobrinho. Coorientador: Prof. Dr. André Luis de Jesus Pereira. Defesa em 16/09/2021. Publicada em 2021.

[11.] RESUMO:

This thesis aims to demonstrate a new method to produce thin black TiO$_2$ films from pure TiO$_2$ films in the anatase phase. The method consists of immersing the TiO$_2$ films for fifteen minutes in a hydrogen plasma generated by a PECVD-RF system with a hollow cathode geometry, resulting in an efficient darkening of the TiO$_2$. The growth of pure TiO$_2$ films in the anatase phase on glass and c-Si substrates was carried out using a magnetron sputtering system and subsequent heat treatment at 450 °C for 2h in order to achieve a preponderance of the anatase phase. Before and after the H$_2$ plasma treatment, the samples were characterized for their morphological, microstructural, chemical, optical, electrical, and wettability characteristics. For this purpose, analyzes of mechanical profilometry, scanning electron microscopy by field emission and atomic force, UV-Vis-NIR spectrophotometry, X-ray diffraction, Raman spectroscopy, X-ray excited photoelectron spectroscopy, measurements of sheet resistance by four-point probe, and goniometry. In addition, the photocatalytic potential of the films produced through the degradation of the methylene blue dye was evaluated, in addition to an investigation of the characteristics of the hydrogen plasma generated during the hydrogenation process. The results obtained show that the use of a hollow cathode for the hydrogenation process was decisive for the efficient hydrogenation of the black TiO$_2$ films. After treatment in hydrogen plasma, the films show a significant increase in the absorption of light across the solar spectrum, a significant decrease in sheet resistance, and a significant increase in the surface area. These results are mainly related to an increase in O vacancies and an increase in the presence of OH hydroxyl groups on the surface of the films. These characteristics led to a significant improvement in its photocatalytic activity under UV-Vis irradiation.

[12.] GRAU DE SIGILO:

(X) **OSTENSIVO**   ( ) **RESERVADO**   ( ) **SECRETO**